J Mammal Evol (2014) 21:127–172
DOI 10.1007/s10914-013-9236-3

ORIGINAL PAPER

The Osteology and Systematics of the Enigmatic Australian Oligo-Miocene Metatherian *Yalkaparidon* (Yalkaparidontidae; Yalkaparidontia; ?Australidelphia; Marsupialia)

Robin M. D. Beck · Kenny J. Travouillon · Ken P. Aplin · Henk Godthelp · Michael Archer

Published online: 24 September 2013

Abstract We provide the first detailed description of the osteology of the enigmatic Oligo-Miocene Australian metatherian *Yalkaparidon*. This taxon exhibits a number of unusual craniodental apomorphies but appears to be plesiomorphic within Metatheria in retaining four molars, rather than three as previously reported. We demonstrate that the only known skull of *Yalkaparidon* almost certainly represents a single individual. We also tentatively refer a number of isolated tarsals to the genus. Maximum parsimony analyses of a 258 character morphological matrix (with information from the tarsals described here either included or excluded) place *Yalkaparidon* within the superordinal clade Australidelphia, but Bayesian analyses of the same matrix are less well resolved, placing *Yalkaparidon* within Marsupialia but without unequivocally supporting australidelphian affinities. Bayesian analyses of a total evidence matrix that combines the morphological data with 9 kb of sequence data from five nuclear protein-coding genes (APOB, BRCA1, IRBP, RAG1 and VWF), 78 indels, and 53 retroposon insertion characters are similarly poorly resolved and do not clarify the supraordinal relationships of *Yalkaparidon* beyond suggesting that it is probably a member of Marsupialia. However, if the tarsal remains are correctly attributed to *Yalkaparidon*, then membership of Australidelphia seems likely, as these specimens exhibit characteristic australidelphian apomorphies. We conclude that the ordinal status of *Yalkaparidon* remains justified based on current evidence, and we present a revised diagnosis for Yalkaparidontia. We maintain the two currently recognized species, *Y. coheni* and *Y. jonesi*, but present revised specific diagnoses. We suggest a revised phylogenetic definition for Marsupialia, and provide phylogenetic definitions for Eomarsupialia (the clade comprising all extant Australian marsupial orders) and for the clade comprising Dasyuromorphia, Peramelemorphia, and Notoryctemorphia to the exclusion of Diprotodontia; we propose the name Agreodontia for the latter clade.

Keywords *Yalkaparidon* · Zalambdodont · Marsupialia · Metatheria · Australidelphia · Riversleigh

Electronic supplementary material The online version of this article (doi:10.1007/s10914-013-9236-3) contains supplementary material, which is available to authorized users.

R. M. D. Beck (✉) · K. J. Travouillon · H. Godthelp · M. Archer
School of Biological, Earth and Environmental Sciences, University of New South Wales, Sydney, NSW 2052, Australia
e-mail: robin.beck@unsw.edu.au

R. M. D. Beck · K. P. Aplin
Department of Mammalogy, American Museum of Natural History, Central Park West at 79th Street, New York, NY 10024-5192, USA

K. J. Travouillon
School of Earth Sciences, University of Queensland, St Lucia, QLD 4072, Australia

K. P. Aplin
National Museum of Natural History, Division of Mammals, Smithsonian Institution, Washington, DC 20013-7012, USA

Introduction

Yalkaparidon is one of the most intriguing of all the Australian fossil metatherians discovered to date. Originally described by Archer et al. 1988, *Yalkaparidon* is known only from Oligo-Miocene freshwater limestone deposits at Riversleigh World Heritage Area, northwestern Queensland. Hundreds of isolated teeth, dozens of dentaries, several cranial fragments, and a single relatively well-preserved partial skull of this taxon have now been obtained from acid processing of limestone blocks collected from multiple Oligo-Miocene sites at Riversleigh. In this paper, we also tentatively refer isolated tarsal elements recovered from several Riversleigh sites to *Yalkaparidon*.

Based on craniodental specimens collected prior to 1987, Archer et al. (1988) described two species: *Yalkaparidon coheni* (which includes the partial skull) and *Y. jonesi*. The

unique dentition of *Yalkaparidon*—comprising diprotodont lower incisors, hypseledont first upper and lower incisors, and extremely zalambdodont molars—together with the highly plesiomorphic basicranial features preserved in the single known skull, led Archer et al. (1988) to assign the genus to its own family (Yalkaparidontidae) and order (Yalkaparidontia). Marshall et al. (1990) and Szalay (1994) both suggested that *Yalkaparidon* is in fact a member of Diprotodontia, based largely on the shared presence of enlarged ("diprotodont") anterior lower incisors; however, diprotodonty appears to have evolved at least twice within Metatheria (Ride 1962; Marshall 1982). Woodburne and Case (1996) placed *Yalkaparidon* in Notoryctemorphia, presumably because both *Yalkaparidon* and the exant notoryctemorphian *Notoryctes* possess zalambdodont molars and despite Archer et al.'s (1988) convincing arguments against notoryctemorphian affinities. Most recent studies (Kirsch et al. 1997; McKenna and Bell 1997; Springer et al. 1997; Kemp 2005; Archer and Kirsch 2006) have followed Archer et al. (1988) in placing *Yalkaparidon* in its own order, rendering Yalkaparidontia the only recognized order of Australian metatherians without living representatives.

The relationships of Yalkaparidontia to other metatherian orders remain obscure. It has yet to be firmly established whether *Yalkaparidon* is a member of Australidelphia (the clade that includes all extant Australian marsupial orders and the South American microbiotherians; Szalay 1982, 1994; Springer et al. 1998; Amrine-Madsen et al. 2003; Nilsson et al. 2004, 2010; Beck 2008; Beck et al. 2008b; Meredith et al. 2008, 2009a), or even if it is a crown-group marsupial. Archer et al. (1988) argued that australidelphian affinities for *Yalkaparidon* seemed likely based on biogeographical grounds and overall basicranial similarities to peramelemorphians, but indicated that there was insufficient anatomical evidence for referring it with confidence to Australidelphia rather than Ameridelphia. However, Beck's (2012) recent description of a calcaneus of a non-australidelphian marsupial from the early Eocene Tingamarra fauna demonstrates that the Australian metatherian fauna has not always been restricted to members of Australidelphia. Furthermore, *Y. coheni* is basicranially plesiomorphic relative to most undoubted australidelphians (Archer et al. 1988; Wroe 1997; Wroe et al. 1998), notably in its lack of a squamosal epitympanic sinus. It is therefore possible that *Yalkaparidon* is not a member of Australidelphia. However, a squamosal epitympanic sinus is also absent in a number of undoubted australidelphians, namely the microbiotheriids *Dromiciops* and *Microbiotherium* (see Segall 1969), some peramelemorphians (Muirhead 2000), the wynyardiid diprotodontians *Wynyardia* (see Aplin 1987) and *Namilamadeta* (see Pledge 2005), and the thylacinid *Badjcinus* (see Muirhead and Wroe 1998). Thus, the absence of this structure in *Yalkaparidon* is not, by itself, compelling evidence of non-australidelphian affinities.

A study of the enamel microstructure of *Y. coheni* (Lester et al. 1988) found similarities to a number of living and extinct Australian marsupials but failed to identify unambiguous synapomorphies linking it with any other Australian order. However, the significance of Lester et al.'s (1988) findings is limited by the fact that non-Australian metatherians were not examined. *Yalkaparidon* and *Notoryctes* both possess zalambdodont molars, a distinctive dental morphology potentially indicative of a close relationship (as proposed by Woodburne and Case 1996). However, fundamental differences in dental morphology between the two taxa (Archer et al. 1988) and the discovery of a pre-zalambdodont but fossorially-adapted notoryctid from early Miocene deposits at Riversleigh (*Naraboryctes philcreaseri;* Warburton 2003; Archer et al. 2011) collectively represent strong evidence that zalambdodonty was convergently acquired by *Yalkaparidon* and *Notoryctes*. Current evidence indicates that zalambdodont molars have evolved a minimum of five times within therian mammals (Asher and Sánchez-Villagra 2005; Seiffert et al. 2007). The basicrania of *Yalkaparidon* and *Notoryctes* also show significant differences, although this is largely because *Yalkaparidon* retains numerous plesiomorphic basicranial features relative to the highly derived and extensively fused basicranium of *Notoryctes* (Archer 1976; Aplin 1990; Ladevèze et al. 2008). Ultimately, none of these hypotheses regarding the affinities of *Yalkaparidon* is supported by formal phylogenetic analyses, and so they remain untested.

Study of the anatomy and phylogeny of *Yalkaparidon* is complicated by the fact that the only known cranium (QM F13008, the holotype of *Y. coheni*, which also includes an associated partial right mandible) was recovered as separate rostral and braincase units that were reported as non-overlapping (Archer et al. 1988). They could therefore potentially represent two different taxa (a possibility acknowledged by Archer et al. 1988), although they were found in close association in a single block of limestone. The rostral unit undoubtedly represents *Yalkaparidon* because it preserves the distinctive incisors and molars characteristic of the genus, as does the associated mandible; however, it is possible that the braincase unit represents a second, otherwise unknown metatherian.

In light of these unresolved mysteries, and given that *Yalkaparidon* is known from relatively well-preserved remains, a comprehensive study of this taxon would seem timely. We initially consider whether the two units of the QM F13008 cranium could feasibly be from different taxa. We provide a detailed description of the known craniodental anatomy of *Yalkaparidon*, expanding on the original, brief report by Archer et al. (1988) and correcting a number of errors. We describe the morphology of isolated astragali and calcanea that we tentatively refer to *Yalkaparidon* based on size, relative abundance, and comparative morphology. We also re-examine the differences in size and dental formula that

led Archer et al. (1988) to recognize the two species *Y. coheni* and *Y. jonesi*, and use specimens collected since the initial description to reassess the species-level taxonomy of the genus. We briefly reassess Beck's (2009) conclusions regarding the functional morphology and likely paleoecology of *Yalkaparidon* based on its craniodental anatomy, incorporating new information provided by the tarsal material described here. We present the first phylogenetic analyses to include *Yalkaparidon*, using a modified version of the morphological matrix of Beck (2012) and the methodologies of maximum parsimony and Bayesian inference. We also employ a "total evidence" approach by combining the morphological matrix with 9 kb of sequence data from five nuclear genes, 78 indel characters coded from the nuclear sequence data, and 53 retroposon insertion characters taken from Nilsson et al. (2010), and analyze the combined dataset using Bayesian inference. Finally, based on its known anatomy and on the results of our phylogenetic analyses, we discuss whether *Yalkaparidon* should continue to be placed in its own order, Yalkaparidontia, and we provide a revised diagnosis for the taxon.

Materials and Methods

Specimens

All specimens of *Yalkaparidon* discussed here are registered in the Queensland Museum Fossil Collection (prefix QM F). A full list of all known specimens is given in the Electronic Supplementary Material, including the Riversleigh sites from which the specimens were collected, the species represented (based on the revised diagnoses presented here; see "Species-Level Taxonomy" and Table 1) and dental dimensions (maximum depth and mesiodistal width of the lower first incisor, following Freeman and Lemen 2008; maximum mesiodistal length and maximum labiolingual width for postcanine teeth; see Figs. 15 and 16) for each tooth preserved in the specimen. All measurements of specimens were made using a Wild MMS235 Digital Length Measuring Set attached to a Wild 3 MB stereomicroscope. We follow Archer et al. (1988) in recognizing two species of *Yalkaparidon*, *Y. coheni* and *Y. jonesi*, but provide a revised diagnosis for each species (see "Species-Level Taxonomy").

The cranial description given here is based primarily on the cranium of QM F13008 (the holotype of *Y. coheni*), which is largely complete except that the posterior part of the rostrum, the rostral part of the basicranium, and the right zygomatic arch are all missing, the left zygomatic arch is incomplete, and the palate is badly damaged. Additional cranial specimens of *Yalkaparidon* are highly fragmentary and largely duplicate regions of QM F13008. However, the following specimens provide significant additional information: QM F52942 (a partial right premaxilla and maxilla), QM F36546, F52755, and F52756 (partial maxillae), QM F40095 (the glenoid region of a right squamosal), and QM F52958 (an isolated partial left petrosal). Description of the mandible is based largely on the partial right mandible associated with the cranium of QM F13008, QM F13009 (the holotype of *Y. jonesi*, a partial right mandible), QM F36544 (a left mandible), and QM F36545 (a right mandible). The latter two specimens appear to represent a single individual and retain largely intact dental condyles, coronoid processes, and inflected mandibular angles, all of which are damaged in most other specimens.

Description of the upper dentition is largely based on QM F13008 (the cranial portion of which preserves I1-3 and M3), QM F13011 (a right partial maxilla preserving P3 and M2, which was designated as the paratype of *Y. coheni* by Archer et al. 1988) and QM F52756 (a left partial maxilla preserving P3 and M1-3). Although *Yalkaparidon* apparently retained four upper molars (contra Archer et al. 1988; see the "Skull Description - Maxilla" and "Dental Description – Upper Dentition"), M4 is not preserved in any cranial specimen, and we have been unable to identify plausible candidates for this tooth from amongst the thousands of isolated mammalian teeth that have been collected from the numerous Oligo-Miocene sites at Riversleigh.

Description of the lower dentition is largely based on the mandible of QM F13008, which preserves i1 and m2, and the following additional specimens: QM F13009 (the holotype of *Y. jonesi*, a partial right mandible preserving i1 and m1), QM F20723 (a left mandible preserving i1 and m2–3), QM F36544 (a left mandible preserving i1, the posterior root of m1, m2, and the mesial half of m4), QM F36548 (a right mandible preserving i1 and m1–2), QM F39984 (a right mandible preserving part of i1 and m1), QM F50794 (a left mandible preserving part of i1 and m2–3), and QM F52963 (a right mandible preserving i1 and a tiny unicuspid tooth occupying one of the alveoli between i1 and m1). Two alveoli for a double-rooted m4 are present in all known mandibles of *Yalkaparidon* that preserve this region, but of these only QM F36544 retains m4 in situ, and this tooth is broken distally in this specimen. We have tentatively identified a number of isolated *Yalkaparidon* molars as m4s based on comparison with the remnants of this tooth in QM F36544 and on extrapolation of meristic gradients inferred from m1–3. The differences in lower dental formula between the holotypes of *Y. coheni* and *Y. jonesi*, as well as further variation seen in additional isolated *Yalkaparidon* dentaries, are discussed in "Species-Level Taxonomy."

We tentatively refer nine isolated astragali (QM F39989, F40091, F40093, F40096, F52957, F52982, F53637, F53638, and F53639) to *Yalkaparidon*. While they are clearly referable to an australidelphian marsupial, they show significant differences to those of all other australidelphians known to have been present at Riversleigh during the Oligo-Miocene (namely members of the modern Australian marsupial orders Dasyuromorphia,

Table 1 List of mandibular and maxillary specimens of *Yalkaparidon*. The number of alveoli between i1 and m1 in the mandibular specimens is listed, and where possible specimens are identified to species-level, based on the revised diagnoses presented here. Measurements of i1 depth and width at the alveolus were taken following Freeman and Lemen (2008), while those for total jaw length, lower molar row length and upper molar row length were taken following Myers (2001). All linear measurements are in mm. Body mass estimates in grams were calculated using the "total jaw length," "lower molar row length," and "upper molar row length" regression equations of Myers (2001) for the "all species excluding dasyuromorphians" dataset, and incorporate the appropriate smearing estimate (Myers 2001: table 3). Specimens are arranged by Riversleigh Faunal Zone (A-C) and by site. Abbreviations: BM: estimated body mass; FZ: Riversleigh Faunal Zone; i1D: depth of i1 at alveolus; i1W; width of i1 at alveolus; LMRL: lower molar row length; TJL: total jaw length; UMRL: upper molar row length

FZ	Site	Specimen number	Specimen type	number of alveoli between i1 and m1	Species	i1D	i1W	TJL	LMRL	UMRL	BM
A	Quantum Leap	QM F50794	left mandible	3+?i2	*Y. coheni*	3.80	1.72	?	6.9	-	143.3 (LMRL)
B	Camel Sputum	QM F13008	partial cranium and associated right mandible	2	*Y. coheni*	4.11	1.78	?	8.3	7.7	248.4 (LMRL) 219.1 (UMRL)
B	Creaser's Ramparts	QM F20366	right mandible	2+?i2	*Y. coheni*	3.02	1.57	?	8.1	-	231.0 (LMRL)
B	Creaser's Ramparts	QM F24361	right mandible	2	*Y. coheni*	3.76	1.69	?	7.6	-	191.1 (LMRL)
B	Dirk's Towers	QM F36345	left mandible	? (postincisive region damaged)	*Y.* sp. indet.	3.94	1.88	?	7.6	-	191.1 (LMRL)
B	Dirk's Towers 4	QM F36415	left mandible	3+?i2	*Y. coheni*	3.76	1.82	?	7.2	-	162.7 (LMRL)
B	Inabeyance	QM F52757	left mandible	at least 1 (postincisive region damaged)	*Y. coheni*	3.79	1.70	?	8.2	-	239.6 (LMRL)
B	Judith Horizontalis	QM F31370	right mandible	1	*Y. coheni*	2.68	1.32	25	6.6	-	76.0 (TJL) 125 LMRL)
B	Neville's Garden	QM F36543	left mandible	2	*Y. coheni*	3.30	1.64	?	8.1	-	231.0 (LMRL)
B	Upper	QM F13010[d]	right mandible	2 (?i2 alveolus may also have been present, but postincisive region damaged)	*Y. coheni*	3.58	1.70	?	8.3	-	248.4 (LMRL)
B	Upper	QM F36544	left mandible	3	*Y. coheni*	3.74	1.79	?	6.0	-	
B	Upper	QM F36545	right mandible	1	*Y. coheni*	3.54	1.70	29.5	6.6	-	126.1 (TJL) 125 (LMRL)
B	Upper	QM F36548	right mandible	1	*Y. coheni*	3.65	1.83	?	8.1	-	231.0 (LMRL)
B	Upper	QM F36549	right mandible	2 (?i2 alveolus may also have been present, but postincisive region damaged)	*Y. coheni*	?	?	?	8.3	-	248.4 (LMRL)
B	Upper	QM F36551	left mandible	2+?i2	*Y. coheni*			?	8.2	-	239.6 (LMRL)
B	Upper	QM F39984	right mandible	2+?i2	*Y. coheni*			?	7.9	-	214.4 (LMRL)
B	Upper	QM F40068	left mandible	2	*Y. coheni*	3.44	1.71	?	?	-	?
B	Upper	QM F52755	right maxilla	-	*Y.* sp. indet.			-	-	6.9	159.8 (UMRL)
B	Upper	QM F52756	left maxilla	-	*Y.* sp. indet.			-	-	7.2	180.6 (UMRL)
B	Upper	QM F52759	left mandible	2	*Y. coheni*	3.82	1.74	?	7.9	-	214.4 (LMRL)
B	Upper	QM F52760	right mandible	2	*Y. coheni*	3.49	1.60	?	8.3	-	248.4 (LMRL)
B	Upper	QM F52761	left mandible	2+?i2	*Y. coheni*			?	7.9	-	214.4 (LMRL)
B	Wayne's Wok	QM F20723	left mandible	2	*Y. coheni*	3.74	1.70	?	7.8	-	206.5 (LMRL)
B	Wayne's Wok	QM F23526	right mandible	2	*Y. coheni*	3.60	1.58	?	8.0	-	222.6 (LMRL)
B	Wayne's Wok	QM F36550	right mandible	2 (?i2 alveolus may also have been present, but postincisive region damaged)	*Y. coheni*			?	7.2	-	162.7 (LMRL)
B	Wayne's Wok	QM F52758	right mandible	2+?i2	*Y. coheni*	2.88	1.42	?	7.8	-	206.5 (LMRL)
C	Gag	QM F13009[e]	right mandible	0	*Y. jonesi*	3.32	1.72	?	7.5	-	183.7 (LMRL)

Diprotodontia, Notoryctemorphia, and Peramelemorphia), and they are of approximately the right size to belong to *Yalkaparidon*. We also identified two calcanea (QM F53640 and F53641) from the Riversleigh Upper Site that correspond to the astragali in terms of the size and morphology of the conarticular lower ankle joint facets, and that also show significant differences to those of all other known australidelphians (see "Tarsals Description").

Anatomical References and Terminology

The cranial description presented here draws heavily on the following works on metatherian and general mammalian anatomy: Archer (1976); Aplin (1987, 1990); Wible (1990, 2003); Evans (1993); Muirhead (1994, 2000); Marshall and Muizon (1995); Wroe (1997); Muizon (1998); Rougier et al. (1998); Wroe et al. (1998); Wible et al. (2001, 2004); Crosby (2002); Crosby and Norris (2003); Voss and Jansa (2003, 2009); Ladevèze (2004, 2007); Ladevèze and Muizon (2007, 2010); Forasiepi (2009). In an attempt to maintain consistency with other recent works, we have largely followed the anatomical terminology used in recent, detailed descriptions of mammalian osteology by Wible and co-workers (e.g., Wible 1990, 2003; Wible et al. 2001, 2004, 2005). However, in certain cases (e.g., for the palatal fenestrae and the paroccipital process) we have preferred the terminology of Voss and Jansa (2003, 2009); we have noted the cases where these two terminologies conflict.

Upper and lower incisors, canines, premolars, and molars are identified by upper and lower case initials respectively, i.e., "I, C, P, M" and "i, c, p, m." We refer to the maximum lower incisor formula for Metatheria as i1–4, rather than formally endorsing Hershkovitz's (1982, 1995) hypothesis that i1 has been lost in metatherians (in which case, the lower incisors represent i2–5). We follow Luckett (1993) in assuming that the plesiomorphic molar formula for Metatheria is M1–4 m1–4, and that P3 and p3 are the only dental loci to show replacement in metatherians. Although the first two premolar loci were argued by Luckett (1993) to represent unreplaced deciduous teeth, we refer to them here as P1–2 and p1–2 to maintain consistency with the majority of the metatherian literature (see also Voss and Jansa 2009: table 7; Aplin et al. 2010: 7). Thus, the plesiomorphic adult dental formula of Metatheria (with the possible exception of *Sinodelphys* – see Luo et al. 2003; Vullo et al. 2009) is considered here to be I1–5 C1 P1–3 M1–4 for the upper dentition and i1–4 c1 p1–3 m1–4 for the lower dentition, with replacement of dP3 and dp3 by P3 and p3, respectively. Terminology for molar morphology follows Kielan-Jaworowska et al. (2004: fig. 11.1).

It should be noted that in their original description of *Yalkaparidon*, Archer et al. (1988) followed Archer's (1978) alternative hypothesis regarding the dental formula of metatherians, which assumes that (1) adult metatherians have five upper and lower molars, and (2) that "M1" and "m1" (dP3 and dp3 according to Luckett 1993) are evicted by the erupting P3 and p3 respectively. Thus, all references to specific molar loci by Archer et al. (1988) are "one ahead" of those in this paper, i.e., "M2" of Archer et al. (1988) = M1 here, "M3" of Archer et al. (1988) = M2 here, and so on.

Interpretation and terminology of the tarsal specimens follows works by Szalay (1982, 1994), Marshall and Sigogneau-Russell (1995), Muizon (1998), Szalay and Sargis (2001, 2006), Argot (2002), Muizon and Argot (2003), Beck et al. (2008b), Forasiepi (2009), and Beck (2012). For the description of the tarsal specimens, "proximal" and "distal" are used rather than "anterior" and "posterior," and "ectal facet" is preferred over "(posterior) calcaneoastragalar facet," following Hooker (2001).

Taxonomy

We have followed the stem-based phylogenetic definition for Metatheria proposed by Sereno (2006: table 10.1), namely the most inclusive clade containing *Didelphis marsupialis* but not *Mus musculus*. We restrict Marsupialia to crown-group metatherians, following most recent studies (e.g., Rougier et al. 1998; Horovitz and Sánchez-Villagra 2003; Luo et al. 2003; Asher et al. 2004, 2007; Forasiepi 2009) but contra several others (e.g., Kielan-Jaworowska et al. 2004; Fox and Naylor 2006; Davis 2007; Beck et al. 2008a).

Sereno (2006: table 10.1) also provided a crown-based phylogenetic definition for Marsupialia, namely "the least inclusive clade containing *Didelphis marsupialis* and *Phalanger orientalis*." Implicit in this definition is the assumption that Didelphimorphia is the sister-group to all other extant marsupials. Whilst most recent studies have supported this position for Didelphimorphia (e.g., Amrine-Madsen et al. 2003; Horovitz and Sánchez-Villagra 2003; Asher et al. 2004; Nilsson et al. 2004; Beck et al. 2008b; Meredith et al. 2008; Horovitz et al. 2009), others have instead placed Paucituberculata (the caenolestid "rat" or "shrew" opossums) as the sister-group to all other extant marsupials, or cannot statistically distinguish between the two alternatives (Baker et al. 2004; Beck 2008; Meredith et al. 2009a, 2009b, 2011; Nilsson et al. 2010). Szalay and Sargis (2001, 2006) have also argued that Paucituberculata is the sister-group of the other extant marsupials based on tarsal morphology. This uncertain position of Paucituberculata means that Sereno's (2006) definition of Marsupialia may not refer to the entire crown-group. We therefore suggest the following modified phylogenetic definition for Marsupialia: the least inclusive clade containing *Didelphis marsupialis*, *Caenolestes fuliginosus*, and *Phalanger orientalis*.

Recent molecular sequence analyses typically support monophyly of extant Australian marsupials to the exclusion of the only extant South American australidelphian, the microbiotherian *Dromiciops*, particularly when apparent biases in base composition are corrected for (Amrine-Madsen et al. 2003; Phillips et al. 2006; Beck 2008; Meredith et al. 2008, 2011). Nilsson et al. (2010) also found four homoplasy-free retroposon insertions supporting monophyly of this Australian marsupial clade, which represents statistically significant support (p=0.0123; see Waddell et al. 2001). Archer (1984a) named this clade Eomarsupialia - Simpson (1970) had earlier suggested the name Eometatheria for the same clade, but Eometatheria is now usually recognized as referring to Australidelphia minus Peramelemorphia, following Kirsch et al. (1997; see e.g., Burk et al. 1999; Amrine-Madsen et al.

2003; Asher et al. 2004). The name Euaustralidelphia proposed by Nilsson et al. (2010) is a junior synonym (see Beck 2012). We propose the following crown-based phylogenetic definition for Eomarsupialia: the least inclusive clade containing *Phalanger orientalis*, *Perameles nasuta*, *Notoryctes typhlops*, and *Dasyurus maculatus*.

A clade comprising the extant Australian orders Dasyuromorphia, Peramelemorphia, and Notoryctemorphia is also consistently supported by molecular data (Amrine-Madsen et al. 2003; Phillips et al. 2006; Beck 2008; Meredith et al. 2008, 2009a, 2009b, 2011) and was recovered in the morphological and total evidence analyses of Beck et al. (2008b) and the molecular scaffold analyses of Beck (2012), but is currently unnamed. We propose the name Agreodontia (from the Ancient Greek *agreos* – "hunter," and *odous* – "tooth") for this clade, in reference to the faunivorous dental adaptations characteristic of many of its members, and to mirror the name of its sister-group, Diprotodontia. We propose the following stem-based phylogenetic definition for Agreodontia: the most inclusive clade including *Perameles nasuta*, *Notoryctes typhlops*, and *Dasyurus maculatus*, but excluding *Phalanger orientalis*.

Phylogenetic Analyses

The phylogenetic analyses presented here are based on the morphological matrix of Beck (2012), which is the most comprehensive currently available for investigating higher-level metatherian relationships, although taxon sampling is still somewhat limited (a much larger analysis currently in preparation should shed further light on the relationships of *Yalkaparidon* and other metatherians—Voss and Beck, in prep.). This morphological matrix has been modified from previous studies (Horovitz and Sánchez-Villagra 2003; Sánchez-Villagra et al. 2007; Beck et al. 2008b; Horovitz et al. 2008, 2009; Abello and Candela 2010). It has been further revised for this study by the addition of *Yalkaparidon*, and one new cranial character, namely presence or absence of a squamosal epitympanic sinus. Character scores for *Yalkaparidon* are based on personal observations of the specimens described in this paper. Scoring of the presence or absence of a squamosal epitympanic sinus is based on personal observations and on the relevant literature (Segall 1969; Archer 1976; Aplin 1987, 1990; Marshall and Muizon 1995; Wroe 1997; Muizon 1998; Wroe et al. 1998; Muirhead 2000; Voss and Jansa 2009). Additional character scores for *Dasyurus* and *Herpetotherium* have been taken from the unpublished thesis of Maga (2008: table 2.4). Scores for Peradectidae were modified based on observations on specimens of *Mimoperadectes labrus*, *M. houdei*, and *Peradectes elegans* (R. S. Voss pers. comm. to R.M.D. Beck) and on Williamson et al. (2012).

The final morphological matrix comprised 258 characters, of which 254 are parsimony-informative and 49 are ordered. These characters were scored for 38 taxa: 33 metatherian ingroup taxa (23 extant, ten fossil), and two fossil eutherians (*Asioryctes* and *Ukhaatherium*), one stem-therian (*Vincelestes*) and two extant monotremes (*Ornithorhynchus* and *Tachyglossus*) as outgroups. A full list of character scores and justifications for scoring decisions is given in the Electronic Supplementary Material. Two different versions of the matrix were prepared. In the first, *Yalkaparidon* was coded only for craniodental characters, and could be meaningfully scored (i.e., discounting characters scored as either missing or inapplicable) for 73 characters, rendering it 28.3 % complete. In the second, the isolated tarsals that we have tentatively referred to *Yalkaparidon*, together with craniodental specimens, were used to score characters; in this version, *Yalkaparidon* could be meaningfully scored for 105 characters, rendering it 40.7 % complete. Both versions of the morphology-only matrix are available for download from Morphobank (http://www.morphobank.org, Project 929) and from Dryad (http://www.datadryad.org; doi: 10.5061/dryad.25nt8).

For total evidence analyses, the morphological matrix was combined with nuclear sequence data from five nuclear protein-coding genes—namely APOB, BRCA1, IRBP, RAG1, and VWF—for the 23 extant marsupial terminals and two extant monotreme outgroups (*Ornithorhynchus* and *Tachyglossus*) present in the matrix. Alignments for these genes were taken from Meredith et al. (2011), with additional sequences downloaded from GenBank and added manually. The GenBank accession numbers of all sequences for each taxon are given in the Electronic Supplementary Material. Indels in the sequence data were coded using the "simple coding" method of Simmons and Ochoterena (2000), as implemented by the IndelCoder module of SeqState 1.4 (Müller 2005). Retroposon insertion characters for 12 of the extant marsupial terminals (*Didelphis*, *Monodelphis*, *Caenolestes*, *Dasyurus*, *Phascogale*, *Notoryctes*, *Perameles*, *Dromiciops*, *Trichosurus*, Pseudocheiridae, *Macropus*, and *Vombatus*) were taken from Nilsson et al. (2010). The final total evidence matrix comprised 9012 bp of molecular sequence data, 78 nuclear indel characters, 53 retroposon insertion characters, and 258 morphological characters. Both versions of the total evidence matrix (i.e., including or excluding character scores for the putative *Yalkaparidon* tarsals) are available for download from Dryad (http://www.datadryad.org; doi: 10.5061/dryad.25nt8).

The two versions of the morphology-only matrix (i.e., with the tarsals tentatively assigned to *Yalkaparidon* either excluded or included) were analyzed using maximum parsimony as implemented in PAUP*4.0b10 (Swofford 2002). Tree searches used the two-stage heuristic search strategy of Worthy et al. (2006). Polymorphic characters were treated as variable, and branches were collapsed if it were possible for them to have a length of zero. Support values were calculated using bootstrapping (2000 replicates, using default search settings; Felsenstein 1985), jackknifing with 25 % deletion of characters (2000 replicates, using default search settings), and the decay

index (using inverse constraint trees in combination with the same two-stage search strategy employed for the original tree search; Bremer 1988). Both versions of the morphology-only matrix were also analyzed by Bayesian inference, as implemented by MrBayes 3.2 (Ronquist et al. 2012). The Bayesian analyses used the Mk model (Lewis 2001), with the assumption that only parsimony informative characters were scored and with a gamma distribution to model rate heterogeneity between characters (see Ronquist et al. 2005). The MrBayes analysis of each version of the morphology-only matrix comprised two independent runs of four chains (three "heated," one "cold"), sampling trees every 500 generations. Each analysis was run for 5×10^6 generations, by which time convergence appeared to have been reached, given that the average standard deviation of split frequencies between the two runs was <0.01. The first 25 % of trees saved were discarded as burn-in; stationarity was reached among the post-burn-in trees in both analyses, as indicated by plots of log likelihood against generation number, and a minimum effective sample size (ESS) of >5000 and potential scale reduction factor (PSRF) of 1.00 for all parameters. The post-burn-in trees were summarized using 50 % majority rule consensus, with Bayesian posterior probabilities (BPPs) as support values.

Total evidence analyses of the combined morphological and molecular supermatrix were carried out using Bayesian inference, again as implemented in MrBayes 3.2. As for the morphology-only Bayesian analyses, the Mk model, assuming that only parsimony informative characters were scored and with a gamma distribution to model rate heterogeneity between characters, was applied to the morphological partition. The sequence data were initially partitioned by gene and codon position, resulting in 15 partitions (five genes, three codon positions for each gene). The program PartitionFinder v1.0.1 (Lanfear et al. 2012) was then used to identify the most appropriate partitioning scheme and models for the different partitions. PartitionFinder was run twice, firstly assuming branch lengths were linked between partitions and a second time assuming branch lengths were unlinked. For both analyses, the "greedy" heuristic search algorithm was used, only models implemented by MrBayes were tested, and the Bayesian Information Criterion (BIC) was used for model selection. For the analysis with linked branch lengths, the best partitioning scheme comprised eight partitions, with a BIC of 116485.82. For the analysis with unlinked branch lengths, the best partitioning scheme comprised three partitions, with a BIC of 117470.78. We have used the linked branch length partitioning sheme, based on its better (lower) BIC score. The nuclear indel and retroposon insertion characters was assigned separate restriction site (binary) models, in both cases with the assumption that only variable characters were coded, as recommended by Ronquist et al. (2005). In total, 11 separate partitions were modelled in the total evidence analyses: eight for the sequence data (based on the PartitionFinder output), one for the nuclear indels, one for the retroposon insertions, and one for the morphological data. Analyses of the two versions of the total evidence matrix (i.e., with and without information from the tarsals tentatively referred to *Yalkaparidon*) in MrBayes 3.2 each comprised four independent runs of four chains (three "heated," one "cold") each, running for a total of 10×10^6 generations and sampling trees every 2000 generations. The temperature of the heated chains was increased from the default value of 0.1 to 0.2. In both analyses, convergence between chains was indicated by an average standard deviation of split frequencies of 0.01–0.02. As for the morphology-only Bayesian analyses, the first 25 % of trees saved were discarded as burn-in; stationarity was reached among the post-burn-in trees, as indicated by plots of log likelihood against generation number, and a minimum ESS of >500 and PSRF of 1.00 for all parameters. The post-burn-in trees were summarized using 50 % majority rule consensus, with BPPs as support values, as in the morphology-only Bayesian analyses.

Evidence That the Cranium of QM F13008 Represents a Single Individual

The cranium of QM F13008 was recovered as two separate units following acid dissolution of a single block of limestone collected from Camel Sputum site (Riversleigh Faunal Zone B = early Miocene; Archer et al. 1988, 1989, 1997; Travouillon et al. 2006). Archer et al. (1988) stated that, although the left zygomatic process of the jugal of the rostral unit and the left zygomatic process of the squamosal of the braincase unit approach each other very closely, there is no actual point of contact. Although Archer et al. (1988) considered it highly unlikely, they acknowledged the possibility that the rostral and braincase units of the skull belong to different taxa. If so, the rostral unit, with the distinctive enlarged and open-rooted I1 and zalambdodont left M3 (the only postincisive tooth preserved), represents *Yalkaparidon*, whilst the braincase unit would represent another, potentially unknown taxon with a basicranium that appears to be highly plesiomorphic relative to most known Australian marsupials. However, several independent lines of evidence support Archer et al.'s (1988) preferred hypothesis that the two cranial units represent the same taxon and individual.

Firstly, there is no duplication of any element in QM F13008, the rostral and braincase units were found in close juxtaposition in single block of limestone, and the units are of compatible size. Archer et al. (1988) argued that, if the braincase unit was not referable to *Yalkaparidon*, it might represent a plesiomorphic peramelemorphian, based on unspecified basicranial features—they were presumably referring to the lack of squamosal epitympanic sinuses, which are also absent in the fossil peramelemorphian *Yarala burchfieldi* and in extant peroryctine and echymiperine peramelemorphians. However,

absence of squamosal epitympanic sinuses is a marsupial plesiomorphy and hence does not support peramelemorphian affinities per se. Furthermore, the cranium of QM F13008 differs from those of all known peramelemorphians in at least two features—lack of inflation of the epitympanic recess and retention of a large interparietal.

The braincase unit of QM F13008 also lacks modifications of the auditory region that might convincingly link it with another australidelphian order, such as (1) fusion of the rostral and caudal tympanic processes of the petrosal into a "petrosal plate" (seen in modern dasyurids, *Dromiciops*, *Notoryctes*, *Tarsipes*, and acrobatids; Aplin 1990; Wroe 1999; Sánchez-Villagra and Wible 2002; Ladevèze 2004, 2007; Ladevèze et al. 2008), (2) presence of a complete stylomastoid foramen (seen in modern dasyurids, *Dromiciops*, *Notoryctes*, and some diprotodontians; Aplin 1990; Wroe 1999; Sánchez-Villagra and Wible 2002; Ladevèze 2004, 2007; Ladevèze et al. 2008), (3) ventral enclosure of the post-promontorial tympanic sinus by the caudal tympanic process of the petrosal (present in dasyurids, *Dromiciops*, *Notoryctes*, some diprotodontians, and some peramelemorphians; Aplin and Archer 1987; Aplin 1990; Wroe 1999; Sánchez-Villagra and Wible 2002; Ladevèze 2004, 2007; Ladevèze et al. 2008), (4) a squamosal tympanic process (present in most vombatimorphian diprotodontians; Aplin 1987; Murray et al. 1987; Aplin 1990), or (5) a greatly inflated hypotympanic sinus and ventrally directed promontorium of the petrosal (present in *Phascolarctos*; Aplin 1987, 1990).

Further compelling evidence that the two units are from a single individual is found in the extremely weak postglenoid process and wide, almost planar glenoid fossa of the braincase unit (Figs. 6, 7 and 8). These are adaptations commonly seen in mammals with enlarged incisors used for gnawing. Furthermore, the very posterior position and robust nature of the entopterygoid crests (which may be connected with the position of the transverse foramen posterior to the carotid foramen; Figs. 6, 7 and 8: **enpc**) also finds parallels in other taxa that use their enlarged incisors for woodgouging (e.g., *Dactylopsila* and *Daubentonia*; Cartmill 1974; Beck 2009), and may be an adaptation to resist stresses generated by dorsal bending of the rostrum (see Beck 2009). Thus, the presence of enlarged incisors in the rostral unit and associated mandible of QM F13008 would be predicted from the morphology of the braincase unit, and represents strong evidence that they represent a single taxon.

Finally, close examination of the zygomatic arch of QM F13008 suggests that the jugal and squamosal probably overlap by approximately 2 mm. The relative widths of the facet for squamosal on the dorsal face of the jugal and of the facet for the jugal on the ventral face of the squamosal are congruent with this interpretation (Figs. 1 and 2: **area of overlap**). In conclusion, we argue that there is compelling evidence in favor of Archer et al.'s (1988) preferred hypothesis that the rostral and braincase units of QM F13008 represent a single taxon.

Skull Description

Cranium as a Whole

The maximum anteroposterior length of the cranium of QM F13008 is 48 mm (Figs. 1 and 2). However, this is probably a slight overestimate, as: (1) we believe that the preserved jugal and squamosal parts of the left zygomatic arch of QM F13008 should overlap by approximately 2 mm (Figs. 1a, c and 2: **area of overlap**); (2) Beck (2009) suggested that the intact cranium may have been somewhat klinorhynch, based on the orientation of the cribriform plate (although the precise degree of klinorhynchy cannot be determined in QM F13008 due to the severe damage to the posterior part of the rostrum and the rostral part of the basicranium). The overall proportions of the cranium of QM F13008 approximate those of other similarly-sized generalized metatherians, such as didelphids and dasyurids. However, the rostrum is relatively short and tall (Fig. 1) and the infratemporal fossa is very large (Figs. 1c and 2) – Beck (2009) interpreted these and several other craniodental features as evidence that *Yalkaparidon* was probably a "mammalian woodpecker" similar to the strepsirhine primate *Daubentonia madagascariensis*, the petaurid marsupials *Dactylopsila* spp., and the Palaeogene eutherian apatemyids. In lateral view (Fig. 1a), the zygomatic arch (only 2 mm deep at the deepest point preserved in QM F13008) appears more delicate than those of most metatherians; in this respect, *Yalkaparidon* resembles caenolestids and many peramelemorphians. Neither the frontal process of the jugal nor the postorbital process of the frontal that would indicate the points of attachment of the postorbital ligament are identifiable. However, the broad and gently concave curve of the infraorbital margin of the jugal suggests that the orbit of *Yalkaparidon* was large and faced somewhat more dorsally than in most metatherians (Fig. 1a, b; see Beck 2009).

Nasal

Only a small rectangular strip representing the posterior part of the right nasal is preserved in QM F13008 (Figs. 1a, c and 3a: **na**). It is unclear whether the lateral margin of this remnant is intact, or whether the nasal was in fact laterally more extensive when complete. Its external surface is slightly convex when viewed laterally (Fig. 1a), but this appears to be the result of post-mortem damage. In dorsal view, the suture between the paired nasals and frontals appears to have been weakly W-shaped, with the base of the W pointing posteriorly (Fig. 1c; see Beck 2009). The naso-frontal suture is approximately level with the alveolus for M4 in the reconstructed skull (Fig. 1a); however, if, as we believe, the preserved parts of the jugal and squamosal overlapped by approximately 2 mm (Figs. 1a, c and 2: **area of overlap**), then the naso-

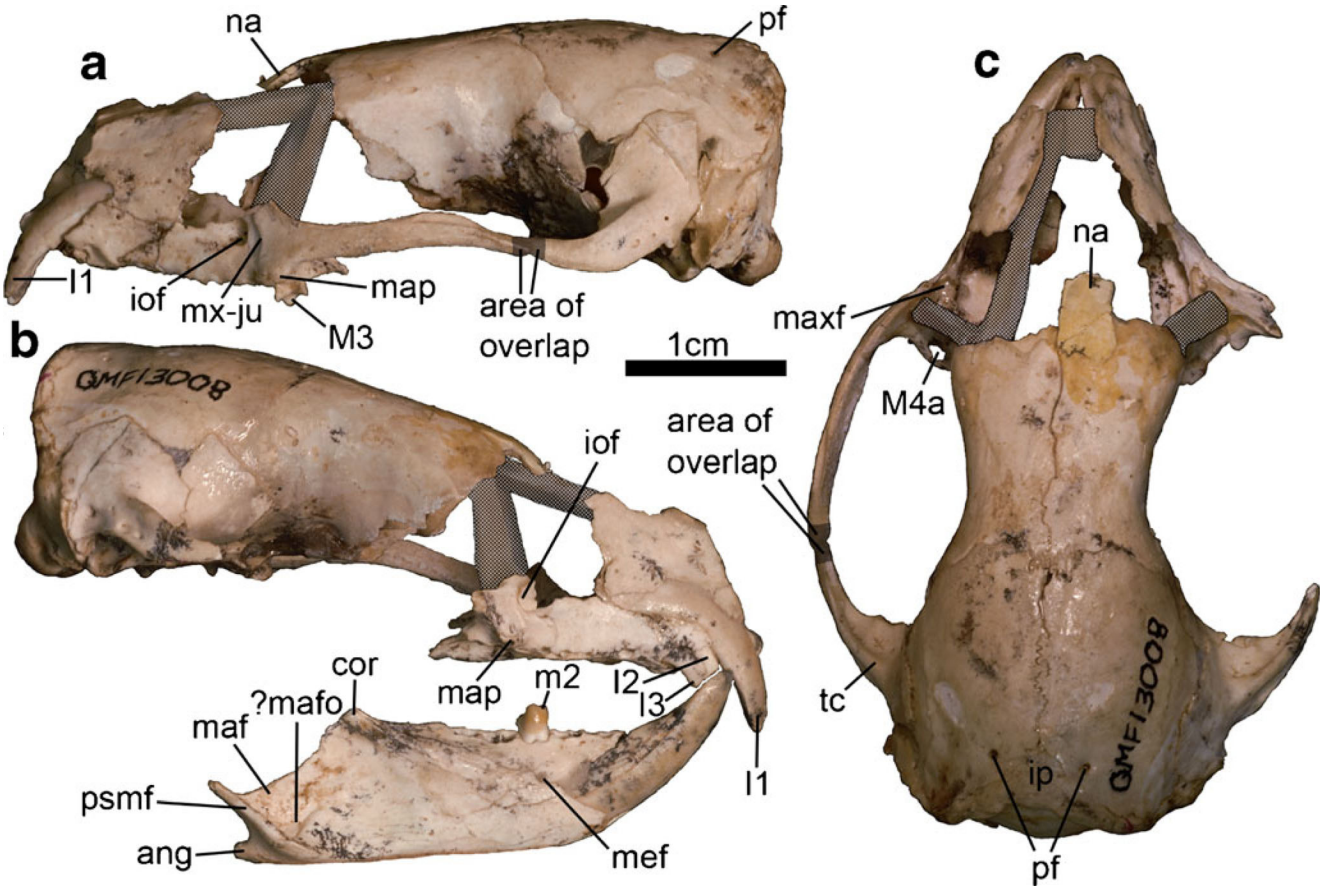

Fig. 1 Cranium of *Yalkaparidon coheni* (QM F13008 - holotype). Hatched areas are not part of the specimen. **a** left lateral view. **b** right lateral view, with associated right mandible in approximate articulation. **c** dorsal view. Abbreviations: **ang** = angular process; **cor** = coronoid process; **iof** = infraorbital foramen; **ip** = interparietal; **M4a** = fourth upper molar alveolus; **maf** = masseteric fossa; **?mafo** = ?masseteric foramen; **map** = masseteric process; **maxf** = maxillary foramen; **mx-ju** = maxilla-jugal suture; **na** = nasal; **pf** = parietal foramen; **psmf** = posterior shelf of the masseteric fossa; **tc** = temporal crest; **vc** = vascular canal

frontal suture would be located slightly more anteriorly, approximately level with the septum between M2 and M3.

Because the right nasal is broken anteriorly (and possibly also laterally) and the left nasal is entirely missing, the precise shape and extent of the intact bones cannot be ascertained. For the same reason, the exact sutural relationships between the nasals and the other elements of the rostrum (the premaxillae, maxillae, and lacrimals) are unknown. However, the facial process of the left premaxilla appears to be largely intact in QM F13008 and its dorsal border (which would have contacted the anterolateral border of the nasal) is angled slightly posterolaterally to anteromedially (Fig. 1c); this suggests that the nasals broadened posteriorly, as in most other metatherians (Archer 1984b; Horovitz and Sánchez-Villagra 2003).

Premaxilla

Following Wible (2003), the paired premaxillae can be considered as each comprising a roughly vertical facial process that forms the sidewalls of the anterior part of the rostrum, a horizontal palatal process that floors the anterior part of the hard palate, and an alveolar process that houses the three upper incisors. In QM F13008, the left and right premaxillae are relatively well preserved, although both show damage to the lateral wall of the facial process, exposing parts of the roots of both the left and right I1 (Fig. 1a, b). The medial part of the palatal process is also damaged in QM F13008, and hence the septum that separates the left and right incisive foramina (the "medial palatine process of the premaxilla" sensu Wible 2003) is missing (Fig. 2). Four isolated premaxillary fragments (QM F39999, F52942, F52943, and F52953) are also known. Of these, QM F52942 (comprising a partial right premaxilla with a largely complete facial process, as well as the anterior part of the right maxilla) is the best preserved and forms the basis of the description of the premaxilla given here (Fig. 4).

In lateral view (Fig. 4a), the facial process of the premaxilla is tall (8.8 mm tall at its tallest point in QM F52942, which may not be complete posterodorsally) and is gently convex dorsoventrally. The facial process is roughly rectangular in

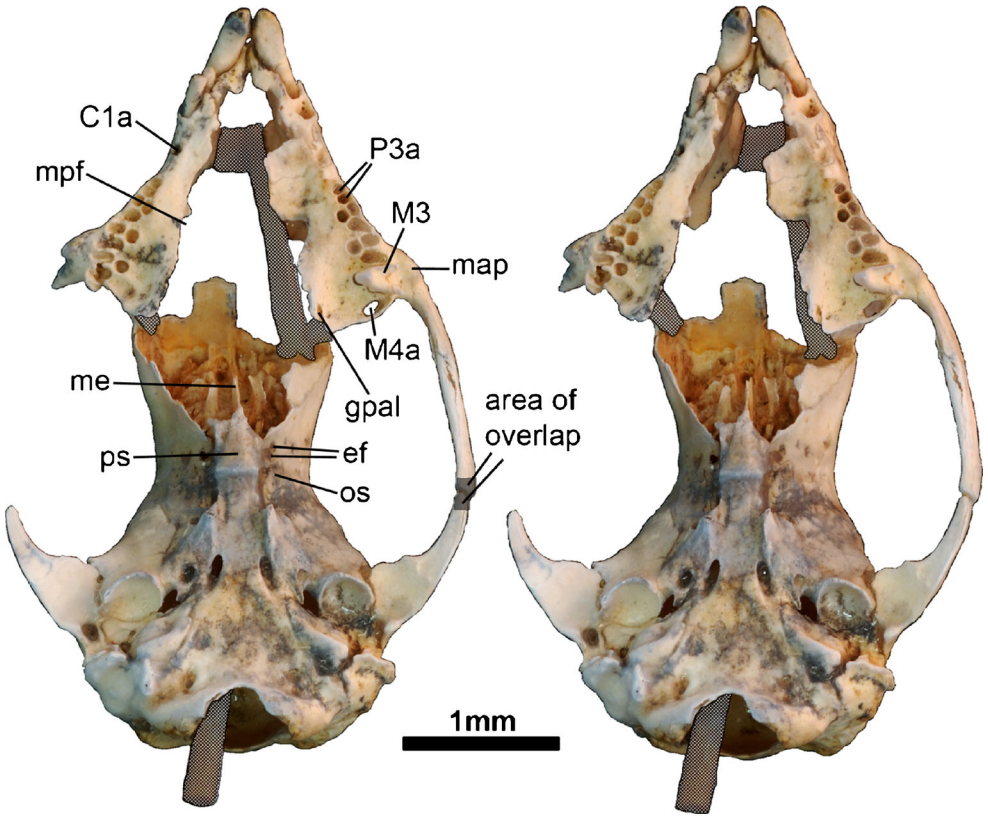

Fig. 2 Cranium of *Yalkaparidon coheni* (QM F13008 – holotype) in stereo-ventral view. Hatched areas are not part of the specimen. Abbreviations: **C1a** = upper canine alveolus; **ef** = ethmoidal foramina (separate foramina for the ethmoidal artery and nerve are present on the left side); **gpal** = groove for the palatine; **M4a** = fourth upper molar alveolus; **map** = masseteric process; **me** = mesethmoid; **mpf** = maxillopalatine fenestra; **os** = orbitosphenoid; **P3a** = third upper premolar alveolus; **ps** = presphenoid

outline, but it is overlapped posteroventrally by a fingerlike anteroventral extension of the facial process of the maxilla (this extension is damaged on both sides of QM F13008 but it is intact in QM F52942; Fig. 4a: **fmx**). Beck (2009) suggested that this extension of the maxilla may help buttress the rostrum against bending forces generated by woodgouging. The dorsal half of the anterior border of the facial process of the premaxilla, which forms the lateral rim of the external nasal aperture (Fig. 4a: **ena**), is gently concave; a second, slightly smaller concavity ventral to this is the lateral rim of the alveolus for I1. The I1 alveolus faces anteriorly. The root of I1 extends posteriorly within the facial process of the premaxilla, producing a distinct bulge in the lateral wall of the rostrum. The root then continues posteriorly within the maxilla, the facial process of which overlaps the premaxilla medially inside the nasal cavity (visible in QM F52942). The dorsal border of the facial process of the premaxilla, which would have contacted the nasal in life, slopes slightly posterodorsally to anteroventrally. There is no distinct posterodorsal process (sensu Wible 2003; where present, this process extends posteriorly between the nasal and maxilla) identifiable in either QM F13008 or F52942, but it may have broken off both specimens postmortem. Multiple small foramina (presumably nutrient foramina) are visible in the lateral surface of the facial process of the premaxilla, which Beck (2009) interpreted as suggesting the presence of well-developed sensory vibrissae.

The suture between the facial process of the premaxilla and the maxilla comprises three sections (Fig. 4a: **pm-mx**): (1) rostroventrally, a short, curved section (1.5 mm tall in QM F52942) just posterodorsal to the I3 alveolus and mirroring the curved rim of this alveolus; (2) a roughly horizontal section (4.1 mm long in QM F52942) that extends posteriorly below the bulge caused by the root of I1, to a point level with the posterior rim of the C1 alveolus; (3) lastly, a roughly vertical section that extends dorsally and slightly posteriorly along the entire posterior border of the premaxilla, and which presumably would have terminated at the nasal. A paracanine fossa is not present, which is unsurprising given that the lower canine is either absent or greatly reduced (see the "Lower Dentition" section of "Dental Description").

In ventral view (Fig. 4b), three alveoli for I1–3 are visible, arranged along the rostrolateral border of the premaxilla. The upper incisor arcade as a whole forms a broad v- or u-shape (Figs. 2 and 4b). The alveolus for I1, at the anterior end of the premaxilla, faces anteriorly and is considerably larger than those for I2–3. The alveolus for I2, immediately posterior and

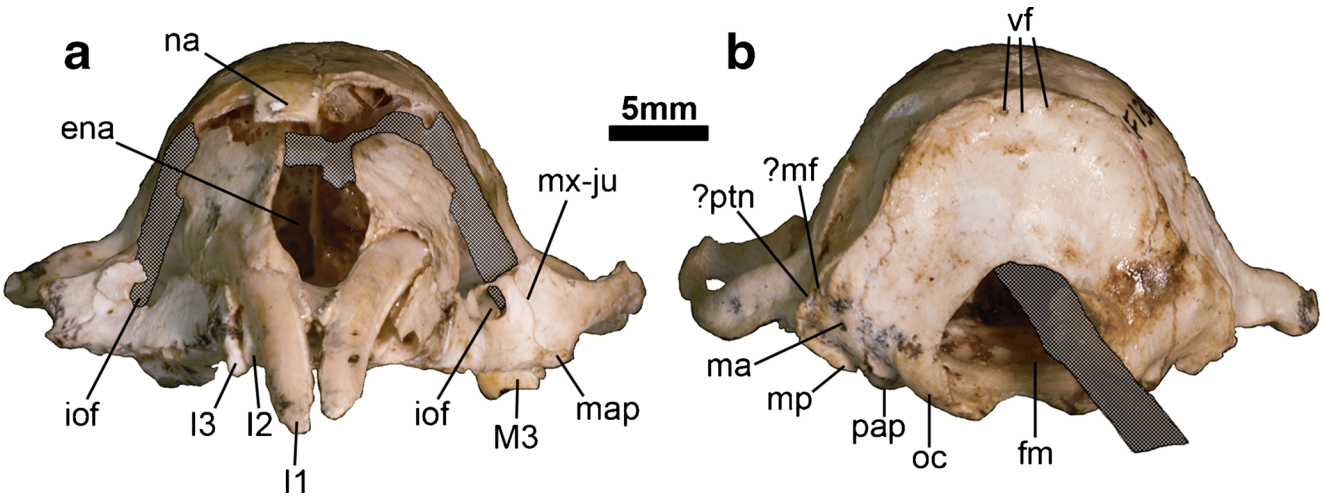

Fig. 3 Cranium of *Yalkaparidon coheni* (QM F13008 - holotype). Hatched areas are not part of the specimen. **a** rostral view. **b** occipital view. Abbreviations: **ena** = external nasal aperture; **fm** = foramen magnum; **iof** = infraorbital foramen; **ma** = mastoid exposure of the petrosal; **map** = masseteric process; **?mf** = ?mastoid foramen; **mp** = mastoid process; **mx-ju** = maxilla-jugal suture; **na** = nasal; **oc** = occipital condyle; **pap** = paroccipital process; **?ptn** = ?posttemporal notch

slightly lateral to the I1 alveolus, is much smaller and faces anteroventrally. The alveoli for I1 and I2 do not appear to have been separated by a bony septum. The I3 alveolus, immediately posterior and slightly lateral to the I2 alveolus, is slightly larger than that for I2 and also faces anteroventrally. A bony septum separates the alveoli for I2 and I3. The rostral tip of the premaxilla (preserved on the left side of QM F13008 and in QM F52942) does not extend much beyond the anterior border of I1. Distortion of the right side of QM F13008 means that the left and right premaxillae are no longer in contact between I1 and I2 (Fig. 2). The medial parts of the palatal processes of the premaxillae and maxillae are missing in both QM F13008 (Fig. 2a) and QM F52942 (Fig. 4b); however, the lateral rim of the incisive foramen (which presumably transmitted the nasopalatine duct and branches of the greater palatine artery and nasopalatine nerve; Evans 1993; Sánchez-Villagra 2001; Wible 2003; Forasiepi 2009) is identifiable medial to I2 and I3 (Fig. 4b: **inf**). The incisive foramen appears to have been quite short (extending for approximately 2 mm from level with the anterior border of the I2 alveolus to level with the middle of the I3 alveolus) and narrow (approximately 0.7 mm wide at its widest point). A short, narrow, fingerlike projection of premaxilla, bordered laterally by the rostral extension of the facial process of the maxilla and medially by the palatal process of the maxilla, extends posteriorly for 1.5 mm from behind the I3 alveolus towards the canine alveolus in the maxilla; it is most obvious on the left side of QM F13008 (Fig. 2).

Maxilla

Following Wible (2003), the facial process of each of the paired maxillae forms the sidewall of the posterior part of the rostrum,

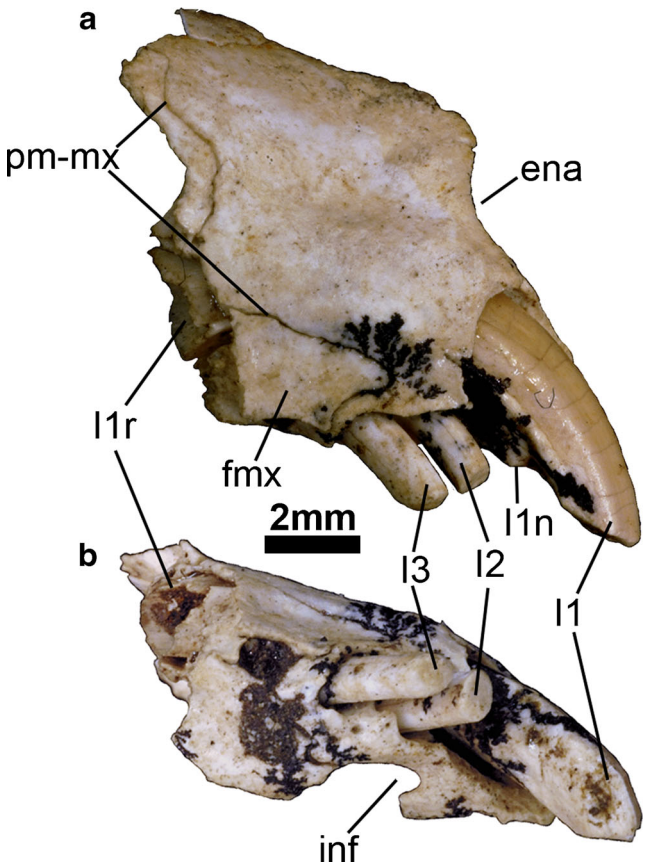

Fig. 4 Isolated partial right premaxilla and maxilla of *Yalkaparidon* sp. indet. (QM F52942). **a** lateral view. **b** ventral view. Abbreviations: **ena** = external nasal aperture; **fmx** = facial process of the maxilla; **I1n** = notch on the distal surface of the first upper incisor for contact with the tip of the first lower incisor; **I1r** = open root of the first upper incisor; **inf** = incisive foramen; **pm-mx** = premaxilla-maxilla suture

whilst the palatal process forms most of the floor of the hard palate. The maxillae also house the maxillary dentition (which in *Yalkaparidon* comprises C1, P3, and M1–4) and contribute to the anterior floor of the orbit. Only the ventral part of the facial process (up to the level of the infraorbital foramen) and the lateral part of the palatal process (including the region that floors the orbit) of both the left and right maxilla are preserved in QM F13008 (Fig. 1a, b). Isolated partial maxillae (QM F13011, F36546, F36547, F39986, F52753, F52754, F52755, F52756, and F52956) are also known, but these also preserve only the ventral part of the facial process and the lateral part of the palatal process. Both maxillae of QM F13008 are damaged posteriorly and both palatine bones are entirely missing (Fig. 2). As a result, the size and number of the palatal fenestrae, the morphology of the posterior palatal margin, and the position and morphology of the posterolateral palatal foramen sensu Voss and Jansa (2003; = "minor palatal foramen" sensu Wible 2003) are all uncertain.

As noted above, in lateral view the rostroventral part of the facial process of the maxilla overlaps the premaxilla almost as far as the alveolus for I3, and its rostral end is curved, mirroring the curve of the rim of the I3 alveolus (Fig. 4b: **fmx**). The remainder of the suture between the premaxilla and maxilla extends posteriorly from a point dorsal to I3 to a point above the alveolus for C1, and then continues dorsally along the posterior border of the premaxilla. The infraorbital foramen is entirely within the maxilla and is roughly level with the anterior part of M2 and posterior part of M1 (Fig. 1a, b and 3a: **iof**). The opening for the incisivomaxillary canal (which transmitted nerves and blood vessels to the anterior dentition; Evans 1993) is visible in the ventromedial wall of the infraorbital foramen of QM F13008, close to its anterior margin. There is a small foramen anterior to the ventral rim of the infraorbital foramen on the left side of QM F13008, while on the right side a similar foramen is present posterior to the ventral rim of the infraorbital foramen, just anterior to maxilla-jugal suture. There are further tiny foramina scattered across the surface of the facial process of the maxilla. Breakage of the facial process dorsal to the infraorbital foramen in QM F13008 and in all other maxillary specimens of *Yalkaparidon* means that the precise contribution of the maxilla to the lateral wall of the rostrum is uncertain, as are its relationships with the nasal, lacrimal, and frontal bones.

Posterior to the infraorbital foramen and above M2, the maxilla contacts the jugal along a shallowly v-shaped suture (Figs. 1a and 3a: **mx-ju**). The region of the maxilla between the "legs" of the jugal is the point of origin for the zygomaticus and levator labii muscles; it is marked by a very slight depression, in contrast to the sizeable nasolabial fossa seen in many peramelemorphians (Muirhead 2000). The dorsal extent of the maxilla-jugal suture cannot be assessed because both bones are broken dorsal to the infraorbital foramen. The maxilla extends ventral to the inferior leg of the jugal and forms a small, low masseteric process, level with the posterior root of M2 and anterior root of M3 (Figs. 1a, 2 and 3a: **map**). The masseteric process is the point of attachment of the superficial masseter; in *Yalkaparidon*, this process protrudes only very slightly below the level of the dental alveoli.

In ventral view, a small alveolus for the single-rooted upper canine is visible at the anterolateral end of the maxilla (Figs. 2 and 5: **C1a**), separated from the I3 alveolus in the premaxilla by a 2 mm long diastema. The anterior border of the canine alveolus is closely approached by a narrow, fingerlike posterior extension of the premaxilla, but this process does not actually contribute to the rim of the alveolus; thus, the upper canine is housed entirely within the maxilla. There are two vascular foramina between C1 and P3 in QM F52756 (Fig. 5b: **vf**). Posterior to the canine alveolus, and separated from it by a 2 mm long diastema (within which there is a small foramen), QM F13008 preserves two alveoli that are arranged anteroposteriorly; these would have housed a double-rooted P3 (Fig. 2: **P3a**). Whilst P3 was double-rooted in QM F13008, it appears to have been single-rooted in QM F52754 and F52755 (which may be from the same individual) and QM F36546. P3 is preserved in situ in QM F52756 (Fig. 5), where it is clearly double-rooted, and in QM F13011, where it may be single-rooted (see "Species-Level Taxonomy"). No specimens show any sign of alveoli between C1 and P3, indicating that *Yalkaparidon* has only a single upper premolar (contra Archer et al. 1988, who incorrectly stated that three upper premolars were present).

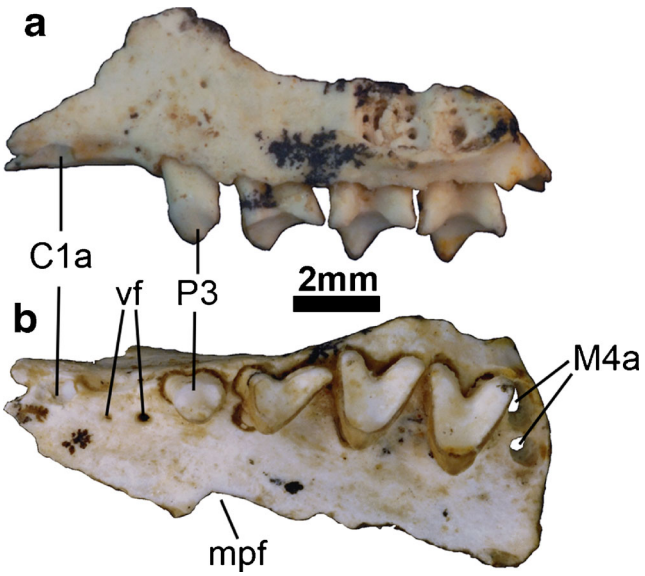

Fig. 5 Isolated partial left maxilla of *Yalkaparidon* sp. indet. preserving P3 M1-3 (QM F52756). **a** ventral view. **b** lateral view. Abbreviations: **C1a** = upper canine alveolus; **M4a** = fourth upper molar alveoli; **mpf** = maxillopalatine fenestra; **vf** = vascular foramina

Immediately posterior to P3, there are three sets of three alveoli for M1–3 (Figs. 2 and 5); each set of three alveoli is arranged in a triangular pattern, with the base facing laterally and the apex pointing medially and slightly anteriorly. The alveoli for M2 are distinctly larger than those for M1, but similar in size to those for M3. Multiple small foramina are present in the palatal process of the maxilla immediately lateral to and between the molar alveoli. Lateral to the alveolar septum between M2 and M3 and to the anterior root of M2, the small masseteric process of the maxilla is visible (Figs. 1a, b, 2 and 3: **map**). A small foramen is present posteromedial to the masseteric process and lateral to M3 on both left and right sides of QM F13008. The lateral rim of the maxillopalatine fenestra (sensu Voss and Jansa 2003; the "major palatine foramen" sensu Wible 2003), which would have transmitted the major palatine artery and nerve, is identifiable in a number of specimens. In QM F36546, its rostral end is level with the septum between P3 and M1, whereas in the QM F13008 it is slightly more anterior, level with posterior root of P3 (Fig. 2: **mpf**). The posterior extent of the maxillopalatine fenestra is uncertain because the palatine, which would form its posteromedial margin, is entirely missing in all known specimens. We therefore disagree with Archer et al.'s (1988) original assertion that the maxillopalatine fenestra (the "maxillary palatal vacuity" sensu Archer et al. 1988) can be described as "very small" based on available specimens.

On the left side of QM F13008, there is a relatively large opening in the maxilla immediately posterior to M3 (Fig. 2: **M4a**; only the lateralmost part of the rim of this opening is preserved on the right side). This opening extends through the bone such that it is visible in dorsal view (Fig. 1c: **M4a**), within the roughly triangular maxillary contribution to the orbital floor. Similar ventral openings are present in all the isolated maxillae in which this region is intact (QM F13011, F36546, F39986, F52753, F52756, and F52956; Fig. 5b: **M4a**). The rim of this opening is slightly raised, and its lateral border slopes ventrolaterally, as in the posterolateral alveolus of M1–3. We suggest here that the opening is an alveolus for M4 and that the thin bone roofing the alveolus has been damaged so that the alveolus is now open dorsally. By contrast, Archer et al. (1988) suggested that this opening is the posterolateral palatal foramen (which transmits the minor palatine artery and nerve; Wible 2003), stating that *Yalkaparidon* has only three upper molars and describing it as having a "very large posterolateral palatal foramen." Archer et al.'s (1988) interpretation appears erroneous because, in all other metatherians that we have examined or for which illustrations are available, the posterolateral palatal foramen: (1) lies on the maxillopalatine suture; (2) faces at least partly anteriorly (allowing the minor palatine artery that passes through the foramen to extend rostrally along the palate); and (3) is medial to, and well-separated from, the last upper molar. By contrast, the opening in *Yalkaparidon*: (1) is entirely within the maxilla; (2) faces directly ventrally; and (3) is immediately posterior to M3 (Figs. 1c, 2 and 5b: **M4a**). It therefore seems more likely that this opening housed M4 rather than transmitted the minor palatine artery and nerve. Furthermore, in QM F52755 and F52756 (Fig. 5b: **M4a**), this region is largely roofed by bone, confirming that the dorsally open condition in QM F13008 is probably the result of damage. In QM F13008 (Figs. 1c and 2: **M4a**) and F36546, there is no evidence of a septum that might have divided the M4 alveolus, and the alveolus as a whole is roughly similar in dimensions to the posterolateral alveolus of M2 and M3; M4 may have been single-rooted in these specimens. In QM F52753, F52755, F52756 (Fig. 5b: **M4a**), and F52956, however, a transverse dividing septum is present, suggesting that M4 was double-rooted in these specimens.

A 1.5 mm groove in the posteromedial corner of the preserved part of the left maxilla of QM F13008 may have housed a process of the palatine (Fig. 2: **gpal**). A small foramen immediately lateral to this groove has an exit on the nasal surface of the maxilla; its likely contents are unclear, but may have been a small branch of the minor palatine artery and/or nerve. This foramen is probably not an accessory palatine foramen sensu Wible (2003) because it lies within the maxilla rather than within the palatine. Neither QM F13008 nor any of the isolated maxillary fragments preserve any portion of the posterolateral palatal foramen, so it is unclear whether this foramen was complete or whether it was an incomplete notch (as it is in most dasyurids; Archer 1984a; Wroe 1997).

In dorsal view, the maxillary foramen (the posterior opening of the infraorbital foramen) is visible on the left side of QM F13008 within the maxilla, medial to the maxilla-jugal suture (Fig. 1c: **maxf**). The maxilla makes only a very narrow (0.25 mm at its narrowest point) contribution to the dorsal roof of the maxillary foramen. This may be the result of damage, but more likely indicates that the lacrimal (which is missing in all specimens of *Yalkaparidon*) also roofed this foramen, as it does in most other metatherians. Extending posteromedially from the medial margin of the maxillary foramen, a low ridge indicates the point of contact with the palatine. The contribution of the maxilla to the floor of the orbit is small and triangular, delimited by this ridge anteromedially, the jugal anterolaterally, and the posterior margin of the maxilla posteriorly. The dorsally open M4 alveolus of QM F13008 (Fig. 1c: **M4a**) is visible within this region, close to the posterior margin of the maxilla. Isolated maxillae (e.g., QM F52755 and F52756) preserve the same overall morphology.

Lacrimal

Both lacrimals are missing in QM F13008, and are not preserved in any other known *Yalkaparidon* specimen.

Palatine

Both palatines are missing in QM F13008 and are not preserved in any other known *Yalkaparidon* specimen.

Jugal

In lateral view, the maxilla-jugal suture, posterior to the infraorbital foramen, is weakly v-shaped (Figs. 1a and 3: **mx-ju**). At its anterior end, the jugal bifurcates into a very short inferior process (1.8 mm in length), which terminates dorsal to the masseteric process of the maxilla, and a superior process, which forms the ventrolateral border of the orbit (Fig. 1a). The preserved part of the superior process of the jugal is 2.0 mm long, but its full extent when intact is uncertain because it is broken dorsally. The superior and inferior processes meet at an angle of about 150°. Posterior to the maxilla-jugal suture, the zygomatic process of the jugal is shallow, approximately 2 mm deep at its deepest point (Fig. 1a). As a result, the zygomatic arch of *Yalkaparidon* appears delicate relative to the overall dimensions of the skull. There is no frontal process on the dorsal surface of the jugal that would indicate the point of attachment of the postorbital ligament.

A facet for contact with the zygomatic process of the squamosal is visible on the superior aspect of the lateral face of the zygomatic process of the jugal, about two-thirds along its preserved length (Fig. 1a). The shape of the facet indicates that the jugal-squamosal suture was roughly v-shaped, with the base of the v facing anteriorly and the jugal forming a superior and an inferior process. The superior process is very short (approximately 1.2 mm long). Although broken posteriorly, the inferior process is much longer, forming the posteriormost preserved part of the jugal in QM F13008 and contacting the anteriormost preserved part of the squamosal (Fig. 1a). When intact, the inferior process of the jugal would have extended as far as the glenoid fossa, based on the shape of the facet for the jugal on the ventral surface of the squamosal (Fig. 2).

In ventral view, the root of the zygomatic process of the jugal is gently curved, but the process is almost straight more posteriorly (Fig. 2). The zygomatic arch as a whole appears to be longer than in most other metatherians because the root of the zygomatic process of the jugal is located more anteriorly, a feature that may reflect the functional demands of woodgouging (see Cartmill 1974; Beck 2009). As discussed in further detail below (see "Evidence that the Cranium of QM F13008 Represents a Single Individual"), it seems likely that in QM F13008 the preserved part of the zygomatic process of the left jugal underlapped the anteriormost part of the preserved section of the zygomatic process of the squamosal by approximately 2 mm (Figs. 1a, c and 2: **area of overlap**); thus, there does appear to be a small point of contact between the rostral and braincase sections of QM F13008, contra Archer et al. (1988). The facet for the jugal on the ventral surface of the zygomatic process of squamosal (Fig. 2) indicates that the intact jugal extended as far as glenoid fossa, but gives no indication as to the morphology of the preglenoid process of the jugal. However, given the almost planar glenoid fossa and extremely weak, vestigial postglenoid process of the squamosal (both of which imply extensive palinal movement of the mandible; Fig. 8), it is likely that the preglenoid process of the jugal would also have been poorly developed.

Frontals

The paired frontals form the region of the skull roof between the nasals and parietals, the medial wall of the orbital fossa and the anteromedial wall of the temporal fossa. They appear to be largely intact in QM F13008, apart from damage to their anterior and anteroventral margins (Fig. 1).

In dorsal view (Fig. 1c), there is no identifiable postorbital process at any point along the lateral border of either frontal. The postorbital constriction of the lateral margin of the frontals is quite weak relative to most other metatherians, and the frontals are quite broad anterior to this constriction, suggesting the presence of enlarged olfactory lobes and frontal cortex (confirmed by CT scans of QM F13008; Beck 2009). The suture between the paired frontals extends along the midline for approximately 12 mm; it is gently sinuous in its anterior half but becomes slightly more complex posteriorly (Fig. 1c). Although only the posteromedial part of the right nasal is preserved, the suture between the paired nasals and frontals appears to have been W-shaped (Fig. 1c; see Beck 2009). Caudally, the frontals are overlapped by the parietals, the suture forming a very weak, broad W-shape with the base of the W facing anteriorly (Fig. 1c). The frontal-parietal suture is tightly interdigitated dorsally, close to the midline (this suture has been slightly pulled apart in QM F13008), but much straighter ventrolaterally (Fig. 1c). Extremely weak paired temporal crests are just visible on the frontals, extending posteromedially from the anterolateral corner of each frontal and continuing onto the parietals. Slightly rugose areas immediately lateral to each temporal crest and close to the suture with the parietal may represent areas of attachment of the temporalis muscles.

In lateral view, the lacrimal and palatine are missing from both sides of QM F13008, as are the bones forming the primary palate, and the region of the maxilla posterior to M4 is not preserved; hence the relationships between these bones and the frontals are uncertain. Dorsally, a foramen for the frontal diploic vein is visible on the left frontal of QM F13008, about 6 mm from its anterior margin (Fig. 6: **fdv**); a second apparent opening 1.7 mm anterodorsal to this is probably artefactual. On the right side there are several (probably three) much smaller foramina in roughly the equivalent position (Fig. 7: **fdv**), although this region is somewhat obscured

by adhesive. Ventrally, the ventralmost preserved part of each frontal closely approaches the preserved part of the presphenoid (Fig. 2), although it is unclear if these bones would have been in contact in life. Posterodorsal to this region, the frontal contacts the orbitosphenoid (Fig. 7). Within the frontal-orbitosphenoid suture, immediately adjacent to the anterodorsal corner of the orbitosphenoid, is the ethmoidal foramen. On the left side of QM F13008, the ethmoidal foramen is divided by a narrow septum into a relatively large foramen on the frontal-orbitosphenoid suture and a smaller foramen anterodorsal to this that lies entirely within the frontal (Figs. 2 and 6: **ef**); presumably, one foramen transmitted the external ethmoidal nerve whilst the other transmitted the ethmoidal artery (see Evans 1993; Giannini et al. 2006). On the right side of QM F13008, the ethmoidal foramen is visible as a single opening (Fig. 7: **ef**), although remnants of a bony septum that may have originally divided this foramen into two separate openings are identifiable around its rim. Dorsal to the orbitosphenoid, the frontal forms a long, relatively straight suture (Fig. 7), first with the alisphenoid (for approximately 8 mm) and then with the parietal (for approximately 8 mm).

In anteroventral view, breakage of the frontals and the loss of bones of the primary and secondary plate have exposed the cribriform plate (which is angled at about 50° to vertical) and the posterior parts of the nasal turbinates (Fig. 2). The bony part of the nasal septum (the mesethmoid, following Rowe et al. 2005) is visible extending dorsoventrally along the midline of the cribriform plate (Fig. 2: **me**). Paired frontal sinuses are present on either side of the dorsal end of the nasal septum. Beck (2009) presented CT scans demonstrating that the cribriform plate is very large and densely perforated in QM F13008, suggesting that olfaction was particularly well developed in *Yalkaparidon*.

Orbitosphenoid

The orbitosphenoid is more obvious on the left than the right side of QM F13008 (Figs. 2 and 7: **os**). In lateral view, it makes a small (3.4 mm in length, 2 mm in height), roughly parallelogram-shaped contribution to the ventromedial wall of the orbit and contacts the frontal anterodorsally and the alisphenoid posterodorsally. At its rostral end, the orbitosphenoid forms the posterior rim of the ethmoidal foramen (which is completed by the frontal) and extends slightly dorsal to this foramen. Ventrally, the relationship between the orbitosphenoid, presphenoid, and basisphenoid is obscured by adhesive in QM F13008.

Presphenoid

In QM F13008, only the posteriormost part of the presphenoid is preserved (Fig. 2: **ps**). In ventral view, this remnant forms a small flat plate, 2.7 mm wide and 4.4 mm long, anterior to the basisphenoid (with which it forms a well-marked, transverse suture) and ventromedial to the frontal and orbitosphenoid;

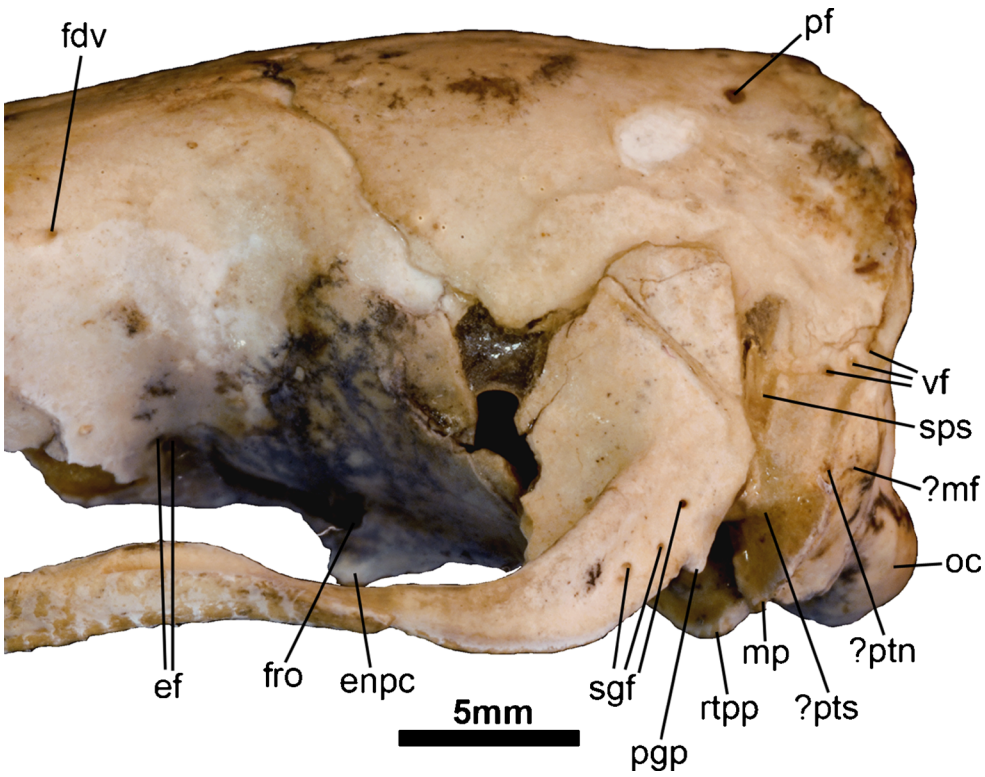

Fig. 6 Braincase of *Yalkaparidon coheni* (QM F13008) in left lateral view. Abbreviations: **ef** = ethmoidal foramina (separate foramina for the ethmoidal artery and nerve are present); **enpc** = entopterygoid crest; **fdv** = foramen for the frontal diploic vein; **fro** = foramen rotundum; **?mf** = ?mastoid foramen; **mp** = mastoid process; **oc** = occipital condyle; **pf** = parietal foramen; **pgp** = postglenoid process; **?ptn** = posttemporal notch; **?pts** = ?posttemporal sulcus; **rtpp** = rostral tympanic process of the petrosal; **sgf** = supraglenoid foramina; **sps** = sulcus for the prootic sinus; **vf** = vascular foramina

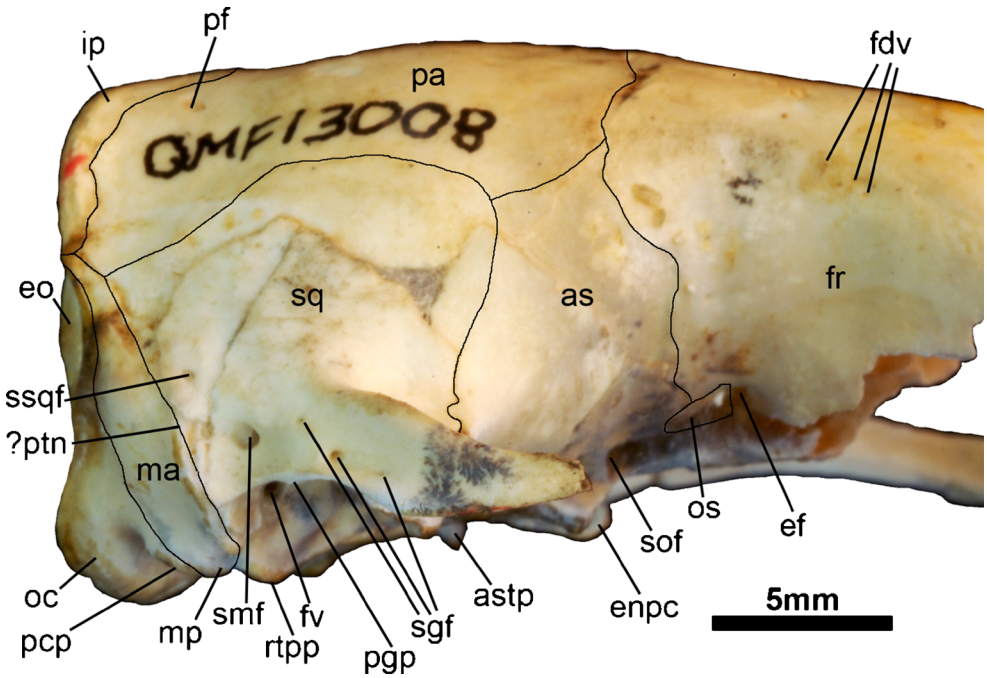

Fig. 7 Braincase of *Yalkaparidon coheni* (QM F13008) in right lateral view, with the inferred extent of the cranial sutures (prior to damage) indicated. Abbreviations: **as** = alisphenoid; **astp** = alisphenoid tympanic process; **ef** = ethmoidal foramen; **enpc** = entopterygoid crest; **eo** = exoccipital; **fdv** = foramina for the frontal diploic vein; **fr** = frontal; **fv** = fenestral vestibuli; **ip** = interparietal; **ma** = mastoid exposure of the petrosal; **mp** = mastoid process; **oc** = occipital condyle; **os** = orbitosphenoid; **pa** = parietal; **pcp** = paroccipital process; **pf** = parietal foramen; **pgp** = postglenoid process; **?ptn** = ?posttemporal notch; **rtpp** = rostral tympanic process of the petrosal; **sgf** = supraglenoid foramina; **smf** = suprameatal foramen; **sof** = sphenorbital fissure; **sq** = squamosal; **ssqf** = subsquamosal foramen

sutural relationships with these latter bones are obscured by adhesive. QM F13008 is damaged anterior to the nasal-frontal suture; as a result, it can be seen that the presphenoid is fused dorsally with the ossified nasal septum (mesethmoid sensu Rowe et al. 2005; Fig. 2: **me**).

Alisphenoid

The alisphenoid and basisphenoid are seamlessly fused in QM F13008. We therefore follow Wible's (2003) criteria for delimiting the boundary between these bones, namely that the foramen rotundum lies entirely within the alisphenoid while the transverse canal and carotid foramina lie entirely within the basisphenoid.

In lateral view, the precise extent of the alisphenoid in QM F13008 is difficult to ascertain because much of the thin bone that would have overlapped the frontal, parietal, and squamosal bones has flaked off; nevertheless, faint ridges on these bones allow the approximate boundaries of sutures to be inferred (Fig. 7). Anteriorly, the alisphenoid forms a roughly vertical suture with the frontal (this suture is more obvious on the right side of QM F13008), which extends dorsally from the orbitosphenoid for about 8 mm and terminates at the parietal about two-thirds up the medial orbital wall. Posterior to this, the intact alisphenoid would have contacted the parietal along a 4 mm long, roughly horizontal suture; thus, *Yalkaparidon* exhibits alisphenoid-parietal contact on the lateral wall of the braincase (Fig. 7). Wroe et al. (1998) incorrectly stated that frontal-squamosal contact is present in *Yalkaparidon*, presumably because they failed to account for the damage to the alisphenoid in QM F13008. The anteroventral border of the alisphenoid contacts the orbitosphenoid. Posterior to this, the alisphenoid forms the lateral wall and dorsal roof of the sphenorbital fissure (Fig. 7: **sof**). The foramen rotundum, which is immediately posterolateral and slightly dorsal to the sphenorbital fissure on the left side of QM F13008 (Fig. 6: **fro**) but slightly more posterior on the right side (Fig. 8: **fro**), is housed entirely within the alisphenoid. Lateral to the transverse canal foramen (Fig. 8: **tf**), which is within the basisphenoid, is the partially broken tympanic process of the alisphenoid (which forms the anterior wall and at least part of the floor of the tympanic bulla; Figs. 7 and 8: **astp**) and, posterior to this, the alisphenoid contribution to the roof of the hypotympanic sinus (Fig. 8: **ashs**). Medial to the hypotympanic sinus, the large foramen ovale (Fig. 8: **fo**), which lies between the alisphenoid and petrosal, is visible. Extending dorsally for about 7.5 mm from the anterior margin of the root of the squamosal zygomatic process to the parietal (approximately two-thirds the way up the medial wall of the braincase), the alisphenoid forms a roughly vertical suture with the squamosal (Fig. 7). Much of the squamosal and alisphenoid in this region has flaked off in QM F13008.

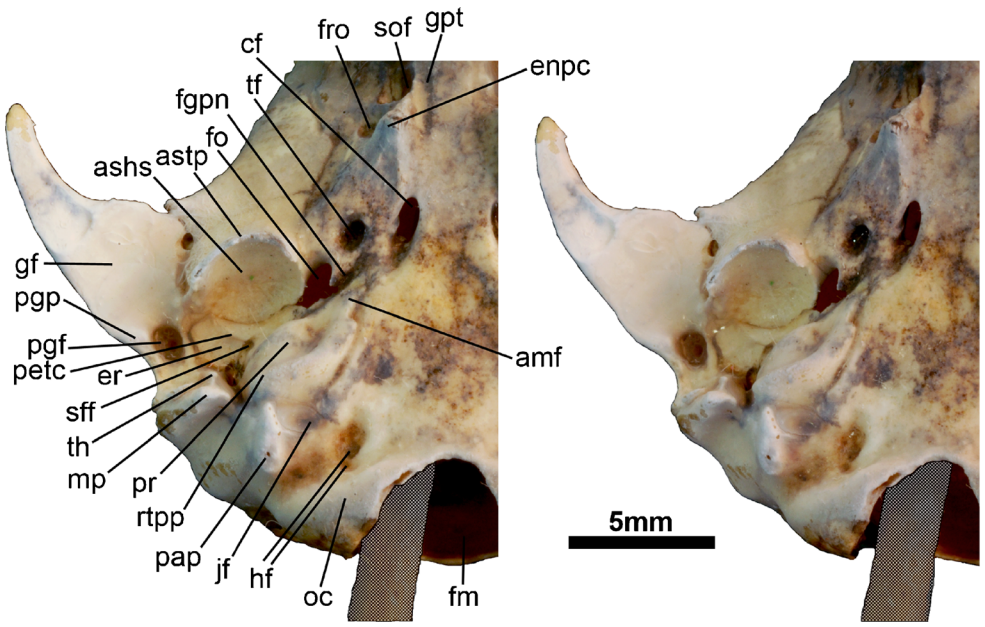

Fig. 8 Right auditory region of *Yalkaparidon coheni* (QM F13008) in stereo-ventral view. Hatched areas are not part of the specimen. Abbreviations: **amf** = anteromedial flange; **ashs** = alisphenoid hypotympanic sinus; **astp** = alisphenoid tympanic process; **cf** = carotid foramen; **enpc** = entopterygoid crest; **er** = epitympanic recess; **fgpn** = (incomplete) foramen for the greater petrosal nerve; **fm** = foramen magnum; **fo** = foramen ovale; **fro** = foramen rotundum; **gf** = glenoid fossa; **gpt** = groove on the basisphenoid for the pterygoid; **hf** = hypoglossal foramina; **jf** = jugular foramen; **mp** = mastoid process; **oc** = occipital condyle; **pap** = paroccipital process; **petc** = petrosal crest (sensu Archer 1976); **pgf** = postglenoid foramen; **pgp** = postglenoid process; **pr** = promontorium; **rtpp** = rostral tympanic process of the petrosal; **sff** = secondary facial foramen; **sof** = sphenorbital fissure; **tf** = transverse canal foramen; **th** = tympanohyal

In ventral view (Figs. 2 and 8), the alisphenoid contacts the squamosal posterolaterally, medial to the glenoid fossa. The alisphenoid makes a very small contribution to the anteromedial border of the posterior root of the zygomatic arch, anterior to the glenoid fossa (Fig. 8) Although this region is damaged on both the left and right sides of QM F13008, a facet on the squamosal indicates that a thin strip of the alisphenoid (the alisphenoid glenoid process sensu Wible 2003; Forasiepi 2009; the entoglenoid process of the alisphenoid sensu Muizon 1998, 1999) extended laterally for about a third the width of the glenoid fossa (approximately 1.3 mm; Fig. 8).

Medial to the posterior half of the glenoid fossa, the alisphenoid forms the majority of the domed dorsal roof of the hypotympanic sinus (Fig. 8: **ashs**); the remainder is excavated in the petrosal immediately posterior to the alisphenoid contribution. Anterior to the hypotympanic sinus, a well-developed alisphenoid tympanic process forms the anterior wall and at least part of the floor of an auditory bulla (Fig. 8: **astp**). The alisphenoid hypotympanic sinus and alisphenoid tympanic process together form a distinct bowl-like structure in QM F13008 (Figs. 2 and 8), with the alisphenoid tympanic process forming the anteroventral rim of the bowl, but this morphology is at least partly due to breakage of the alisphenoid tympanic process ventrally. Damage to the alisphenoid tympanic process on both the left and right sides of QM F13008 means that the precise extent of the intact bulla is unclear, including whether or not it extended far enough posteromedially to contact the rostral tympanic process of the petrosal.

Medial to the hypotympanic sinus, between the alisphenoid and petrosal, is a large, roughly oval-shaped opening, the foramen ovale (the exit for the mandibular branch of the trigeminal nerve; Fig. 8: **fo**). A small, posterolaterally-directed prong of the alisphenoid on the anteromedial border of the foramen ovale may define a partially separate, but incomplete, foramen for the greater petrosal nerve (Fig. 8: **fgpn**). Although the alisphenoid tympanic process is damaged, a complete secondary foramen ovale (i.e., full enclosure by an outgrowth of the alisphenoid; see Gaudin et al. 1996; Wroe 1997) was almost certainly not present, because there is no evidence for a point of attachment for such an outgrowth anteromedial to the tympanic process. However, a partially enclosed secondary foramen ovale—in which an outgrowth extended from the alisphenoid tympanic process but did not contact the basicranium anteromedially (see e.g., Gaudin et al. 1996: Fig. 6)—may have been present.

In dorsal view, the contribution of the alisphenoid to the anteromedial border of the root of the zygomatic arch can be seen (Fig. 1c). This region is damaged on both sides of QM F13008, but a facet on the squamosal indicates that the alisphenoid extended laterally for approximately half the width of root of the zygomatic arch (roughly 2 mm).

Basisphenoid

In ventral view, the rostral end of the basisphenoid forms a well-marked, transverse, straight suture with the presphenoid at a point that is approximately level with the alisphenoid-frontal suture and midway between the ethmoidal foramen and sphenorbital fissure (Figs. 2 and 8). Immediately posterior to the presphenoid-basisphenoid suture, a broad antero-posterior groove occupies the lateral part of the basisphenoid ventromedial to the sphenorbital fissure and extends posteriorly for approximately 4 mm (Fig. 8: **gpt**); comparison with intact skulls of other metatherians suggest that it housed the pterygoid.

Posteroventral to the sphenorbital fissure and level with the foramen rotundum in the alisphenoid, the basisphenoid sends out a stout, ventrally directed entopterygoid crest (Fig. 8: **enpc**); together, the left and right entopterygoid crests form the lateral walls of the nasopharyngeal fossa. The entopterygoid crest of *Yalkaparidon* is much thicker and is located more posteriorly than those of most other similarly-sized metatherians, such as dasyurids, didelphids, and peramelemorphians. Beck (2009) argued that this feature is functionally related to woodgouging, specifically, to strengthen the skull against stresses generated when the rostrum is bent upward (see Cartmill 1974). Both the left and right entopterygoid crests of QM F13008 are broken anteriorly and hence their full extent is uncertain, but when complete they would have been much more extensive rostrally and presumably contacted both the pterygoid and palatine. The medial face of the entopterygoid crest bears an extensive facet for contact with the pterygoid; a tiny piece of bone attached to the posterior part of this facet on the left entopterygoid crest in QM F13008 may be a remnant of the pterygoid. There is no distinct pterygoid fossa or ectopterygoid crest lateral to the entopterygoid crest.

Posterior to the entopterygoid crest is the lumen of the carotid foramen (Fig. 8: **cf**). In QM F13008, the right carotid foramen appears larger than the left due to damage to the dorsal roof of the groove running into the right foramen. This groove extends posteriorly and slightly laterally from the carotid foramen and indicates the course of the internal carotid artery. Posterolateral and slightly dorsal to the entopterygoid crest, the foramen of the transverse canal is visible (Fig. 8: **tf**). This foramen is lateral and slightly posterior to the carotid foramen, anteromedial to the foramen ovale in the alisphenoid, and faces posterolaterally. The anterior rim of the transverse canal foramen is approximately level with the posterior rim of the carotid foramen, in contrast to other marsupials in which the transverse canal foramen is anterior of the carotid foramen (with the exception of *Metachirus*, in which these foramina are reported to be level; Sánchez-Villagra and Wible 2002). The seemingly unique position of the transverse foramen in *Yalkaparidon* was remarked upon by Sánchez-Villagra and Wible (2002), and may be related to the posterior extension and robusticity of the entopterygoid crest (see Beck 2009). When a bright light is shone directly into the endocranial cavity, light is clearly visible in the lumen of both the left and right transverse canal foramen, suggesting that the transverse canal foramina open directly into the cranial cavity, rather than having an intramural connection with a complete dorsal roof of bone.

A groove in the basisphenoid extends from just anterior to the rostral pole of petrosal, between the carotid foramen and the transverse canal foramen, towards the entopterygoid crest. This groove, which is more obvious on the left side, probably housed the greater petrosal nerve as it extended from the petrosal towards the pterygoid canal (the pterygoid canal is not preserved in QM F13008 due to loss of the pterygoids and palatines). The suture between the basisphenoid and basioccipital that delimits the basisphenoid posteriorly cannot be identified in QM F13008.

Pterygoid

Both left and right pterygoids are entirely missing from QM F13008, with the possible exception of a tiny fragment of bone attached to the posterior part of the medial face of the left entopterygoid crest of the basisphenoid. The pterygoids are not preserved in any other *Yalkaparidon* specimen.

Parietal

The paired, domed parietals form the dorsolateral walls of the posterior part of the braincase. The parietals contact the frontals anteriorly, the alisphenoid anterolaterally, the squamosal laterally, the wedge-shaped interparietal posteromedially, and the dorsal part of the mastoid exposure of the petrosal posterolaterally.

In dorsal view (Fig. 1c), the parietal overlaps the frontal anteriorly, and is overlapped by the squamosal and alisphenoid ventrolaterally (although the overlapping portions of these bones are broken off, their extent is indicated by faint ridges on the parietal; Fig. 7). The suture between the parietals extends along the midline for 10.4 mm and is unfused, although it becomes tightly interdigitated in its middle third (Fig. 1c). Very weak temporal lines are just visible on the parietals (as they are on the frontals), extending posteriorly and slightly medially close to the midline; they meet on the midline 2.5 mm anterior of the suture with the interparietal, but do not form a distinct sagittal crest. Posterodorsally, a large parietal foramen is present on both sides 1.2 mm lateral of the rostralmost end of the interparietal (Figs 1a, c, 6 and 7: **pf**). Examination of the endocranial space of QM F13008 through the foramen magnum indicates that these parietal foramina connect to the transverse sinuses.

In lateral view, a small foramen is present on the left parietal of QM F13008, close to its posteroventral edge,

0.8 mm anterior to the dorsalmost extent of the mastoid exposure and 1.0 mm dorsal of the posteriormost part of the parietal-squamosal suture. No such foramen is present on the right side.

Interparietal

As in *Monodelphis* (see Wible 2003), the interparietal of *Yalkaparidon* is an unpaired bone that is roughly moustache-shaped in dorsal view (Fig. 1c). Rostrally, the interparietal forms a triangular wedge between the parietals; posteriorly, it extends laterally and ventrally along the posterior border of the skull, thinning as it does so (Figs. 1c and 7: **ip**). The posterior margin of the interparietal is developed into a nuchal crest ventrolaterally, but there is no crest in its medial section (Figs. 1c and 3b); this somewhat resembles the condition in peramelemorphians, but sutures that might indicate the presence of lambdoidal sesamoids in this region (as seen in peramelemorphians; Filan 1990) are not visible. An obvious suture marking the boundary between the interparietal and the supraoccipital cannot be identified, although faint remnants of this suture may be present along the nuchal crest. Damage to the left side of the interparietal, just lateral to the midline, has partly exposed a canal that extends to a foramen in the supraoccipital, just below the dorsal margin of the skull, and which may connect to the parietal foramen. In lateral view, it can be seen that the ventrolateral end of the interparietal contacts the most dorsal point of the mastoid exposure of the petrosal (Fig. 7).

Occipital Complex

We assume here that the occipital complex comprises four bones (as in e.g., *Monodelphis*; Wible 2003): the basioccipital, supraoccipital, and paired exoccipitals. However, sutures demarcating the boundaries between these bones are not visible in QM F13008, and the occipital complex is not preserved in any other known *Yalkaparidon* specimen. We therefore describe the occipital complex in two parts: the ventral occipital (which forms the floor of the rear part of the braincase, and comprises the fused basioccipital and exoccipitals), and the occipital plate (which forms the posterior wall of the braincase, and comprises the fused supraoccipital and exoccipitals).

Ventral Occipital

In ventral view (Figs. 2 and 8), the ventral occipital is roughly triangular in outline, except where its posterior border is notched by the foramen magnum. The occipital condyles are clearly visible lateral to the foramen magnum (Fig. 8: **oc**). Paired hypoglossal foramina are present on both sides, anterior to each occipital condyle (Fig. 8: **hf**). They are most obvious on the right side of QM F13008 and are arranged anteroposteriorly, with the anterior foramen roughly twice as large as the posterior. The occipital condyles and hypoglossal foramina were presumably formed by the exoccipitals (as in e.g., *Monodelphis*; Wible 2003). Anterolateral to the hypoglossal foramina, the ventral occipital forms the medial and posterior rim of the jugular foramen (Fig. 8: **jf**), which is completed anterolaterally by the promontorium of the petrosal. A separate foramen for the inferior petrosal sinus, anterior to the jugular foramen, is not clearly identifiable, but may have been present, as this region is obscured by adhesive on both the left and right sides of QM F13008. A separate foramen for the inferior petrosal sinus is present in the metatherians *Monodelphis*, *Didelphis*, *Dasyurus*, and *Pucadelphys* (Wible 2003), but it shares a common opening with the jugular foramen in the eutherian *Zalambdalestes* (see Wible et al. 2004) and also some diprotodontians. The jugular foramen is bordered posterolaterally by the paroccipital process sensu Voss and Jansa (2003; = "paracondylar process" sensu Wible 2003; Fig. 8: **pap**), which has broken off the left side of QM F13008 and is damaged posteriorly on the right side. The paraoccipital process (presumably formed by the exoccipital, as in e.g., *Monodelphis*; Wible 2003) is very small, short, and directed anteroventrally, almost contacting the posterior surface of the promontorium of the petrosal. Immediately lateral to the paroccipital process, the ventral occipital contacts the mastoid exposure of the petrosal. At the rostral end of the ventral occipital (presumably formed by the basioccipital, as in e.g., *Monodelphis*; Wible 2003), the suture with the basisphenoid is not identifiable.

Occipital Plate

In posterior view (Fig. 3b), the occipital plate is roughly trapezoidal in outline. Although the occipital plate presumably comprises the supraoccipital dorsally and paired exoccipitals ventrolaterally, sutures between these elements are not visible. The occipital plate forms the entire posterior wall of the skull except the posterolateral corners, which are formed by the mastoid exposures of the two petrosals (Fig. 3b: **ma**). The occipital plate is dominated by the large, ventromedial foramen magnum (Fig. 3b: **fm**), the rim of which is smoothly rounded and lacks a sharply defined dorsal incisura. The occipital plate is delimited dorsally and dorsolaterally by the nuchal crest, except for 1.5 mm immediately either side of the midline where this crest is absent (Fig. 3b). The nuchal crest probably coincides with the boundary between the supraoccipital and interparietal, but the suture between these two bones is not identifiable. Three vascular foramina are present immediately below the dorsal margin of the occipital plate, close to the midline (Fig. 3b: **vf**; Wible 2003 reported a single, centrally placed foramen in this region in *Monodelphis*); of these, the left foramen is the largest, whereas the middle and right foramina are distinctly smaller. Multiple

small foramina are also present around the rim of the occipital plate close to the nuchal crest. Ventrolaterally, the occipital plate contacts the mastoid exposure of the petrosal, which is about half the height of the occipital plate. The occipital condyles (Fig. 3b: **oc**) form the ventrolateral border of foramen magnum and are roughly comma-shaped, with the "tail" of each comma pointing ventromedially.

Squamosal

In lateral view (Figs. 1a, b, 6 and 7), the squamosal forms the posterior part of the zygomatic arch and contributes to the lateral wall of braincase. The squamosal overlaps the alisphenoid anteriorly, the parietal dorsally, and the mastoid exposure of the petrosal posteriorly (Fig. 7: **sq**). A large suprameatal foramen (sensu Wible 2003; Fig. 7: **smf**), dorsal to the external auditory meatus, is preserved on the right side of QM F13008, but this region is damaged on the left side. A small subsquamosal foramen (sensu Wible 2003; Fig. 7: **ssqf**) also appears to be present 3 mm posterodorsal to the suprameatal foramen, close to the suture with the petrosal. There are three anterolateral-facing foramina (Figs. 6 and 7: **sgf**) visible in the lateral face of the zygomatic process of the squamosal, anterior to the suprameatal foramen, on both the left and right sides of QM F13008; we refer to them here as "supraglenoid foramina." Wible (2003) reported a single foramen in a similar location in *Monodelphis*, and this also appears to correspond to "foramen X" identified by Horovitz et al. (2008) in skulls of the metatherian *Herpetotherium* from the early Oligocene of Wyoming. In QM F13008, the largest of the three supraglenoid foramina (the middle foramen on the right side, the anterior foramen on the left) has a distinct sulcus extending anteriorly, grooving the zygomatic process of the squamosal. In QM F40095 (an isolated glenoid region of a right squamosal), it can be seen that these foramina communicate with the postglenoid foramen. Beck (2009) tentatively suggested that the supraglenoid foramina of *Yalkaparidon* may reflect the presence of enlarged pinnae (which would have required an increased blood supply), but also noted that some extant mammals with similar foramina (e.g., the tapir *Tapirus* and the rice tenrec *Orizoryctes*; Koenigswald 1990; Salton 2005) have relatively small pinnae. Alternatively, they may simply transmit arterial and venous blood to and from the posterior part of the temporalis.

On the right side of QM F13008, there is a notch in the squamosal along its suture with the petrosal, immediately posterior to the suprameatal foramen, which may be the posttemporal notch (Fig. 7: **?ptn**). On the left side, the squamosal in this region has largely broken off, but there is notch in the petrosal along a vertical ridge that marks its suture with the squamosal, which again may represent the posttemporal notch (Fig. 6: **?ptn**). The postglenoid process (Figs. 6 and 7: **pgp**) is barely visible in lateral view, forming a slight "bump" in the ventral border of the zygomatic process of the squamosal, anteroventral to the suprameatal foramen and immediately anterior to the inferred position of the external auditory meatus. Posterior to the external auditory meatus, a small, ventrally directed postympanic process of the squamosal overlaps the anterolateral part of the petrosal. The squamosal does not contribute to the hypotympanic sinus or tympanic wing in *Yalkaparidon*, and there are no squamosal epitympanic sinuses.

In ventral view, the squamosal contribution to the glenoid fossa and surrounding area is better preserved on the right side of QM F13008 (Fig. 8). The glenoid fossa (Fig. 8: **gf**) is wide and essentially planar; there is no evidence of the separate articular eminence and mandibular fossa that characterize the "complex" glenoid fossa of most diprotodontians (Aplin 1987). The postglenoid process (Fig. 8: **pgp**) is extremely weak, being little more than a very low ridge that extends anterolaterally from the lateral rim of the postglenoid foramen for approximately 1.5 mm. Posterior to the medial region of the glenoid fossa, immediately medial to the postglenoid process and lateral to the epitympanic recess of the petrosal, the large postglenoid foramen (Fig. 8: **pgf**) is entirely enclosed by the squamosal. Postzygomatic foramina (sensu Gregory 1910; see Wible 2003) are not visible within the right postglenoid foramen of the right side of QM F13008 because this region is obscured by adhesive. However, in QM F40095 (an isolated glenoid region of a right squamosal), two small foramina are visible within the lumen of the postglenoid foramen: one foramen, which opens in the lateral wall of the lumen of the postglenoid foramen, communicates with one of the supraglenoid foramina on the lateral wall of the root of the squamosal zygomatic process; a second foramen, in the anterior wall, penetrates the substance of the squamosal but its exit is uncertain (it may be via another of the supraglenoid foramina). QM F40095 also confirms that the suprameatal foramen connects to the postglenoid foramen in *Yalkaparidon*, as in other marsupials (Wible 2003).

In dorsal view, a distinct temporal crest (sensu Evans 1993) is present along the lateral margin of the squamosal zygomatic process (Fig. 1c: **tc**); this crest forms the posterolateral wall of a depression (enclosed medially by the braincase) on the dorsal surface of the root of the squamosal zygomatic process. This depression represents the origin of the pars zygomatica of the temporalis muscle (Turnbull 1970), and several small foramina are visible within the depression in dorsal view.

Petrosal

The petrosal houses the cochlea and semicircular canals, provides attachments for the muscles and ligaments of the auditory ossicles, and exhibits grooves, canals, and foramina for various blood vessels and nerves. It is the most complex bone of the mammalian skull, and is also one of the most commonly preserved in fossil deposits due to its high density. Numerous studies demonstrate its utility in inferring

phylogenetic affinities (e.g., Wible 1990; Wible et al. 2001; Ladevèze 2004, 2007; Ladevèze and Muizon 2007; Beck et al. 2008b). QM F13008 preserves both left and right petrosals largely intact, apart from slight damage to the left promontorium anterior to the fenestra vestibuli. An isolated partial left petrosal (QM F52958; Fig. 9) that preserves the pars cochlearis and the ventral portion of the pars canalicularis is tentatively referred to *Yalkaparidon* here. Comparison of QM F52958 with QM F13008 suggests that the former is indeed from *Yalkaparidon*, although it is slightly smaller (QM F13008 appears to represent a particularly large individual; see Table 1) and shows some minor morphological differences relative to QM F13008. We first describe the features of the petrosal that are visible in QM F13008 and go on to discuss additional details revealed by QM F52958.

In ventral view, the petrosal contacts the occipital complex medially and posteromedially, the alisphenoid anterolaterally, and the squamosal laterally (Fig. 8). The jugular foramen (Fig. 8: **jf**) is posteromedial to the petrosal, lying between it and the basioccipital, while the foramen ovale (Fig. 8: **fo**) and the smaller, incomplete foramen for greater petrosal nerve (Fig. 8: **fgpn**) are anterior to the petrosal, between it and the alisphenoid. The petrosal is dominated by the promontorium (Fig. 8: **pr**), which houses the cochlea. The promontorium itself appears to be roughly hemispherical in shape, but its outline is distorted by a ridgelike rostral tympanic process (Fig. 8: **rtpp**) that extends anteromedially along the ventral surface of the promontorium from just ventral to the fenestra cochleae to the point of contact between the petrosal and the basioccipital. Anteromedially, the promontorium extends into a flat piece of bone (Fig. 8: **amf**; the anteromedial flange sensu Wible 2003) that is oriented at an angle of about 45° with respect to the sagittal plane. The anteromedial flange forms the posteromedial border of the foramen ovale and overlaps the basisphenoid lateral to this.

Within the promontorium, the laterally-facing fenestra vestibuli is roughly oval and is recessed within a fossula; it is largely concealed in ventral view but is visible in lateral view on the right side of QM F13008 (Fig. 7: **fv**). The fenestra cochleae, which opens in the posterior flank of the promontorium dorsal to the posterior end of the rostral tympanic process, is also barely visible in ventral view on either side of QM F13008. A roughly triangular sheet of bone, which we term the anterior lamina following Ladevèze (2004; but see Rougier and Wible 2006), extends lateral to the promontorium. Anteriorly, the anterior lamina is partly excavated by the part of the hypotympanic sinus that lies within the petrosal (the majority of the hypotympanic sinus lies within the alisphenoid, anterior to the petrosal). A low crest (Fig. 8: **petc**; the petrosal crest sensu Archer 1976) divides the petrosal contribution to the hypotympanic sinus from the epitympanic recess (Fig. 8: **er**) immediately behind it. The precise morphology of the

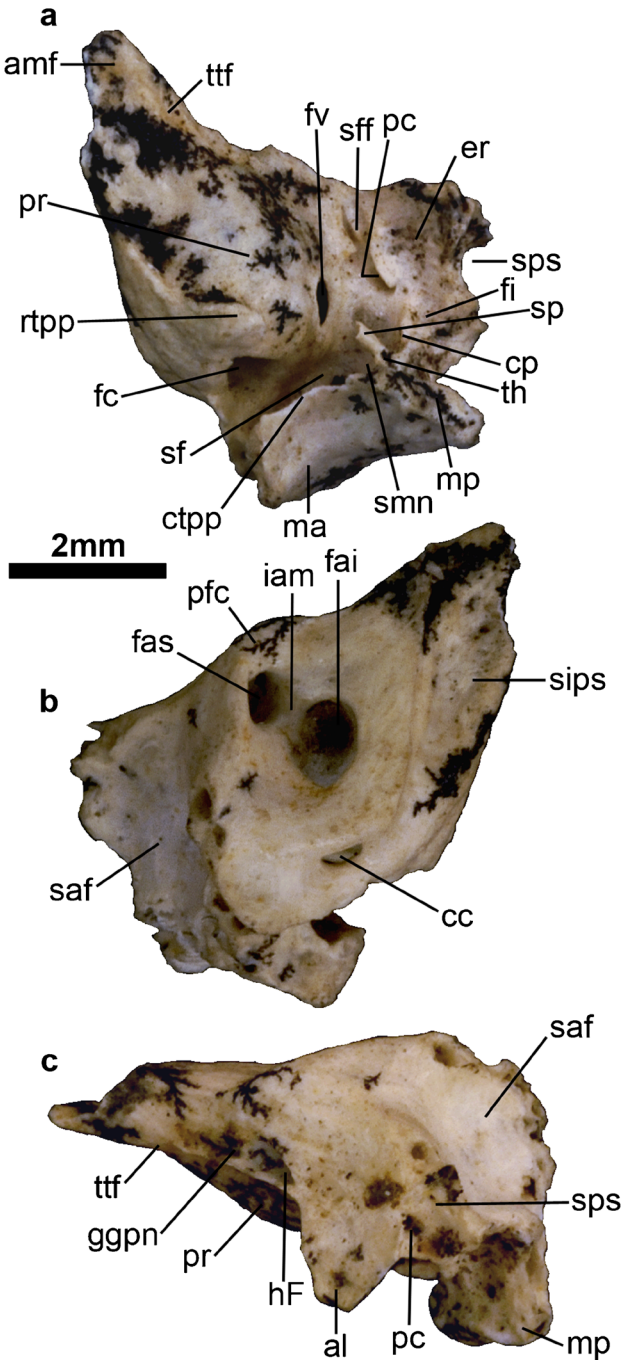

Fig. 9 Isolated partial left petrosal of *Yalkaparidon* sp. indet. (QM F52958). a dorsal (cerebellar) view. b ventral (tympanic) view. c lateral (squamosal) view. Abbreviations: **al** = anterior lamina (sensu Ladevèze 2004); **amf** = anteromedial flange; **cc** = cochlear canaliculus; **cp** = crista parotica; **ctpp** = caudal tympanic process of the petrosal; **er** = epitympanic recess; **fai** = foramen acusticum inferius; **fas** = foramen acusticum superius; **fc** = fenestra cochleae; **fi** = fossa incudis; **fv** = fenestra vestibuli; **ggpn** = groove for the greater petrosal nerve; **hF** = hiatus Fallopii; **iam** = internal acoustic meatus; **ma** = mastoid exposure of the petrosal; **mp** = mastoid process; **pc** = prootic canal; **pfc** = prefacial commissure; **pr** = promontorium; **rtpp** = rostral tympanic process of the petrosal; **saf** = subarcuate fossa; **sf** = stapedius fossa; **sff** = secondary facial foramen; **sips** = sulcus for the inferior petrosal sinus; **smn** = stylomastoid notch; **sp** = styloid process; **sps** = sulcus for the prootic sinus; **th** = tympanohyal; **ttf** = tensor tympanic fossa

epitympanic recess and the fossa incudis cannot be determined in QM F13008 because they are obscured by adhesive. The secondary facial foramen (Fig. 8: **sff**) for the exit of the facial nerve is visible medial to the epitympanic recess, anterodorsal to the fenestra vestibuli. A relatively large foramen that represents the tympanic opening of the prootic canal is present posterolateral to the secondary facial foramen and posterior and slightly dorsal to the epitympanic recess; the floor of this opening is formed by the fossa incudis.

Posterior to the epitympanic recess, the tympanohyal (Fig. 8: **th**; after the stapes, the most proximal ossification in Reichert's cartilage) is identifiable as a relatively stout, vertically-directed process. A short, posteriorly directed crest connects the tympanohyal to the weak mastoid process (Fig. 8: **mp**). Anterolateral to the mastoid process and lateral to the tympanohyal, the petrosal is covered by the posttympanic process of the squamosal (this process is missing on the left side of the QM F13008). Medial to the tympanohyal and mastoid process is a weak stylomastoid notch for the exit of the facial nerve from the middle ear; *Yalkaparidon* lacks a complete stylomastoid foramen enclosed by the petrosal. Medial to the stylomastoid notch, the caudal tympanic process of the petrosal forms a crest that extends laterally to contact the paroccipital process of the ventral occipital, posterior to the fenestra cochleae.

In lateral view, damage to the squamosal on the left side of QM F13008 has exposed most of the squamosal face of the left petrosal (Fig. 6). Three foramina (Fig. 6: **vf**) close to the dorsal margin of the squamosal face of the left petrosal probably represent exits for branches of the sigmoid sinus. A sulcus extends anteriorly from the most anterior of these foramina for about 1.5 mm towards the vertically directed prootic sinus (Fig. 6: **sps**), the dorsal section of which is visible where the squamosal has broken away. A structure that probably represents the postttemporal notch (Fig. 6: **?ptn**) is identifiable as a distinct notch in the posterolateral margin of the petrosal, about 2.5 mm from its ventral edge. A very weak sulcus (Fig. 6: **?pts**) appears to extend anteriorly from the posttemporal notch along the squamosal face of the petrosal; this may be the posttemporal sulcus, which would have transmitted the the arteria diploëtica magna and accompanying vein towards the prootic sulcus. A small foramen (Figs. 3b and 6b: **?mf**) on the mastoid face of the left petrosal of QM F13008, approximately 1 mm posteromedial to the posttemporal notch, may be a mastoid foramen.

In posterior view, the mastoid exposure of the petrosal (Fig. 3b: **ma**) forms the posterolateral corners of the skull, lateral to the occipital plate. The mastoid exposure is shaped roughly like a dorsally elongate isoceles triangle. It is overlapped by the squamosal anteriorly, and contacts the parietal at its dorsal end (Fig. 7). As previously described, the probable posttemporal notch (Fig. 3b: **?ptn**) is visible in the lateral margin of the mastoid exposure of the left petrosal of QM F13008, about a third of the way up its vertical suture with the squamosal, and there appears to be a small mastoid foramen (Fig. 3b: **?mf**) roughly 1 mm posteromedial to the posttemporal notch; it is uncertain whether a similar foramen is present on the right side because this region is obscured by adhesive.

The isolated left petrosal QM F52958 (Fig. 9) retains a complete pars cochlearis, but the dorsal portion of the pars canalicularis (including the entire mastoid exposure) is missing, such that only the anterior half of the subarcuate fossa is preserved. Examination of QM F52958 confirms many of the anatomical details visible in QM F13008.

In ventral (tympanic) view (Fig. 9a), the rostral tympanic process of the petrosal (Fig. 9a: **rtpp**) is slightly more pronounced posteriorly in QM F52958 than in QM F13008, and forms a distinct knoblike structure. The bony floor of the secondary facial foramen (Fig. 9a: **sff**) has apparently broken away. The fenestra vestibuli (Fig. 9a: **fv**) is oval-shaped and recessed in a well-marked fossula. The fenestra cochleae (Fig. 9a: **fc**) is large and is shaped like a slightly rounded isoceles triangle, the apex of which is directed ventrally. The epitympanic recess (Fig. 9a: **er**) is more clearly visible in QM F52958, and is not greatly enlarged as it is in peramelemorphians. The tympanic aperture of the prootic canal (Fig. 9a: **pc**) is hidden by a ventral "ledge" of bone extending medially from the epitympanic recess; a small notch is present at the posterior end of this ledge. Posterolateral to this notch, the shallow fossa incudis (Fig. 9a: **fi**) is identifiable but is not well separated from the epitympanic recess anterior to it. Immediately medial to the fossa incudis, the crista parotica (Fig. 9a: **cp**) extends posteriorly to the tympanohyal (Fig. 9a: **th**). Extending anteroventrally from the tympanohyal is a delicate process of bone (Fig. 9a: **sp**) that Beck (2009) referred to as the styloid process and which may be a remnant of the stylohyal (the next distal ossification in the hyoid apparatus after the tympanohyal) that has fused to the tympanohyal. This process is not present on either the left or right (Fig. 8) side of QM F13008, but may have broken off during fossilization. Beck (2009) hypothesized that the styloid process of QM F52958 may reflect the presence of a well-developed styloglossus muscle (which attaches to the stylohyal) in *Yalkaparidon*. Medial to the styloid process is the stylomastoid notch (Fig. 9a: **smn**), which (as in QM F13008) clearly does not form a complete foramen. The stapedius fossa (Fig. 9a: **sf**), anterior to the tympanohyal and caudal tympanic process of the petrosal and posterior to the promontorium, is deep and well excavated. The tensor tympani fossa (Fig. 9a: **ttf**) is identifiable as a shallow, elongate groove along the anteolateral border of the anteromedial flange (Fig. 9a: **amf**) of the promontorium.

In dorsal (cerebellar) view, the internal auditory meatus (Fig. 9b: **iam**) is clearly identifiable towards the anteromedial end of the petrosal as a large opening that is subdivided into the more medial foramen acusticum inferius (Fig 9b: **fai**) and

the more lateral foramen acusticum superius (Fig. 9b: **fas**). The passage for the facial nerve from the foramen acusticum superius (which it leaves via the primary facial foramen) to the hiatus Fallopii and secondary facial foramen can be traced. A cribriform dorsal vestibular area for passage of some bundles of the vestibular nerve (Wible 2003) is visible in the posterior wall of the foramen acusticum superius. The internal structure of the foramen acusticum inferius is partially obscured by infilling sediment, but the foramen singulare (which transmits the remaining bundles of vestibular nerve) is visible as a pit in its posterior wall. The prefacial commissure (Fig. 9b: **pfc**), immediately anterolateral to the foramen acusticum superius, is narrow. Posteromedial to the internal acoustic meatus, only the most anterior part of the subarcuate fossa is preserved (Fig. 9b: **saf**), although this is sufficient to demonstrate that the subarcuate fossa was deep and well excavated.

In lateral (squamosal) view, the hiatus Fallopii (Fig. 9c: **hF**) is visible; following the definition of Sánchez-Villagra and Wible (2002), it opens in an approximately "intermediate" position (i.e., neither clearly dorsal nor clearly ventral). A short groove (Fig. 9c: **ggpn**) extending anteriorly from the hiatus Fallopii indicates the course of the greater petrosal nerve. Posterior to the triangular-shaped anterior lamina (sensu Ladevèze 2004; Fig. 9c: **al**), the ventralmost part of the sulcus for the prootic sinus (Fig. 9c: **sps**) is preserved. The sulcus is vertically directed, and the squamosal aperture of the prootic canal (Fig. 9c: **pc**) is present in its anterior wall, although this opening is partially obscured by the posterior part of the anterior lamina. In medial view, the large cochlear canalicularis (which opens into the jugular foramen in the intact skull) is visible dorsal to the fenestra cochleae.

Mandible

Multiple mandibles are known from *Yalkaparidon*, although most have suffered damage to the coronoid process, mandibular condyle, and angular process. QM F36544 and F36545 (Fig. 10a–c) are largely complete and may be from a single individual; together, these form the basis for the description presented here. The overall shape of the mandible is superficially rodentlike, dominated by the enormous, procumbent i1. Following Wible (2003), the mandible comprises the horizontal, tooth-bearing body, the tall, hook-like coronoid process, the relatively low dental condyle (located only slightly above the alveolar margin of the body), and the weakly-developed angular process.

In lateral view, a strong coronoid crest (Fig. 10a: **coc**) is present along the anterior margin of the tall and hook-like coronoid process (Fig. 10a: **cor**). The masseteric fossa (Fig. 10a: **maf**) is well marked and is floored by a ventral ledge (the posterior shelf of the masseteric fossa sensu Marshall and Muizon 1995; Fig. 10a: **psmf**) that is quite wide posteriorly. The masseteric fossa is anteriorly extensive, with its anterior margin roughly level with the posteriormost molar alveolus; Beck (2009) argued that this indicates that a major function of the masseter in *Yalkaparidon* is to shift the mandible anteriorly, bringing the tips of i1 and I1 into occlusion. Several small foramina (Figs. 10a, d, g: **?mafo**) are present within the masseteric fossa, and may be homologous with the masseteric foramen seen in many diprotodontians and in *Caenolestes* (see Osgood 1921; Voss and Jansa 2009: 46). A single mental foramen (Fig. 10: **mf**) is present below the tooth that we identify here as m1 in QM F36544, F36545 (Fig. 10a: **mf**), and in several other specimens; it is located more posteriorly, below m2, in others, e.g., QM F13008 (Fig. 10d: **mf**) F20366, F23526, and F36543. Wible (2003) found that position of the mental foramen in *Monodelphis* was at least partly correlated with size, with the foramen located more anteriorly in smaller individuals, but there is no clear evidence for such a relationship in the *Yalkaparidon* specimens examined here. In QM F13009 (the holotype of *Y. jonesi*; Fig. 10g: **mf**), F31370, and F50794, two mental foramina are present.

In medial view, the symphysis (Fig. 10b: **mas**) is identifiable as a distinct, oval-shaped, roughened area at the anterior end of the mandible; it is approximately 4.5 mm long and 5 mm deep at its deepest point in QM F36544 and F3654. The symphysis is unfused and extends as far posteriorly to a point just anterior to the alveoli that we interpret as housing m1. Posterior to this, the mandible maintains a roughly consistent depth until the coronoid process (Fig. 10a: **cor**). The root of i1 extends posteriorly within the mandible below the entire molar row, producing a clearly visible bulge on the medial face of the mandible, and terminates just anterior to the mandibular foramen, about level with the anterior margin of the coronoid process (confirmed by damaged specimens; Fig. 10h). Posterior to the end of the i1 root, the mandibular foramen (Figs. 10a, e, h: **manf**) is located about halfway up the body of the mandible, level with the anterior margin of the angular process (Figs. 10 a–c: **ang**). In QM F31370, a particularly small right mandible, two mandibular foramina are present, with one distinctly larger and anterodorsal to the other.

In dorsal view, the angular process (Fig. 10c: **ang**) forms a shallow hook extending posteromedially; it shows only a relatively weak medial inflection compared to most metatherians (see Sánchez-Villagra and Smith 1997). The mandibular condyle (Fig. 10c: **con**) is roughly bean-shaped in dorsal view, and is obliquely oriented from posterolateral to anteroventral, with a gently rounded dorsal surface. The dental alveoli terminate posteriorly anterior and slightly medial to the coronoid process, creating a short retromolar space sensu Wible (2003). An apparent retromolar foramen is present in QM F31370, medial to the anterior margin of the coronoid process, but the retromolar space is imperforate in all other *Yalkaparidon* specimens. We discuss the number of dental alveoli in the mandibular body and their implications for the dental formula of *Yalkaparidon* below.

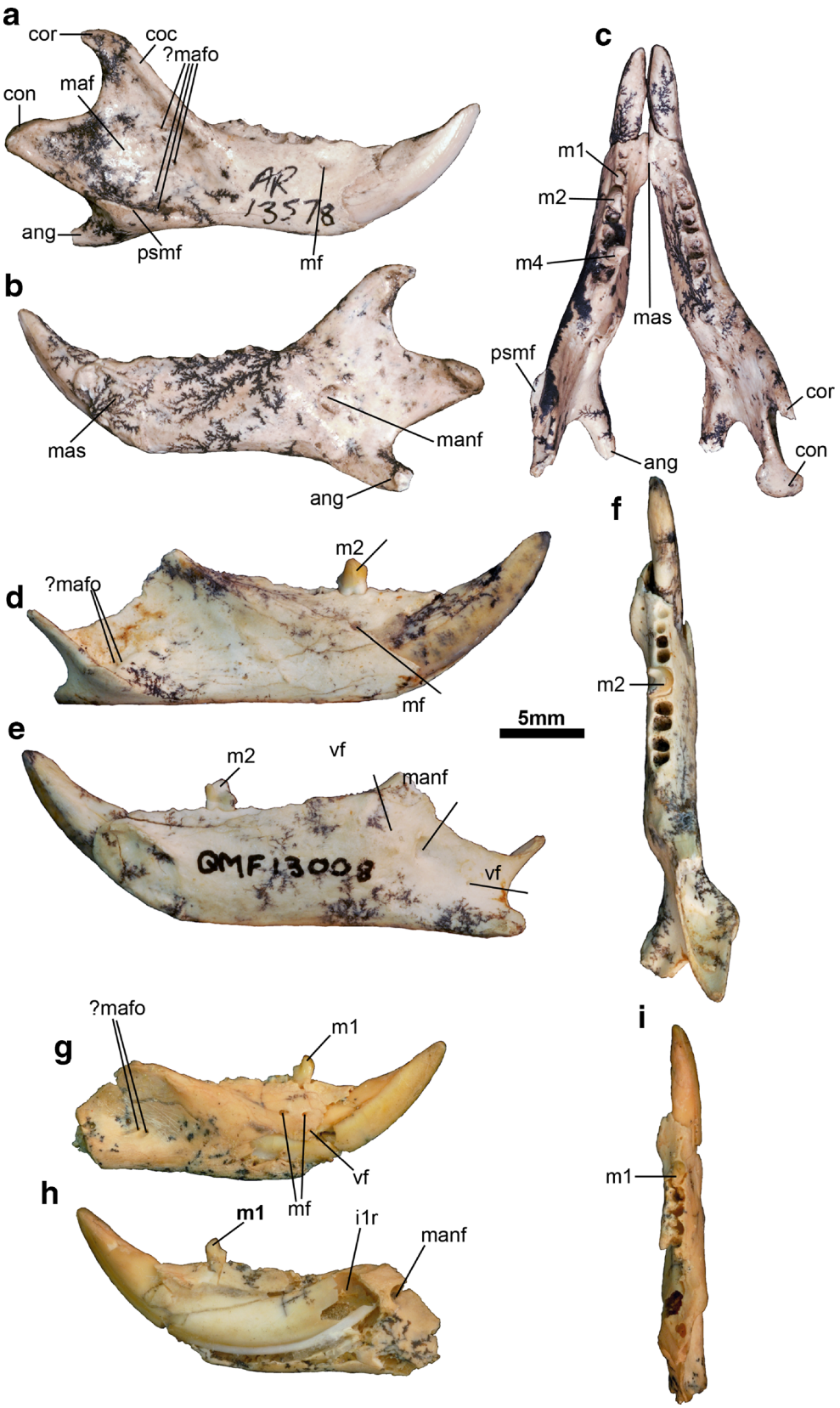

Fig. 10 Mandibular morphology of *Yalkaparidon*. **a** isolated right mandible of *Yalkaparidon coheni* (QM F36545) in labial view. **b** QM F36545 in lingual view. **c** left (QM F36544) and right (QM F36545) mandibles of *Y. coheni* (probably from a single individual) in occlusal view. **d** partial right mandible of holotype of *Y. coheni* (QM F13008) in labial view. **e** QM F13008 in lingual view. **f** QM F13008 in occlusal view. **g** holotype partial right mandible of *Y. jonesi* (QM F13009) in labial view. **h** QM F13009 in lingual view. **i** QM F13009 in occlusal view. Abbreviations: **ang** = angular process; **coc** = coronoid crest; **con** = mandibular condyle; **cor** = coronoid process; **i1r** = open root of first lower incisor; **maf** = masseteric fossa; **?mafo** = ?masseteric foramina; **manf** = mandibular foramen; **mas** = mandibular symphysis; **mf** = mental foramen; **psmf** = posterior shelf of the masseteric fossa; **vf** = vascular foramen

Dental Description

Dentition as a Whole

As noted by Archer et al. (1988), the dentition of *Yalkaparidon* is unique amongst known metatherians (and, indeed, known mammals) in that it combines three highly distinctive dental specializations. Firstly, *Yalkaparidon* is diprotodont, i.e., the anteriormost lower incisor is greatly enlarged and procumbent, or "gliriform" (Figs. 1b and 10). Within Metatheria, diprotodonty is present in diprotodontians and the South American "pseudodiprotodont" groups Paucituberculata and Polydolopimorphia (Goin 2003). Whether the gliriform tooth is homologous across all of these groups remains uncertain: the gliriform tooth of diprotodontians and paucituberculatans is clearly an incisor, but the precise dental locus may differ between these two groups (Ride 1962), and it has been suggested that the gliriform tooth of polydolopimorphians may in fact be a canine (Marshall 1982; Flynn and Wyss 2004). However, in the absence of compelling evidence for non-homology, we assume that the gliriform tooth of diprotodontians, paucituberculatans, and *Yalkaparidon* represents the same locus, namely i1 (we have not included any representatives of Polydolopimorphia in the phylogenetic analysis presented here, and so do not consider the homology of the gliriform tooth of these taxa further).

Secondly, the first upper and lower incisors of *Yalkaparidon* are hypseledont, i.e., open-rooted, and hence grow continuously throughout life (Figs. 4 and 10h). Within Metatheria, hypselodont incisors are also found in some diprotodontians, including the extant vombatids *Lasiorhinus* and *Vombatus*, as well as the South American pseudodiprotodont argyrolagoids (Flynn and Wyss 1999). The enamel of I1 and i1 of *Yalkaparidon* is restricted to the anterolabial face of the tooth (Figs. 1, 3, 4 and 10), a feature that is best known in rodents and lagomorphs but within Metatheria is found in several diprotodontians and some argyrolagoids; this distribution of enamel ensures that the incisors maintain a sharp, chisel-like edge as the teeth wear.

Thirdly, the molars of *Yalkaparidon* are extremely zalambdodont, i.e., the upper and lower molars are highly modified through loss of the protocone and talonid, respectively, and each tooth is dominated by a single major cusp from which two crests emanate, resulting in a distinctive v-shape when seen in occlusal view (Figs. 2, 5, 10, 11 and 12; see Asher et al. 2002; Asher and Sánchez-Villagra 2005; Seiffert et al. 2007). Amongst unequivocal metatherians, zalambdodonty is also present in *Notoryctes*, albeit in a less extreme form than in *Yalkaparidon* in that the protocone is still clearly identifiable (Asher and Sánchez-Villagra 2005; Archer et al. 2011). Incipient zalambdodonty, achieved through paracone reduction, is present in the fossil notoryctid *Naraboryctes philcreaseri* from the early Miocene of Riversleigh (Archer et al. 2011) and in *Kiruwamaq chisu*, a probable metatherian from the ?middle-late Eocene Santa Rosa formation of Peru (Goin and Candela 2004). Murray and Megirian (2006: Fig. 6a–f) described an isolated upper molar (NTM P2815–6) from the late Oligocene Pwerte Marnte Marnte Local Fauna in the Northern Territory that they identified as the M2 of peramelemorphian and which is characterized by a reduced paracone. We suggest that this specimen is probably a plesiomorphic notoryctemorphian (a possibility also acknowledged by Murray and Megirian 2006) that documents an earlier stage (given its larger paracone and metaconule) in the acquisition of zalambdodonty than does *Naraboryctes*. *Necrolestes*, an enigmatic fossorial mammal from the early Miocene of Argentina, has been suggested to be a zalambdodont metatherian (Asher and Sánchez-Villagra 2005; Asher et al. 2007; Ladevèze et al. 2008). However, more recent research indicates that it is a non-therian that diverged from therians prior to the evolution of tribospheny (Chimento et al. 2012; Rougier et al. 2012; Averianov et al. 2013).

The living marsupial mole *Notoryctes* has evolved zalambdodonty by loss of the paracone (Archer et al. 2011). This is in contrast to most zalambdodont placentals, which have lost the metacone (Asher and Sánchez-Villagra 2005).

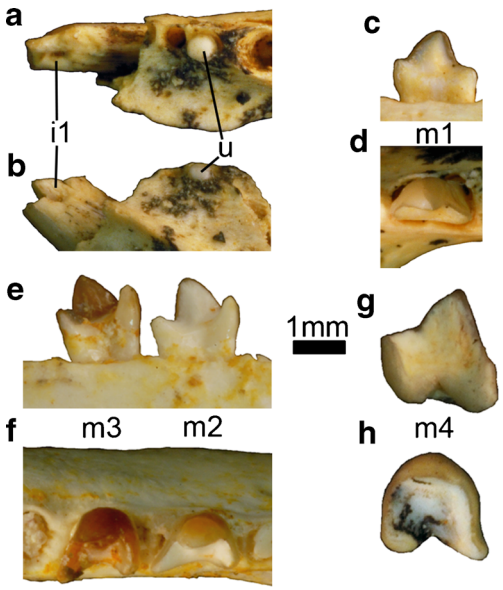

Fig. 11 Details of the lower dentition of *Yalkaparidon*. **a** QM F52963 (right partial mandible of *Yalkaparidon coheni*) in lingual view. **b** QM F52963 in occlusal view. Note broken right i1 and unicuspid tooth in one of the alveoli between i1 and m1. **c** QM F39984 (right mandible of *Y. coheni* preserving m1) in lingual view. **d** QM F39984 in occlusal view. **e** QM F50794 (left partial mandible of *Y. coheni* preserving m2 and m3) in lingual view. **f** QM F50794 in occlusal view. **g** QM F40059 (an isolated right ?m4) in lingual view. **h** QM F40056 in occlusal view. Abbreviations: **u** = unicuspid tooth in the region between i1 and m1

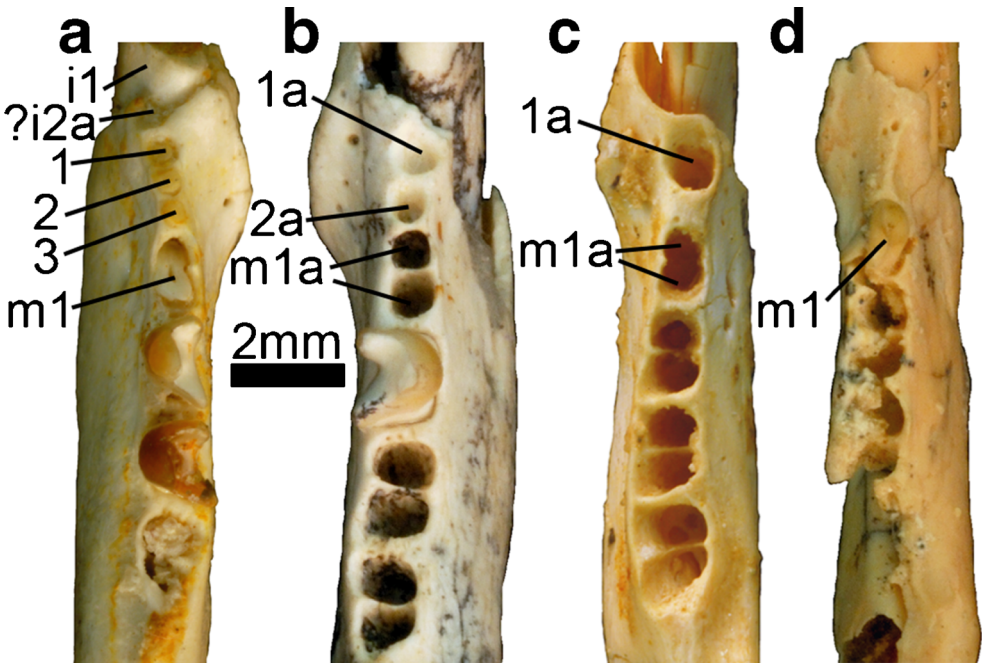

Fig. 12 Variation in the number of alveoli between i1 and m1 in *Yalkaparidon* mandibles. **a** QM F50794 (*Yalkaparidon coheni*). **b** QM F13008 (*Y. coheni holotype*). **c** QM F31370 (*Y. coheni*), **d**, QM F13009 *(Y. jonesi* holotype). Abbreviations: **1–3** = postincisive unicuspid teeth; **1a** = alveolus for first postincisive unicuspid tooth; **2a** = alveolus for first postincisive unicuspid tooth; **i1r** = (open) root of first lower incisor; **?i2a** = ?alveolus for second lower incisor; **m1a** = alveoli for first lower molar

Archer et al. (1988) assumed that *Yalkaparidon* achieved zalambdodonty via the same evolutionary pathway as in *Notoryctes*, i.e., by suppression of the paracone. However, at least one placental, the vespertilionid bat *Harpiocephalus*, has evolved incipient zalambdodonty via paracone reduction (i.e., the pattern typical of metatherians; Asher and Sánchez-Villagra 2005). Thus, zalambdodonty is not always acquired in placentals by suppression of the paracone. This raises the possibility that zalambdodonty in metatherians is not always the result of suppression of the metacone. Until such time as intermediate fossils documenting the evolution of zalambdodonty in *Yalkaparidon* are found, it cannot be assumed a priori that the major cusp of the upper molars of *Yalkaparidon* is the metacone.

Asher and Sánchez-Villagra (2005) and Asher et al. (2007) argued that occlusal relations can be used to infer probable cusp homologies, and we have attempted to apply this approach here to *Yalkaparidon*. When QM F52756 (a left maxilla preserving P3 and M1–3; Fig. 5) is brought into approximate occlusion with QM F20723 (a left mandible preserving i1 and m2–3), the major cusp of the upper molars appears to occlude closer to the paracristid of the more posterior lower molar (data not shown). Following Asher and Sánchez-Villagra (2005) and Asher et al. (2007), we tentatively interpret this as evidence that the major cusp of the upper molars of *Yalkaparidon* is most likely the metacone, as was originally assumed by Archer et al. (1988).

However, occlusal relations are clearly not infallible indicators of cusp homologies: Asher and Sánchez-Villagra (2005) and Asher et al. (2007) used them to conclude that the major lingual cusp of the upper molars of *Necrolestes* is the metacone, whereas it now seems clear that this cusp is in fact the paracone, based on comparison with other meridiolestidans (Rougier et al. 2012). Chimento et al. (2012) used occlusal relations to conclude that the major lingual cusp of the upper molars of *Necrolestes* is the paracone, in agreement with Rougier et al. (2012). However, Chimento et al.'s (2012) model of occlusion in *Necrolestes* is clearly incorrect because it reconstructs the upper and lower molars occluding one-to-one (rather than as interlocking triangles), which would render the molar crests non-functional.

Amongst zalambdodont mammals, *Yalkaparidon* is unusual in that the occlusal and labial surfaces of the upper molars (Fig. 5) and the occlusal and lingual surfaces of the lower molars are entirely enamel-free (Figs. 11 and 12). This distribution of enamel is also seen in the enigmatic mammal *Yingabalanara richardsoni* described by Archer et al. (1990), which is known only from the Faunal Zone B (early Miocene) deposits at Riversleigh (see the "Lower Dentition" section of the "Dental Description"). Beck (2009) observed that this restricted distribution of enamel ensures that the molar crests remain sharp as the molars wear, and proposed that it represents a specific adaptation for feeding on soft-bodied invertebrates.

Archer et al. (1988) briefly described the dentition of *Yalkaparidon*, and Long et al. (2002) included a labelled diagram of its dentition that assumed the dental formula and cusp homologies proposed by Archer et al. (1988). Here we provide the first detailed description of the individual teeth of *Yalkaparidon* and propose a revised interpretation of the dental formula that differs somewhat from that of Archer et al. (1988).

Upper Dentition

The upper dental formula of *Yalkaparidon* is relatively easy to determine from known specimens. I1–3 lie within the premaxilla, as is evident from QM F13008 and F52942 (Figs. 1 and 3). A diastema separates I3 from the single-rooted C1, which lies entirely within the maxilla, as seen in QM F13008 and F52756 (Fig. 2). A second diastema separates C1 from the P3 (Figs. 2 and 5), which may have been single-rooted in some specimens (e.g., QM F52754, F52755, and F36546), but was clearly double-rooted in others (e.g., QM F13008 and F39986; Fig. 2: **P3a**). In QM F13008, there are three sets of three alveoli posterior to P3, with each set arranged in a triangular pattern and the apex of the triangle pointing lingually (Fig. 2); these would have housed M1–3, as confirmed by QM F52756 (Fig. 5), in which M1–3 are preserved in situ. Posterior to M3, there is either a single alveolus (e.g., QM F13008; Fig. 2: **M4a**) or pair of alveoli (e.g., QM F52756; Fig. 5: **M4a**) for a single- or double-rooted M4 (see the "Maxilla" section of "Skull Description"). Thus, the full upper dentition of *Yalkaparidon* is I1–3 C1 P3 M1–4, and not I1–3 C1 P1–3 M1–3 as was originally stated by Archer et al. (1988). The presence of four rather than three molars in *Yalkaparidon* is perhaps not surprising, given that loss of the fourth molar is rare in metatherians, and is usually associated with hypertrophy of the third premolar (Arena et al. 2011), which is clearly not the case in *Yalkaparidon*.

The I1 (Figs. 1, 2, 3 and 4) is by far the largest upper tooth in *Yalkaparidon*, considerably larger than both I2 and I3, and is also hypseledont (Fig. 4). Damage to the facial process of the maxilla on both the left and right sides of QM F13008 means that the open root of I1 can be seen extending back within the premaxilla to a point level with anterior root of P3 (Fig. 1a, b). In lateral view (Figs. 1a, b and 4a), the crown of I1 is relatively featureless, curving smoothly ventrally from the premaxilla to a point 6 mm below the ventral margin of the cranium. Enamel is restricted to the anterolabial face of the tooth. A small notch in the dentine on the posterior face of I1 (Fig. 4a: **I1n**), level with occlusal surfaces of I2 and I3, indicates the point of contact with the tip of i1. In occlusal view (Figs. 2 and 4b), I1 is roughly triangular in cross-section, comprising a flat, unenamelled distal face, a flat, unenamelled lingual face and a rounded, enamelled mesiolabial face.

The I2 (Figs. 1, 2, 3 and 4) is immediately posterior and slightly lateral to I1. In lateral view (Figs. 1a, b and 4a), the crown of I2 curves ventrally for about 2 mm below the premaxilla, and its occlusal surface faces anteroventrally. In occlusal view (Figs. 2 and 4b), the outline of I2 is a mediolaterally compressed oval, and the tooth appears somewhat "squashed" between I1 and I3. Its occlusal surface is essentially flat and featureless, and appears to have been slightly worn through contact with i1. I2 appears to entirely lack enamel, comprising a simple, slightly curved cylinder of dentine.

The I3 (Figs. 1, 2, 3 and 4) is posterolateral to I2, is slightly larger, and in lateral view (Figs. 1a, b and 4a) its occlusal surface faces slightly more anteriorly. Besides this, I3 is very similar in terms of morphology and dimensions to I2, and has a similarly featureless, slightly worn occlusal surface (Figs. 2 and 4b). Like I2, I3 appears to be unenamelled.

The C1 is not preserved in any known specimen of *Yalkaparidon*. However, an alveolus for C1 is preserved in QM F13008 (Fig. 2: **C1a**), F36546, and F52756 (Fig. 5b: **C1a**) and indicates that this tooth was tiny and single rooted; it is unlikely that it played a major role in occlusion.

The P3 is preserved in QM F13011 (a paratype of *Y. coheni*) and F52756 (Fig. 5). Maximum mesiodistal crown length is 1.21 mm and maximum labiolingual crown width is 0.72 mm in QM F52756 (Fig. 5; see Electronic Supplementary Material for measurements of other specimens). In labial view (Fig. 5a), the crown of P3 is roughly triangular, with its posterior crest slightly longer than the anterior crest and with a trace of a cusp present at the end of the posterior crest. In occlusal view (Fig. 5b), its outline is a mediolaterally compressed triangle, with its apex pointing lingually and its posterior half slightly larger than its anterior half. Enamel is entirely restricted to the lingual face of P3 (Fig. 5). As noted above, P3 is clearly double-rooted in some specimens (e.g., QM F13008 and F39986; Fig. 2: **P3a**) but may have been single-rooted in others (e.g., QM F52754, F52755, and F36546; see "Species-Level Taxonomy").

The M1 is preserved in situ in a single maxillary specimen, QM F52756 (Fig. 5), but we have also identified several isolated examples (see Electronic Supplementary Material). Maximum mesiodistal crown length is 2.07 mm and maximum labiolingual crown width is 1.43 mm in QM F52756 (Fig. 5; see Electronic Supplementary Material for measurements of other specimens). In labial view (Fig. 5a), the lingual cusp of M1 (probably the metacone, as discussed above) is considerably taller than the anterolabial and posterolabial cusps (which are presumably stylar in origin, but the exact homologies of which cannot be identified with any certainty). In occlusal view (Fig. 5b), M1 is shaped like a rounded "tick" or "checkmark," with a long tail extending posterolabially. Enamel is present on anterior and posterolingual faces, present but extremely thin on the labial face and entirely absent from the occlusal face (Fig. 5). Three roots are present: anterolingual, anterolabial, and posterolabial (Fig. 2).

The M2 (Fig. 5) is considerably wider and more symmetrical than M1. Maximum mesiodistal crown length is 2.00 mm and maximum labiolingual crown width is 2.34 mm in QM F52756 (Fig. 5; see Electronic Supplementary Material for measurements of other specimens). The tooth is shaped like an arrowhead in occlusal view (Fig. 5b), with a very deep ectoflexus. The anterolabial cusp and posterolabial cusp (at the ends of the anterior and posterior lobes, respectively) are further labial than the equivalent cusps on M1, and the lingual cusp (the metacone) is slightly further lingual. The posterior

lobe is slightly wider than the anterior lobe. The morphology of M2 is otherwise similar to that of M1, with enamel absent from the occlusal face and absent or extremely thin on the lingual face, and with the metacone considerably taller than the anterolabial and posterolabial cusps (Fig. 5). As for M1, three roots are present (Fig. 2).

The M3 (Figs. 2, 3a and 5) is almost identical to M2, but slightly wider (such that the metacone is slightly further lingual), more symmetrical and with a deeper ectoflexus. Maximum mesiodistal crown length is 2.06 mm and maximum labiolingual crown width is 2.49 mm in QM F52756 (Fig. 5; see Electronic Supplementary Material for measurements of other specimens).

The M4 is not preserved in any cranial specimen of *Yalkaparidon* and an examination of isolated molars from various Riversleigh sites failed to identify plausible candidates. Although the presence of either one (e.g., QM F13008; Fig. 2: **M4a**) or two (e.g., QM F52756; Fig. 5b: **M4a**) alveoli in the maxilla posterior to M3 confirms that *Yalkaparidon* retained four molars, the M4 alveolus (or alveoli) is extremely shallow and M4 itself is not preserved in any known specimen. M4 was therefore very short rooted and probably of limited importance in mastication.

Lower Dentition

With the exception of the enormous, open-rooted anterior lower incisor (identified here as i1; Figs. 1b and 10), tooth homologies of the lower dentition of *Yalkaparidon* are rather more difficult to interpret than for the upper dentition. Archer et al. (1988) determined the lower postincisive dental formula of *Yalkaparidon* as comprising between one and three premolars and three molars. However, examination of all known *Yalkaparidon* material, including specimens unavailable to Archer et al. (1988), leads us to an alternative interpretation that we present here.

Of central importance is QM F13008, the holotype of *Y. coheni*, which is the only *Yalkaparidon* specimen with an associated upper and lower dentition. The right mandible of QM F13008 (Figs. 1b, 10d-f and 12b) preserves a single molar that Archer et al. (1988) identified as m1 (but which they referred to as "m2," following the alternative hypothesis of metatherian dental homologies proposed by Archer 1978). However, if the cranium and mandible of QM F13008 are arranged so that the occlusal surface of i1 contacts the occlusal surfaces of I1–3 and the tip of i1 contacts the small notch (Fig. 5a: **I1n**) on the posterior face of I1 (as in Fig. 1b), the single preserved lower molar clearly lies posterior to the alveoli for M1 and anterior to the alveoli for M2. Thus, the lower molar in QM F13008 would appear to be m2, not m1. There are four alveoli posterior to the m2 (Fig. 12b), which presumably housed a double-rooted m3 and a double-rooted m4, and we interpret the two alveoli immediately anterior to m2 (Fig. 12b) as most likely housing a double-rooted m1. Thus, the lower molar formula of QM F13008 is probably m1–4 (not m1–3, as suggested by Archer et al. 1988), as in most metatherians and as would be expected given the presence of four upper molars (see "Upper Dentition" above). Application of this model of dental homologies to the holotype mandible of *Y. jonesi* (QM F13009) suggests that the single preserved tooth is a heavily worn m1 (Figs. 10g–i and 12d), not p3 as argued by Archer et al. (1988). QM F39884 preserves a relatively unworn tooth that appears to be m1 (Fig. 11c, d), given that there are three pairs of alveoli (for m2–4) posterior to it. Comparison of this specimen with QM F13009 confirms that the tooth preserved in the latter is probably m1, albeit with heavy wear.

In the mandible of QM F13008, there are two alveoli between the m1 and i1 (Figs. 10f and 12b: **1a**, **2a**). These alveoli are relatively well separated (the bony septum between them is thicker than that between the alveoli of a single molar), which may indicate that they were occupied by two single-rooted teeth. In apparent agreement with this, QM F52963 preserves a tiny, single-rooted unicuspid tooth (Fig. 11a–b: **u**) with a very low, roughly hemispherical crown, in the alveolus anterior to the alveolus for the anterior root of m1. The precise homology of the teeth between i1 and m1 in QM F13008 is uncertain, but, assuming a maximum of four lower incisors, one canine, and three premolars, they were presumably two out of i2–4, c1, and p1–3. Thus, the lower dental formula of QM F13008 (the holotype of *Y. coheni*) appears to comprise a single enlarged incisor (i1), two single-rooted teeth (two out of i2–4, c1, and p1–3), and four double-rooted molars (m1–4). In contrast, there are no alveoli between i1 and m1 in QM F13009 (Figs. 10i and 12d), suggesting a lower dental formula of i1 c0 p0 m1–4 for this specimen. This variation in dental formula between QM F13008 and F13009 was the major factor that led Archer et al. (1988) to identify them as representing different species. Further variation in the number of alveoli between i1 and m1 is seen in other *Yalkaparidon* dentaries (Fig. 12). In several specimens (e.g., QM F36415, F50794, F39984, F36551, and F20366), a tiny anteriorly-directed alveolus is present immediately posterodorsal to the posterior margin of the i1 alveolus (Fig. 12a: **?i2a**). No tooth has been found preserved in this alveolus in any *Yalkaparidon* specimen, but it may have housed a vestigial i2. Posterior to this, most isolated dentaries show the same morphology as in QM F13008, i.e., two alveoli between i1 and m1 (Fig. 12b; Table 1); however, some specimens (e.g., QM F36415 and F50794) have three alveoli (Fig. 12a; Table 1), and some (e.g., QM F31370, F36545, and F36548) have only a single alveolus (Fig. 12c; Table 1). QM F13009 is the only *Yalkaparidon* mandible currently known to entirely lack alveoli between i1 and m1 (Fig. 12d, Table 1). The implications of this variation in lower dental formula for the species-level taxonomy are discussed in "Species-Level Taxonomy" below.

The i1 (Figs. 1b and 10), is a relatively enormous, curved, procumbent, rodentlike tooth, extending anterodorsally for approximately 8.5 mm beyond the mandible in QM F13008; it is 4.11 mm deep and 1.78 mm wide at the alveolus (measurements follow Freeman and Lemen 2008; see Table 1 and Electronic Supplementary Material for measurements of other specimens). The tooth extends within the mandible beneath the entire molar row as far as the mandibular foramen (Fig. 10h). Isolated teeth and broken dentaries demonstrate that it is open rooted (Fig. 10h). Enamel is restricted to the anterolabial face and the anteroventral margin of the lingual face. The tip of i1 is located approximately 3.5 mm above the alveolar margin of the mandible in QM F13008, and well above the occlusal plane of the lower molars (Figs. 1b and 10d, e). As discussed above, a very small, anteriorly directed alveolus is present immediately behind i1 in some specimens, e.g., QM F50794 (Fig. 12a: **?i2a**; Table 1). No tooth has been found occupying this alveolus, but it may have housed a greatly reduced i2.

As noted above, at least one alveolus is present between i1 and m1 in all known dentaries of *Yalkaparidon*, with the exception of QM F13009 (the holotype of *Y. jonesi*; Fig. 12, Table 1). However, only one specimen (QM F52963) preserves an apparently complete tooth in this region, in the alveolus immediately anterior to m1 (Fig. 11a, b: **u**): this tooth is tiny and single rooted, with a very low, roughly hemispherical crown. Maximum mesiodistal crown length is 0.59 mm and maximum labiolingual crown width is 0.62 mm in QM F52963 (Fig. 11b). The three alveoli between i1 and m1 in QM F50794 are occupied by roots (Fig. 12a), but the crowns of these teeth are either extremely worn or have broken off entirely, as no part of these teeth extends above the alveolar margin. It remains uncertain exactly which dental loci are represented in this region.

The occlusal outline of the lower molars of *Yalkaparidon* (Figs. 10, 11 and 12) differs from that of other zalambdodont mammals, including *Notoryctes* (see figures in Asher and Sánchez-Villagra 2005). In *Yalkaparidon*, the v-shaped crests are considerably less acute and the molars are relatively asymmetrical, with the posterior half of each molar forming a relatively elongate posterolingually-directed "tail" (Figs. 10, 11 and 12). This unusual morphology raises the possibility that the talonid has not been entirely lost in *Yalkaparidon*, and that the posterior "tail" represents the remnant of the talonid; if so, the posterior crest and posterolingual cusp of the lower molars may not be the metacristid and metaconid, respectively. However, in the absence of convincing evidence to the contrary, we have assumed that the talonid has been entirely lost in *Yalkaparidon* and that the posterolingual cusp is the metaconid, as in other zalambdodont taxa.

We note intriguing similarities between the overall morphology of the lower molars of *Yalkaparidon* and the trigonid of the enigmatic Riversleigh mammal *Yingabalanara richardsoni* (Archer et al. 1990; these authors also discussed this resemblance in their "Hypothesis 1" and "Hypothesis 6"). Enamel is absent from the occlusal surface of the trigonid of an isolated lower molar of *Y. richardsoni* (QM F31586), as in *Yalkaparidon*, and the trigonid is approximately the same size as a *Yalkaparidon* lower molar. Given that *Yingabalanara* exhibits an extremely reduced talonid, it is possible that it represents a plesiomorphic pre-zalambdodont yalkaparidontian, but this hypothesis remains speculative in the absence of more complete specimens of this taxon.

The morphology of m1 is best preserved in QM F39984 (Fig. 11c, d) and F36548, but QM F13009 (the holotype of *Y. jonesi*) also preserves a worn m1 (not a p3, contra Archer et al. 1988, as discussed above; Figs. 10g, i and 12d). Maximum mesiodistal crown length is 1.68 mm and maximum labiolingual crown width is 0.98 mm in QM F52756 (Fig. 11d; see Electronic Supplementary Material for measurements of other specimens). The tooth is roughly triangular in occlusal outline, with its distal half only slightly longer than mesial half; hence the posterolingual "tail" is shorter than in the more posterior molars. In QM F39984 (Fig. 11d), the labial border is almost straight, with only a very weak inflection. The apex of the protoconid is located roughly midway along the lingual margin of the tooth. Enamel is entirely absent from the occlusal and labial faces; hence, a labiolingually narrow, enamel-free basin is present labial to the protoconid, enclosed by the paracristid mesially and the metacristid distally, but open labially. In labial view (Fig. 11c), the protoconid is by far the tallest cusp. The paraconid is identifiable as a slight rise at the mesial end of the paracristid, which is notched as a result. The metacristid is distinctly bipartite: it descends at an angle of about 60° from the protoconid, then levels off to form an almost horizontal crest.

The m2 (based on QM F20723 and F50794, which are the least worn known examples; Fig. 11e, f) is considerably larger than m1, the paraconid is much better developed and the posterolingual tail is more elongate, but it is otherwise similar in overall morphology. Maximum mesiodistal crown length is 1.79 mm and maximum labiolingual crown width is 1.14 mm in QM F50794 (Fig. 11f), although this specimen appears to be from a particularly small individual (Table 1; see Electronic Supplementary Material for measurements of other specimens).

The m3 (again based, on QM F20723 and F50794; Fig. 11e, f), is extremely similar to m2 but slightly wider and the paracristid and metacristid are oriented slightly more transversely relative to the long axis of the mandible. Maximum mesiodistal crown length is 1.76 mm and maximum labiolingual crown width is 1.49 mm in QM F50794 (Fig. 11f; see Electronic Supplementary Material for measurements of other specimens).

The m4 of *Yalkaparidon* is preserved in situ in only a single mandible, QM F36544 (Fig. 10c), but the tooth is heavily worn and broken distally in this specimen. We have tentatively

identified a number of isolated, complete m4s based on comparison with QM F36544 and on inferred meristic gradients suggested by m1–3 (e.g., QM F40056 and F40059; Fig. 11g, h; see Electronic Supplementary Material). These specimens indicate that m4 is similar to m3, but the paraconid and metaconid are both slightly longer mesiodistally (Fig. 11g, h), and the paracristid and metacristid are oriented slightly more transversely so that the tooth as a whole does not appear as elongate (Fig. 11h). Maximum mesiodistal crown length is 1.90 mm and maximum labiolingual crown width is 1.81 mm in QM F40056 (Fig. 11h; see Electronic Supplementary Material for measurements of other specimens).

Tarsals Description

We tentatively refer nine isolated astragali (QM F39989, F40091, F40093, F40096, F52957, F52982, F53637, F53638, and F53639) to *Yalkaparidon*, based on relative size, abundance, and comparative morphology. We also identified two calcanea (QM F53640 and F53641) that appear to match the astragali in terms of size and conarticular joint morphology, from amongst isolated postcranial material from Upper Site (the Riversleigh site from which the most *Yalkaparidon* craniodental specimens have been collected to date; see Electronic Supplementary Material). Because the morphology of the tarsus plays a central role in our current understanding of metatherian phylogeny (e.g., Szalay 1982, 1994), these specimens may be particularly useful in deciphering the phylogenetic affinities of *Yalkaparidon*. However, the critical question is whether they can be assigned to *Yalkaparidon* with any degree of confidence.

Collectively, the tarsal specimens appear to represent a member of Australidelphia, given the presence of: (1) partially fused ectal and sustentacular facets, forming the continuous lower ankle joint characteristic of australidelphians; and (2) a tripartite calcaneocuboid facet, which is the second major tarsal synapomorphy of Australidelphia (Figs. 13 and 14; see Szalay 1982, 1994; Beck et al. 2008b; Beck 2012). However, the overall morphology of these tarsals differs significantly from that of all other undoubted australidelphians, namely dasyuromorphians, diprotodontians, notoryctemorphians, and peramelemorphians (members of which are known from the Oligo-Miocene deposits at Riversleigh), the South American microbiotherian *Dromiciops*, and the early Eocene Australian australidelphian *Djarthia* (see Szalay 1982, 1994; Beck et al. 2008b; Beck 2012).

Perhaps the most distinctive features of these tarsals are the extremely elongate astragalar neck (Figs. 13a, b and 14a, b), which is about as long proximodistally as is the body of the astragalus, and the distally extensive sustentacular facet of both the astragalus (Figs. 13b and 14b) and calcaneus (Figs. 13d, f and 14d, f); these two characters are correlated because the sustentacular facet of the astragalus extends onto the ventral surface of the astragalar neck, and hence distal extension of this facet necessitates a concomitant elongation of the astragalar neck. In addition to these features, the tarsals differ from: (1) those of dasyuromorphians in lacking a distal calcaneoastragalar facet at the distal end of the sustentaculum (Szalay 1994; the sustentacular facet instead extends the entire length of the sustentaculum); (2) those of macropodoid diprotodontians (including Miocene taxa from Riversleigh; Kear et al. 2001a, 2001b, 2007) in their smaller size, and in lacking a sharply angled "mortise-and-tenon" upper ankle joint, accessory astragalocalcaneal facet, or strongly "stepped" calcaneocuboid facet (Szalay 1994); (3) those of vombatimorphian diprotodontians in their smaller size and in having less distally extensive medial and lateral astragalotibial facets (Szalay 1994); (4) those of notoryctemorphians in their larger size and in having a narrower astragalofibular facet, a distally less extensive medial astragalotibial facet, and a proportionally shorter and more robust calcaneal tuber (Szalay 1994); (5) those of peramelemorphians (including undescribed specimens from

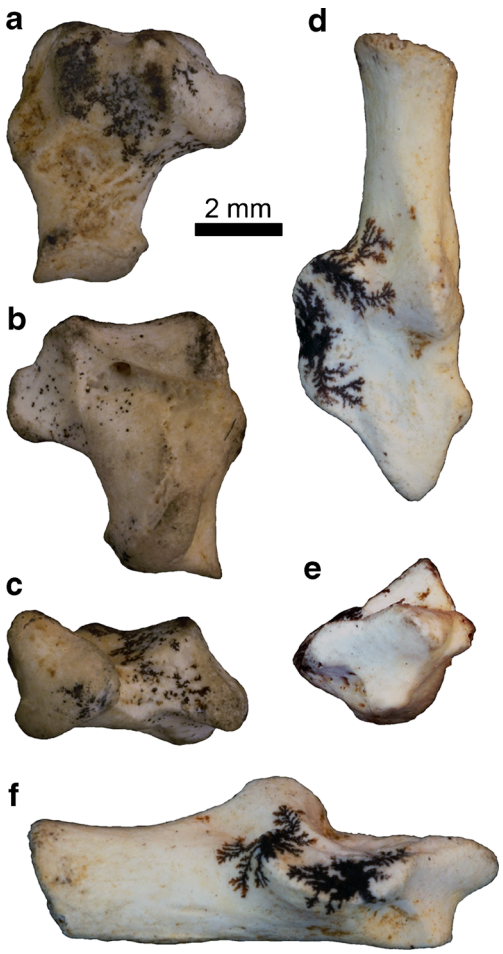

Fig. 13 Isolated tarsals tentatively referred here to *Yalkaparidon* sp. indet. **a** QM F53639 (isolated left astragalus) in dorsal view. **b** QM F53639 in ventral view. **c** QM F53639 in distal view. **d** QM F53641 (isolated left calcaneus) in dorsal view. **e** QM F53641 in distal view. **f** QM F53641 in medial view

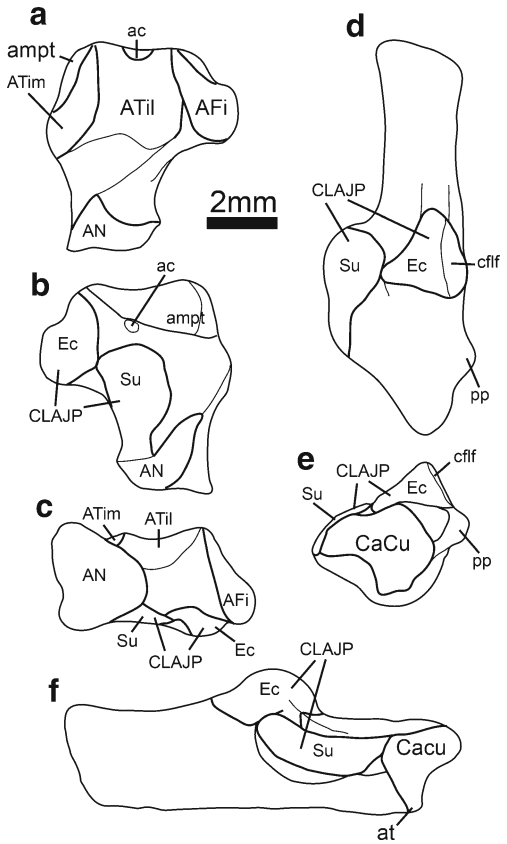

Fig. 14 Labelled diagrams of isolated tarsals tentatively referred here to *Yalkaparidon* sp. indet., with major features indicated. **a** QM F53639 (isolated left astragalus) in dorsal view. **b** QM F53639 in ventral view. **c** QM F53639 in distal view. **d** QM F53641 (isolated left calcaneus) in dorsal view. **e** QM F53641 in distal view. **f** QM F53641 in medial view. Abbreviations: **ac** = astragalar canal; **AFi** = astragalofibular facet; **ampt** = astragalar medial plantar tuberosity; **AN** = astragalonavicular facet; **at** = anterior plantar tubercle; **ATil** = lateral astragalotibial facet; **ATim** = medial astragalotibial facet; **CaCu** = calcaneocuboid facet; **cflf** = calcaneofibular ligament facet; **CLAJP** = continuous lower ankle joint pattern; **Ec** = ectal facet; **pp** = peroneal process; **Su** = sustentacular facet

Riversleigh; pers. obv.) in lacking a sharply angled "mortise-and-tenon" upper ankle joint and a calcaneofibular facet, and in having a less quadrate astragalus and a sustentacular facet that faces more medially (Szalay 1994); (6) those of the plesiomorphic australidelphian *Djarthia*, the microbiotherian *Dromiciops*, and "possum-like" diprotodontians in having a more sharply angled upper ankle joint with crests separating the tibial and fibular facets, distinct "pinching" or "waisting" of the continuous lower ankle joint (i.e., a narrow, rather than broad, connection between the ectal and sustentacular facets) and a less distinct tripartite division of the calcaneocuboid facet (Szalay 1994; Beck et al. 2008b).

Given that: (1) the craniodental morphology of *Yalkaparidon* differs significantly from that of all known australidelphians, (2) *Yalkaparidon* is the only undoubted metatherian currently known from Riversleigh that cannot be assigned to a known order, and (3) the tarsal remains discussed here are likewise very different from those of any other australidelphian and cannot be clearly assigned to any of the australidelphian orders present at Riversleigh, it seems plausible that these highly distinctive metatherian tarsals are indeed referable to *Yalkaparidon*. The alternative requires that either: (1) these tarsals belong to another Riversleigh metatherian taxon that is currently completely unrepresented by craniodental remains, or (2) a member of one of the known marsupial orders present at Riversleigh and known only from craniodental specimens possessed a tarsal morphology that differs radically from that of relatives that are known from associated postcranial material. We consider both possibilities unlikely. However, the referral of these tarsal specimens should, of course, be treated as tentative pending the discovery of associated craniodental and postcranial remains of *Yalkaparidon* (see Gelfo and Lorente 2012 for a general critique of attempts to refer isolated postcranial specimens to taxa known only from craniodental remains). We now present a detailed description of these tarsal specimens.

Astragalus

In dorsal view (Figs. 13a and 14a), the astragalofibular facet is broad and the lateral astragalotibial facet is distinctly trochleated. The medial astragalotibial facet is concave, with its distal margin well distal of the lateral astragalotibial facet and its proximal margin well distal of the proximal margin of the astragalus; as a result, the astragalar medial plantar tuberosity is visible in dorsal view (Figs. 13a and 14a: **ampt**). In distal view (Figs. 13c and 14c), the astragalofibular, lateral astragalotibial, and medial astragalotibial facets are separated from each other by well-marked crests, and the distinctly trochleated shape of the lateral astragalotibial facet is clearly visible. The degree of angulation between the medial astragalotibial and lateral astragalotibial facets and between the lateral astragalotibial and astragalofibular facets is more than in *Djarthia*, *Dromiciops*, and possum-like diprotodontians, but less than in the "mortise-and-tenon" upper ankle joint of peramelemorphians and macropodoids; some dasyoromorphians (e.g., *Antechinomys*; Szalay 1994: fig. 7.38 J) and some didelphids (e.g., *Didelphis*; Szalay 1994: fig. 7.11 J) show a similar degree of angulation. A crest extends from distal to the crest separating the astragalofibular and lateral astragalotibial facets to the dorsomedial corner of the astragalonavicular facet (Figs. 13a, c and 14a, c).

In distal view (Figs. 13c and 14c), the astragalonavicular facet is about as extensive dorsoventrally as it is mediolaterally, and it extends onto the ventromedial part of the astragalar neck. In dorsal (Figs. 13a and 14a) and proximal views, a foramen for the astragalar canal is visible, below the proximal border of lateral astragalotibial facet. The presence of a large astragalar canal (almost certainly a plesiomorphic retention; Szalay 1994; Szalay and Sargis 2006) would probably have limited the degree of plantar flexion possible around the upper ankle joint.

In ventral view (Figs. 13b and 14b), the ectal facet is weakly concave and the sustentacular facet is weakly convex. These two facets contact each other, forming the continuous lower ankle joint pattern ("CLAJP") characteristic of australidelphians, but the point of contact is relatively narrow; this "pinched" morphology of the CLAJP is characteristic of peramelemorphians and macropodoids (Szalay 1994), but also appears to be present to varying degrees in some dasyuromorphians (e.g., *Antechinomys*; Szalay 1994: fig. 7.38) and some "possum-like" diprotodontians (e.g., *Petaurus*; Szalay 1994: fig. 7.55). The proximal margin of the sustentacular facet is distal of the more proximal half of the ectal facet, unlike the condition in peramelemorphians, macropodoids, and some dasyuromorphians (e.g., *Antechinomys* and *Thylacinus*; Szalay 1994: figs. 7.38–39) in which these two facets are aligned mediolaterally. The astragalar medial plantar tuberosity appears relatively small and does not overhang the sustentacular facet. The ventral opening of the astragalar canal, dorsal and slightly lateral to the astragalar medial plantar tuberosity, is partially visible. The astragalonavicular facet is continuous with sustentacular facet in some specimens (e.g., QM F40096, F53639; Figs. 13b and 14b) but apparently not others (e.g., QM F39989), and extends proximally along the ventromedial face of the astragalar neck in all specimens.

Calcaneus

In dorsal view (Figs. 13d and 14d), the calcaneus appears quite slender and elongate (despite loss of the proximal epiphysis in both of the known specimens), with a relatively long tuber. The peroneal process is identifiable as a small but distinct protuberance on the lateral margin of the calcaneus, set well back from its distal end. The sustentaculum is long, and the sustenacular facet extends the entire length of the sustentaculum. The sustentacular facet is concave in medial view (Figs. 13f and 14f), and its anterior half faces more medially than does the posterior half. The ectal facet is anteroposteriorly convex and faces dorsomedially (Figs. 13d, e and 14d, e); as in the astragalus, the proximal part of the ectal facet is further proximal than the sustentacular facet (Figs. 13d and 14d). The sustentacular facet is considerably longer proximodistally than the ectal facet (Figs. 13d, f and 14d, f). As in the astragalus, although the sustentacular and ectal facets of the calcaneus contact each other (forming the australidelphian CLAJP), the area of contact between the two facets is relatively narrow, giving the CLAJP a distinctly "pinched" outline in dorsal view (Figs. 13d and 14d). When viewed medially (Figs. 13f and 14f), there is a distinct "step" at the point where the ectal and sustentacular facets contact each other, with the posterolateral margin of the sustentacular facet located below the level of the medial margin of the ectal facet (also seen in peramelemorphians and macropodoids). A relatively deep sulcus between the posterior regions of the ectal and sustentacular facets would have accepted the part of the astragalus immediately posterior to the astragalofibular facet during extremes of plantar flexion. There is no evidence for a distinct calcaneofibular facet lateral to the ectal facet.

A small but identifiable anterior plantar tubercle (Figs. 13f and 14f: **at**) is present at the ventrodistal end of the calcaneus, below the calcaneocuboid facet. In distal view (Figs. 13e and 14e), the calcaneocuboid facet appears to be tripartite, which is a second tarsal apomorphy characteristic of Australidelphia. However, the division between the three facets is less distinct than in *Dromiciops*, possum-like diprotodontians, or *Djarthia* (Szalay 1994; Beck et al. 2008b); in this respect, the calcaneocuboid facet resembles the condition seen in peramelemorphians (Szalay 1994), except that the dorsolateral part of the facet is more extensive medially in *Yalkaparidon*, extending along the anterior margin of the sustentaculum.

Species-Level Taxonomy

In their original description, Archer et al. (1988) identified two species of *Yalkaparidon*, *Y. coheni* and *Y. jonesi*. The species were distinguished by: (1) the presence in *Y. coheni* of two alveoli between the enlarged, procumbent i1 and the tooth that we identify here as m1 (Figs. 10f and 12b: **1a**, **2a**), whereas a true, edentulous diastema occupies this region in *Y. jonesi* (Figs. 10i and 12d); (2) the slightly larger size of *Y. coheni*. We now consider whether recognition of two species of *Yalkaparidon* still appears reasonable in the light of the larger sample of *Yalkaparidon* specimens now known from Riversleigh.

We observed possible polymorphism in P3 root number, with this tooth clearly double-rooted in some specimens (e.g., QM F13008 and F39986; Fig. 2: **P3a**), but possibly single rooted in others (e.g., QM F52754, F52755, and F36546). However, polymorphism in P3 root number has been reported in the extant dasyurid *Pseudantechinus mimulus* (see Woolley 2011), and variation in the number of premolar roots is observed in several other mammalian taxa (e.g., primates; Kupczik et al. 2005). As a result, we do not consider the apparent P3 variation seen in *Yalkaparidon* to be a basis for recognizing multiple species, particularly given the small size and probable limited functional significance of this tooth.

The holotype of *Y. coheni* (QM F13008) has two alveoli between i1 and m1, as do several additional specimens (e.g., QM F24361, F36543, F52759; Figs. 10f and 12b: **1a**, **2a**; Table 1), but *Yalkaparidon* mandibles with three prominent alveoli between i1 and m1 are now also known (e.g., QM F50794; Fig. 12a; Table 1), as are mandibles with a single alveolus in this region (e.g., QM F31370; Fig. 13c; Table 1). An additional tiny, anteriorly-directed alveolus immediately posterior to i1, possibly for i2, is also present in some

specimens (e.g., QM F20366; Fig. 12a; Table 1). QM F13009, the holotype of *Y. jonesi*, remains the only known *Yalkaparidon* mandible to entirely lack alveoli between i1 and m1 (Fig. 12d; Table 1). Collectively, these specimens may document a gradual anagenetic trend towards loss of the teeth between i1 and m1 within a single lineage, culminating in the true diastema seen in QM F13009.

The temporal distribution of *Yalkaparidon* mandibular specimens may support this hypothesis. QM F50794 (Fig. 12a; Table 1) is putatively the oldest known *Yalkaparidon* mandible, as it comes from Quantum Leap Site, which is usually considered to belong to Riversleigh Faunal Zone A (the oldest of the Riversleigh Faunal Zones, interpreted as late Oligocene in age; Archer et al. 1989, 1997; Travouillon et al. 2006), although it may in fact be part of Faunal Zone B (P. Creaser, pers. comm., June 2008; Travouillon et al. 2013). This specimen has three alveoli between i1 and m1, plus an additional alveolus that may be for i2 (Fig. 12a). QM F13009 (Figs. 10g–i and 12d; Table 1), the holotype of *Y. jonesi*, is the youngest known *Yalkaparidon* mandible, from the Riversleigh Faunal Zone C Gag Site (interpreted as middle Miocene in age; Archer et al. 1989, 1997; Travouillon et al. 2006), and is the only known specimen without alveoli between i1 and m1. The remaining mandibles currently known, in which the number of alveoli varies between one and four (including the tiny ?i2 alveolus), are all from Faunal Zone B sites, which are interpreted as early Miocene in age (Figs. 10a–f and 12b, c; Table 1; Archer et al. 1989, 1997; Travouillon et al. 2006). In a potentially parallel example, the extinct eutherian apatemyids, which may be ecological analogues of *Yalkaparidon* (Beck 2009), appear to show a gradual temporal trend towards the development of a diastema over the course of the Palaeogene, via reduction of p3 and p4 (West 1973).

An alternative interpretation for the differences in alveolus number in known mandibles of *Yalkaparidon* is that it reflects variation within a single species. Rates of dental abnormalities can be surprisingly high in marsupials: Archer's (1975) survey of dasyurids found that 18 % of *Sarcophilus harrisii* specimens and 26 % of *Planigale maculata* specimens examined showed some kind of dental abnormality, and Martin's (2007) study of the microbiotheriid *Dromiciops gliroides* and the caenolestids *Caenolestes fuliginosus* and *Rhyncholestes raphanurus* found that the frequency of anomalies ranged from 8.8 % in *D. gliroides* to 15 % in *C. fuliginosus* and 29.6 % in *R. raphanurus*. Significantly, most of the anomalies in *C. fuliginosus* and *R. raphanurus* reflect supernumerary or missing teeth in the region immediately posterior to the incisors; this is probably because these teeth are of limited importance in mastication (the upper and lower dentitions do not occlude in this region) and so are not under tight functional constraint. Archer (1975) also reported that the number of alveoli between i1 and p3 in the pseudocheirid *Pseudocheirus peregrinus* varied between one and three; in pseudocheirids, as in caenolestids, the teeth in this region do not contact the upper dentition during occlusion. Likewise, in *Yalkaparidon* it appears that the teeth present between i1 and m1 were non-functional or of minimal importance in mastication: these teeth could not have contacted the upper dentition (Fig. 1b), and in the one known mandible that preserves a complete tooth in this region (QM F52963; Fig. 11a, b), the tooth is extremely low-crowned and may even have failed to breach the gum. Thus, a single species of *Yalkaparidon* might be expected to exhibit a similarly high rate of supernumerary and missing teeth in the postincisive region as do the extant *C. fuliginosus* and *R. raphanurus*. However, whether this would extend to complete absence of teeth in this region, in which case QM F13009 could represent *Y. coheni* (rather than a second species *Y. jonesi*), is uncertain. By comparison, none of the *C. fuliginosus* or *R. raphanurus* specimens examined by Martin (2007) and none of the *P. peregrinus* specimens discussed by Archer (1975) entirely lack teeth in the region immediately posterior to the incisors.

The second criterion used by Archer et al. (1988) to distinguish *Y. coheni* from *Y. jonesi* is the slightly larger size of the former, based on comparison of the holotype mandibles of the two species (QM F13008 and F13009, repectively). However, several *Yalkaparidon* specimens with at least one alveolus between i1 and m1 overlap in dental dimensions and estimated body size with QM F13009 (Fig. 16, Table 1); thus, size is not an absolute criterion for distinguishing the two species recognized by Archer et al. (1988). The observed variation in size may reflect differences in the individual age of particular specimens. However, all known *Yalkaparidon* mandibles, including QM F36545 and F31370 (the two smallest known mandibles), exhibit alveoli for m4, indicating that this tooth (the last molar to erupt in marsupials) was fully erupted. CT-scans and dental X-rays of QM F36545 and F31370 also fail to indicate the presence of an unerupted p3 in either specimen (data not shown). Hence, all known *Yalkaparidon* mandibles appear to represent adults.

Other possible explanations for the variation in dental dimensions and estimated body mass include sexual dimorphism (although there is no clear evidence for a bimodal distribution of body sizes; Table 1) and "ordinary" intraspecific variation. If the very low body mass estimate (76.0 g; Table 1) for QM F31370 based on "total jaw length" is excluded, estimated body mass in *Yalkaparidon* ranges from 125 to 248.8 g. Estimated body mass for QM F13009, the holotype of *Y. jonesi*, is 183.7 g, i.e., close to the midpoint of the range seen in *Yalkaparidon* as a whole. A proportionally similar range in body mass is seen in extant *Dactylopsila* species, which may be modern ecological analogues of *Yalkaparidon* (see Beck 2009): body mass is 260–550 g in *D. palpator* and 280–470 g in *D. trivirgata* (Flannery 1994, 1995).

Plots of depth and mesiodistal width of i1 and labiolingual width and mesiodistal length of P3, M1–3, and m1–4 for

known *Yalkaparidon* specimens (Figs. 15 and 16) do not result in obviously discrete clusters that might represent different species. Specimens that lie outside the 95 % confidence ellipses appear to represent heavily worn teeth, the dimensions of which (particularly mesiodistal length) are almost certainly underestimates of their unworn size. The i1 and m1 dimensions of QM F13009 do not represent outliers (Fig. 16). There is no evidence for a relationship between dental dimensions and the relative age of different *Yalkaparidon* specimens (Figs. 15 and 16), assuming that Riversleigh Faunal Zones A, B, and C represent the late Oligocene, early Miocene, and middle Miocene, respectively (following Archer et al. 1989, 1997; Travouillon et al. 2006). Thus, there does not appear to have been a consistent trend regarding change in tooth size over time.

Is there any other source of morphological variation that might be of use in clarifying species boundaries within *Yalkaparidon*? Closely related fossil mammal species are usually distinguished by discrete dental characters, particularly characters of the molars. However, the dental morphology of *Yalkaparidon* is extremely simple compared to most other mammals (Figs. 5, 10, 11 and 12), and most isolated mandibles of *Yalkaparidon* are edentulous, with the molars in those mandibles that preserve them (including QM F13009, the holotype of *Y. jonesi*) often heavily worn. As a result, we have been unable to identify discrete, consistently identifiable dental characters that might be useful in determining species boundaries within *Yalkaparidon*. Furthermore, only one specimen, QM F13008, is known with associated partial upper and lower dentitions, of which only the incisors, a single upper (M3) and a single lower (m2) molar are preserved (Figs. 1, 2, 4, 10d–f and 12b). Thus, it seems impossible, at present, to determine whether isolated lower teeth and mandibles represent the same or different species as isolated upper teeth, premaxillae, and maxillae.

Collectively, these issues render attempts to determine species boundaries within *Yalkaparidon* extremely difficult, given the specimens currently available. We have elected to maintain the two species described by Archer et al. (1988), but we argue that the only diagnostic character that distinguishes the two is presence in of at least one alveolus between i1 and m1 in *Y. coheni* (Fig. 12a–c) versus complete absence of any alveoli in this region (i.e., presence of a true edentulous

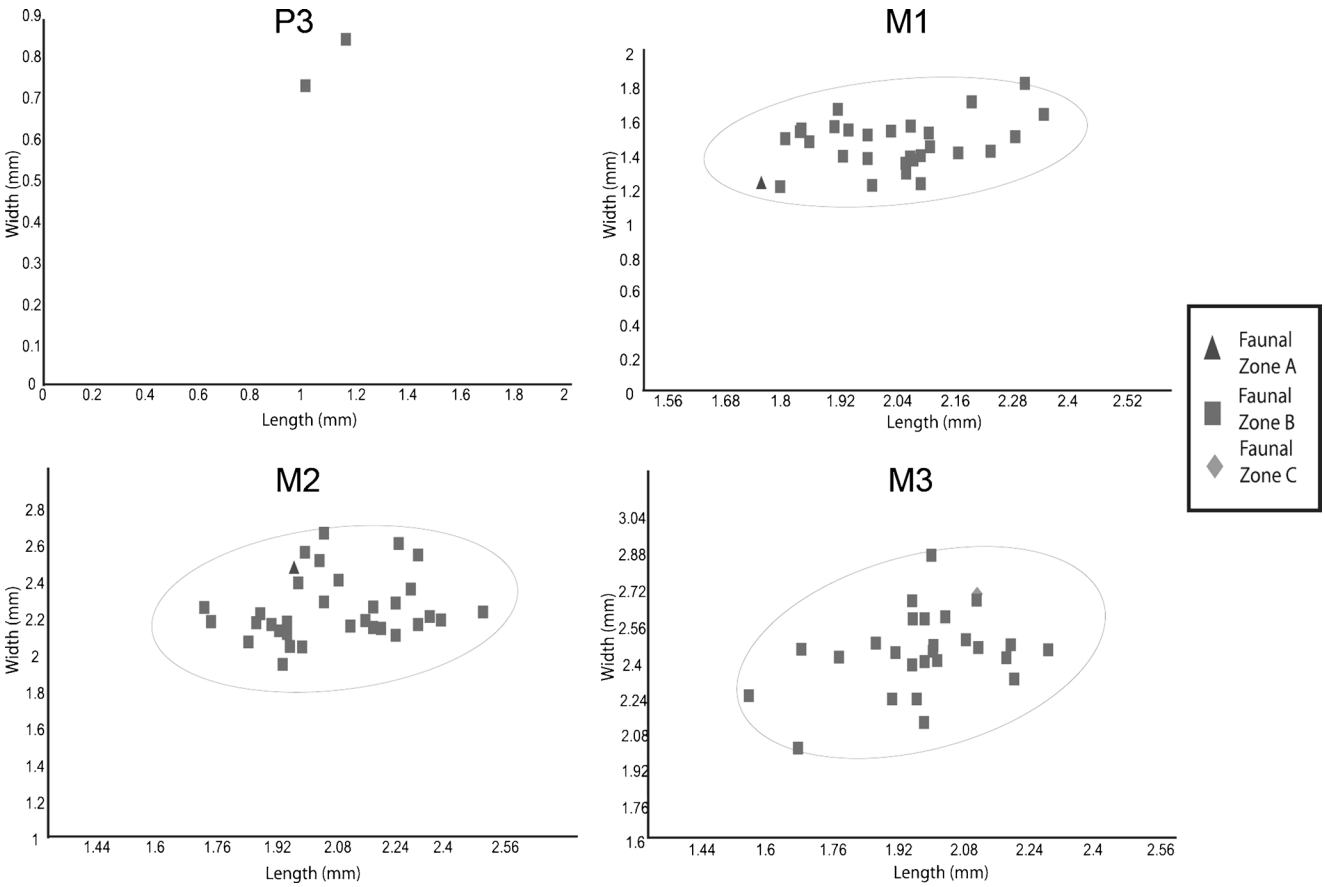

Fig. 15 Graphs of maximum labiolingual width against maximum mesiodistal length for P3 and M1-3 of *Yalkaparidon*. 95 % confidence ellipses (assuming a bivariate normal distribution) are shown, as calculated by PAST (Hammer et al. 2008). Symbols indicate whether specimens are from Riversleigh Faunal Zone A, B or C sites (see Archer et al. 1989, 1997; Travouillon et al., 2006). All specimens and raw measurements are listed in Electronic Supplementary Material

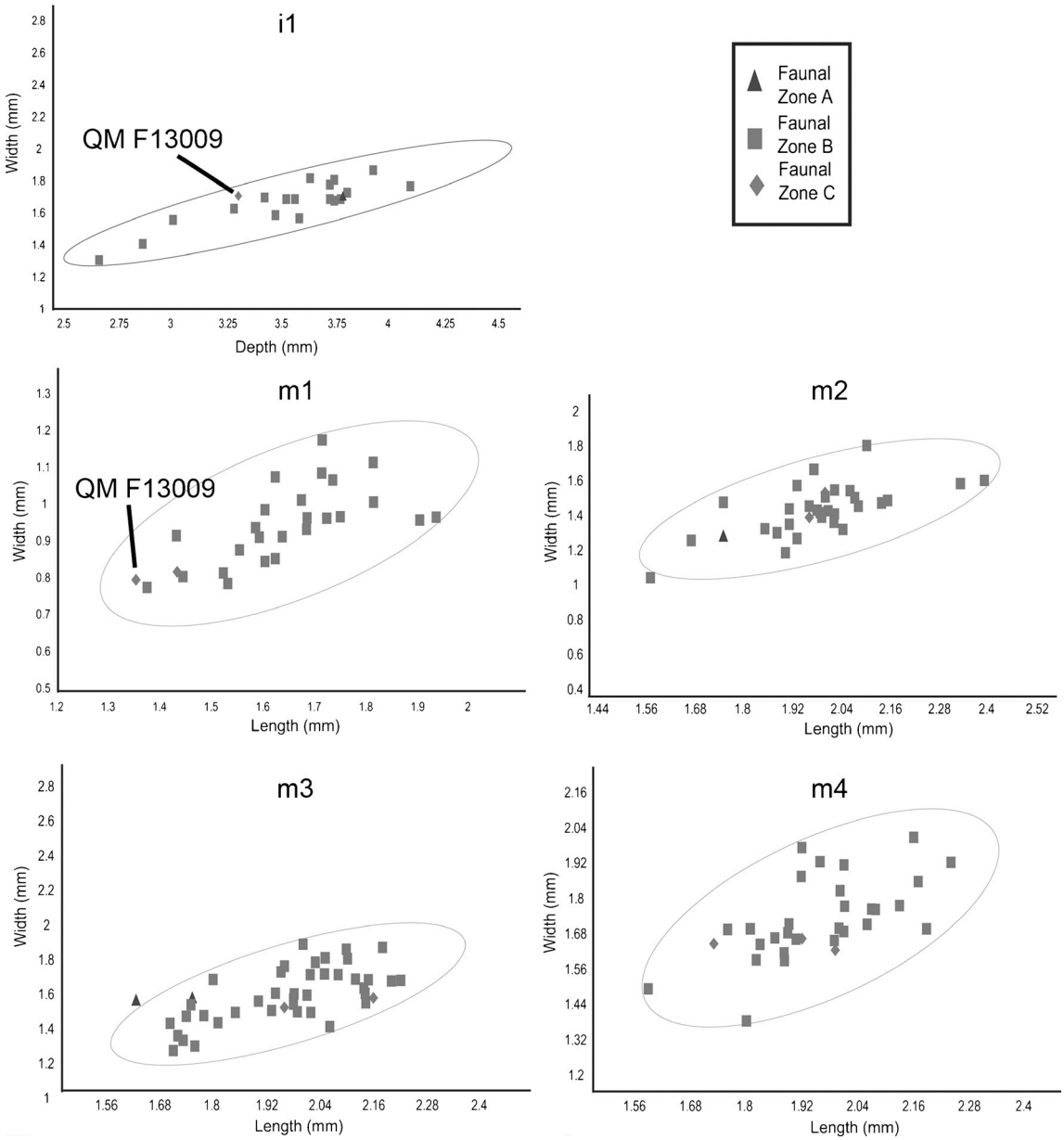

Fig. 16 Graphs of maximum mesiodistal width against depth of i1 at the alveolus (following Freeman and Lemen (2008) and maximum labiolingual width against maximum mesiodistal length for m1-4 of *Yalkaparidon*. 95 % confidence ellipses (assuming a bivariate normal distribution) are shown, as calculated by PAST (Hammer et al. 2008). Symbols indicate whether specimens are from Riversleigh Faunal Zone A, B, or C sites (see Archer et al. 1989, 1997; Travouillon et al., 2006). The i1 and m1 of QM F13009 (the holotype of *Y. jonesi*) are indicated. All specimens and raw measurements are listed in Electronic Supplementary Material

diastema) in *Y. jonesi* (Fig. 12d). Archer et al.'s (1988) use of size as a diagnostic character is not supported by the larger sample of specimens available to us here (Figs. 15 and 16; Table 1). We therefore refer all *Yalkaparidon* mandibles with at least one alveolus between i1 and m1 to *Y. coheni*. QM F13009, the only known mandible that entirely lacks alveoli between i1 and m1, represents *Y. jonesi*.

This approach means that only specimens preserving the postincisive region of the mandible can be identified to species level. We argue that all other specimens should be referred to *Yalkaparidon* sp. indet., pending the identification of additional diagnostic characters. As a result, the paratype of *Y. jonesi* (QM F13012, a right i1) and one of the paratypes of *Y. coheni* (QM F13011, a maxillary fragment with P3 and M2) listed by Archer et al. (1988) should now be considered as *Yalkaparidon* sp. indet. (see Electronic Supplementary Material). The discovery of *Yalkaparidon* specimens with associated upper and lower dentitions and with reasonably

complete cranial material (which might reveal the presence of significant non-dental variation) should permit a more confident resolution of the species-level taxonomy within the genus.

Functional Morphology and Paleoecology

The functional morphology and likely paleoecology of *Yalkaparidon* have been discussed at length by Beck (2009), who proposed that *Yalkaparidon* is a fourth example of a "mammalian woodpecker," after the strepsirhine primate *Daubentonia madagascarensis*, the petaurid possums *Dactylopsila* spp., and the fossil eutherian apatemyids (recently, the South American notoungulate *Hegetotherium mirabile* has been suggested to be a fifth such example; McCoy and Norris 2012). This conclusion was based on the presence of a number of unusual craniodental features in *Yalkaparidon*, particularly the combination of: (1) enlarged, hypselodont incisors, (2) cranial adaptations that appear to strengthen the skull against rostral bending, and (3) extremely zalambdodont, "self-sharpening" molars, which Beck (2009) suggested were a specific adaptation for feeding on soft-bodied invertebrates such as insect larvae.

Although we do not present a detailed functional analysis of the tarsal specimens tentatively referred to *Yalkaparidon* here, their overall morphology does not conflict with the hypothesis of Beck (2009), which was based solely on the craniodental anatomy of *Yalkaparidon*. The ridges and degree of angulation between the astragalotibial and astragalofibular facets of the astragalus (Figs. 13c and 14c) suggest that the upper ankle joint of *Yalkaparidon* was not as mobile as that of *Djarthia*, *Dromiciops*, and "possum-like" diprotodontians (Szalay 1994; Beck et al. 2008b), which may be evidence that *Yalkaparidon* was not a dedicated arborealist. However, the upper ankle joint morphology of *Yalkaparidon* does not approach the cursorially-adapted "mortise-and-tenon" condition of peramelemorphians and macropodoid diprotodontians, and also differs from these taxa in lacking a calcaneofibular facet (which would further stabilize the tarsus). There is only a narrow connection between the ectal and sustentacular facets in *Yalkaparidon*, resulting in a distinctly "pinched" CLAJP (Figs. 13b, d and 14b, d). This morphology is characteristic of peramelemorphians and macropodoids, and probably helps stabilize the lower ankle joint in these cursorial forms (Szalay 1994; Beck et al. 2008b; Beck 2012). However, the lower ankle joint of *Yalkaparidon* appears to have been highly mobile, given (1) the distally elongate sustentacular facet (Figs. 13b, d, f and 14b, d, f), (2) the small size of the (concave) ectal facet of the astragalus compared to the (convex) ectal facet of the calcaneus (Figs. 13b, d and 14b, d), and (3) the fact that the ectal and sustentacular facets are not transversely aligned as they are in peramelemorphians and macropodoids (Figs. 13b, d and 14b, d). Furthermore, the ectal and sustentacular facets of *Yalkaparidon* face dorsomedially (Figs. 13e and 14e), suggesting that the foot was habitually inverted, as in arboreal and scansorial metatherians (Muizon 1998; Beck 2012). By contrast, these facets face more dorsally in the cursorially-adapted peramelemorphians and macropodoids (Szalay 1994) and in the more terrestrial members of Didelphidae (e.g., *Metachirus* and *Monodelphis*; Argot 2002; Muizon and Argot 2003) and Dasyuromorphia (e.g., *Antechinomys* and *Thylacinus*; Szalay 1994: figs. 7.38E, 7.39E).

Thus, the tarsals of *Yalkaparidon* exhibit a combination of arboreal and scansorial/terrestrial adaptations: whereas the upper ankle joint was apparently less mobile than that of habitually arboreal metatherians, the lower ankle joint appears to have been able to accommodate considerable inversion and eversion. It should be noted that Beck's (2009) hypothesis that *Yalkaparidon* was a "mammalian woodpecker" is compatible with a partly terrestrial lifestyle for this taxon: *Dactylopsila palpator*, which shows the most extreme "mammalian woodpecker" adaptations of all *Dactylopsila* species, was reported by Flannery (1994, 1995) to be predominantly terrestrial in habits and to look "awkward and uncomfortable" when placed on narrow branches.

Results of Phylogenetic Analyses

The trees produced by the various phylogenetic analyses are shown in Figs. 17, 18 and 19. Although we present support values (bootstrap values, jackknife, values and decay indices for the maximum parsimony analyses; Bayesian posterior probabilities for the Bayesian analyses), it should be noted that the inclusion of more fossil taxa will typically reduce support for clades (Horovitz 1999; Asher 2005; Cobbett et al. 2007), particularly when these fossils are stem-taxa that subdivide long branches between clades that previously received high support values. As such, differences in support values should not necessarily be interpreted as evidence that a particular clade is more likely to be "correct" than another, but may (in some cases) be an artefact of differences in taxon sampling. Indeed, a major weakness in the analyses presented here is the limited sampling of fossil members of Australidelphia; an ongoing project (Voss and Beck, in prep.) will attempt to remedy these deficiencies.

Maximum parsimony analysis of the morphology-only matrix, with *Yalkaparidon* scored only for craniodental characters, recovers three most parsimonious trees of length 1105; the strict consensus of these is illustrated in Fig. 17a. *Yalkaparidon* is recovered as a member of a monophyletic Australidelphia (bootstrap=<50 %; jackknife=<50 %; DI=+1). The early Eocene Australian taxon *Djarthia* is sister to all other australidelphians including *Yalkaparidon* (bootstrap=<50 %; jackknife=<50 %; DI=+1), the supraordinal relationships of

which are unresolved. When the MP analysis of the morphology-only matrix was repeated including data on the tarsals that we tentatively refer to *Yalkaparidon*, six most parsimonious trees of length 1113 were recovered. The strict consensus of these is slightly more resolved than in the previous analysis (Fig. 17b): *Yalkaparidon* is recovered within Australidelphia (bootstrap=<50 %; jackknife=<50 %; DI=+1), *Djarthia* is sister to all other australidelphians (bootstrap=<50 %; jackknife=<50 %; DI=+1), and *Yalkaparidon* is sister to a clade comprising the five extant australidelphian orders (bootstrap=<50 %; jackknife=<50 %; DI=+1).

Bayesian analysis of the morphology-only matrix, with *Yalkaparidon* scored only for craniodental characters, resulted in a harmonic mean of the log likelihood of the post-burn-in trees of −3429.29. The 50 % majority rule consensus of the post-burn-in trees (i.e., excluding trees from the first 25 % of the 5×10^6 generations) is illustrated in Fig. 18a. Interordinal relationships are largely unresolved, but *Yalkaparidon* is recovered within Marsupialia, in a clade that also includes the four Australian orders, Paucituberculata, and the fossil australidelphian *Djarthia*, to the exclusion of Didelphimorphia. When character scores from the putative *Yalkaparidon* tarsals were included, Bayesian analysis of the morphology-only matrix resulted in a harmonic mean of the log likelihood of the post-burn-in trees of −3448.63. The 50 % majority rule consensus of the post-burn-in trees recovers the same interordinal relationships as when information from the putative *Yalkaparidon* tarsals was excluded (Fig. 18b).

Bayesian analysis of the total evidence matrix, with *Yalkaparidon* scored only for craniodental characters, resulted in a harmonic mean of the log likelihood of the post-burn-in trees of −62641.72. The 50 % majority rule consensus of the post-burn-in trees (i.e., excluding trees from the first 25 % of the 10×10^6 generations) is illustrated in Fig. 19a. The only interordinal relationship recovered within Marsupialia is *Dromiciops* + Diprotodontia (Bayesian posterior probability= 0.80). *Yalkaparidon* is placed in a large polytomy that also includes *Dromiciops* + Diprotodontia, the other extant marsupial orders, *Djarthia*, and the fossil metatherians *Herpetotherium* and Peradectidae. When character scores from the putative *Yalkaparidon* tarsals were included, Bayesian analysis of the total evidence matrix resulted in a harmonic mean of the log likelihood of the post-burn-in trees of −62655.55. The 50 % majority rule consensus of the post-burn-in trees recovers similar interordinal relationships as when information from the putative *Yalkaparidon* tarsals was excluded (Fig. 19b), but is slightly more resolved, with weak support (Bayesian posterior probability=0.54) for a clade comprising *Notoryctes*, dasyurids, and peramelids, i.e., the clade that we name here "Agreodontia" (see the "Taxonomy" section of "Materials and Methods"). *Yalkaparidon* is again placed in a large polytomy that includes the modern Australian marsupial orders, *Djarthia*, *Herpetotherium*, and Peradectidae.

Justification for Ordinal Status of Yalkaparidontia

Archer et al. (1988) argued that *Yalkaparidon* is most appropriately placed in its own order, Yalkaparidontia, based on the absence of convincing craniodental apomorphies linking it with any known metatherian order. The current study has also failed to find compelling apomorphies in either the skull or dentition that would unite *Yalkaparidon* with another order. Furthermore, *Yalkaparidon* is also characterized by a number of striking craniodental apomorphies—notably extreme zalambdodonty of the molars, rostral extension of the facial process of the maxilla, a transverse canal foramen posterior to the carotid foramen, and extreme robusticity of the entopterygoid crests—that are not seen in any other known metatherian and emphasize the distinctiveness of this taxon. The tarsal specimens that we have tentatively referred to *Yalkaparidon* also appear to represent a highly distinctive australidelphian taxon that cannot be easily placed within any known order. Bearing in mind the inherent arbitrary nature of taxonomic ranks, the apparent absence of compelling apomorphies linking *Yalkaparidon* with members of a known metatherian order, combined with its unique specializations, appear to justify ordinal status for this taxon.

This qualitative assessment of the craniodental and tarsal evidence is congruent with the results of our phylogenetic analyses (Figs. 17, 18 and 19). Maximum parsimony analyses of both versions of the morphology-only matrix (i.e., with character scores for the referred tarsals either included or excluded) recovered *Yalkaparidon* within Australidelphia, but without close relationships to any other australidelphian taxon (Fig. 17). Bayesian analyses of the same matrix were less resolved, placing *Yalkaparidon* within Marsupialia but without supporting specifically australidelphian affinities (Fig. 18). Finally, Bayesian analyses of both versions of the total evidence matrix are even less well resolved with regard to the relationships of *Yalkaparidon* (Fig. 19). It is notable that none of the analyses support a particularly close relationship between *Yalkaparidon* and either Diprotodontia or Notoryctemorphia. There is therefore currently no justification for including *Yalkaparidon* in either order (contra Marshall et al. 1990; Szalay 1994; Woodburne and Case 1996). Ultimately, confident resolution of the phylogenetic affinities of *Yalkaparidon* will require a much increased sampling of fossil and extant metatherians, particularly within Australidelphia (Voss and Beck, in prep.). Based on current evidence, we argue that the order Yalkaparidontia should continue to be recognized, and we present the following diagnosis, modified from that of Archer et al. (1988).

SYSTEMATIC PALEONTOLOGY

CLASS MAMMALIA LINNAEUS, 1758
SUBCLASS THERIA PARKER AND HASWELL, 1897

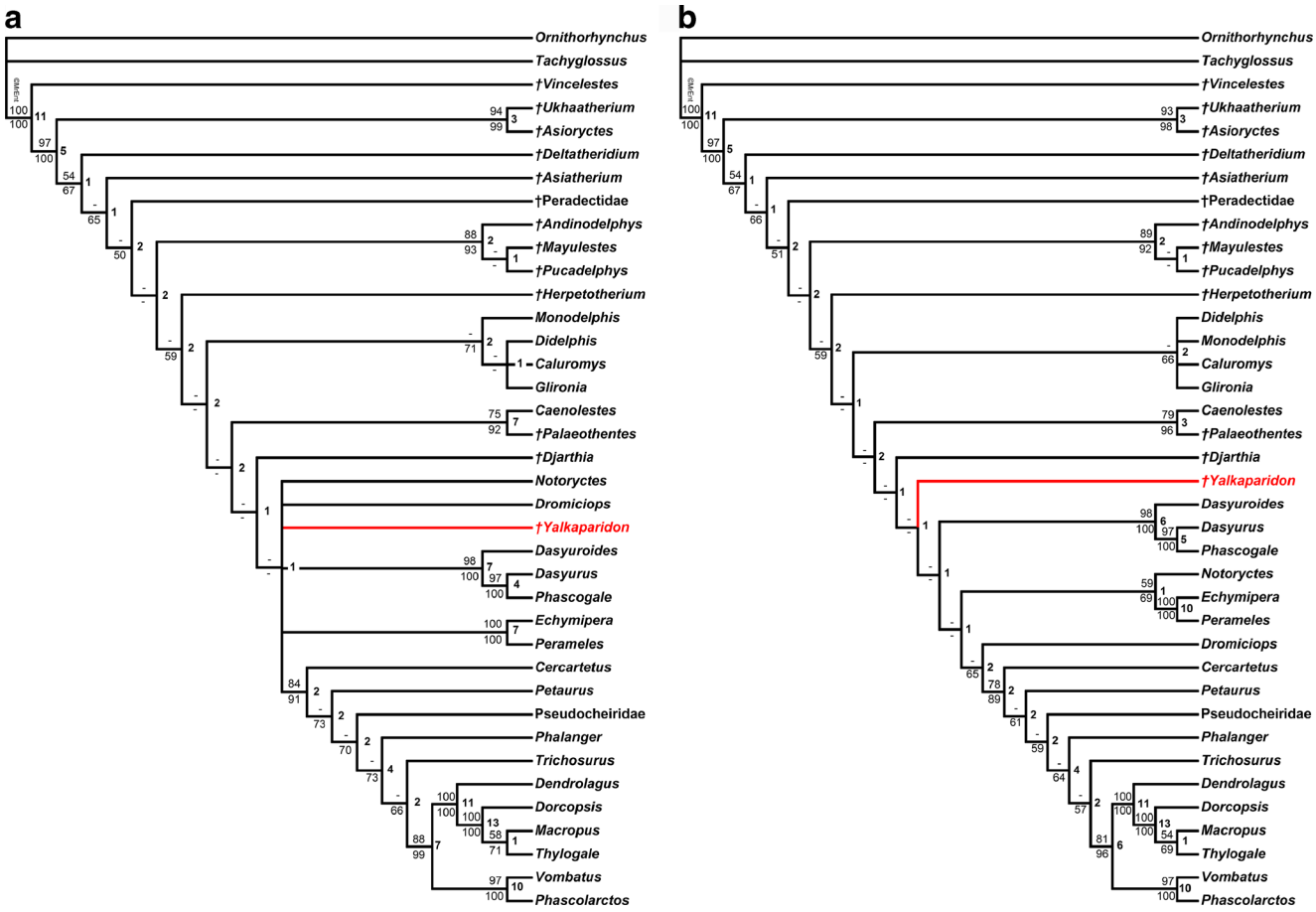

Fig. 17 Phylogenetic relationships of *Yalkaparidon* based on maximum parsimony analysis of the morphology-only matrix. **a** strict consensus of three most parsimonious trees (tree length=1105; consistency index excluding uninformative characters=0.402; retention index=0.644; rescaled consistency index=0.261) following maximum parsimony analysis of the morphology-only matrix with *Yalkaparidon* scored for craniodental characters only. **b** strict consensus of six most parsimonious trees (tree length=1113; consistency index excluding uninformative characters=0.400; retention index=0.642; rescaled consistency index=0.258) following maximum parsimony analysis of the morphology-only matrix with *Yalkaparidon* scored for both craniodental and tarsal characters. Numbers to the left of nodes and above branches represent bootstrap values of ≥50 % (based on 2000 bootstrap replicates); numbers to the left of nodes and below branches represent jackknife values (with 25 % deletion of characters); numbers to the right of nodes represent decay index values. Extinct taxa are identified by daggers. *Yalkaparidon* is indicated in *red* (electronic version) or *gray* (print version)

INFRACLASS METATHERIA HUXLEY, 1880

SUPERCOHORT MARSUPIALIA (ILLIGER, 1811) CUVIER, 1817

COHORT ?AUSTRALIDELPHIA SZALAY, 1982

ORDER YALKAPARIDONTIA ARCHER ET AL., 1988

DIAGNOSIS: That of Yalkaparidontidae until additional families are recognized.

FAMILY YALKAPARIDONTIDAE ARCHER ET AL., 1988

TYPE GENUS: *Yalkaparidon* Archer et al., 1988.

DIAGNOSIS: That of *Yalkaparidon* until additional genera are recognized.

GENUS *YALKAPARIDON* ARCHER ET AL., 1988

TYPE SPECIES: *Yalkaparidon coheni*, Archer et al., 1988.

INCLUDED SPECIES: *Yalkaparidon jonesi*, Archer et al., 1988.

DISTRIBUTION AND AGE: Riversleigh World Heritage Area, northwestern Queensland. *Yalkaparidon* is known from Riversleigh Faunal Zones A, B, and C, which are interpreted as late Oligocene, early Miocene, and middle Miocene in age, respectively (Archer et al. 1989, 1997; Travouillon et al. 2006).

REVISED DIAGNOSIS: *Yalkaparidon* differs from all other metatherians in the following combination of features: upper dental formula comprising I1–3, C1, P3, M1–4; lower dental formula comprising i1 (and possibly i2 in some specimens), between zero and three unicuspid teeth of uncertain homology, m1–4; hypselodont I1 and i1 with enamel restricted to anterolabial face; relatively enormous, procumbent i1; I2 and I3 without enamel; diastemata separating the I3 from C1 and C1 from P3; extreme zalambdodonty, with no trace of protocone on the upper molars or talonid on the lower molars;

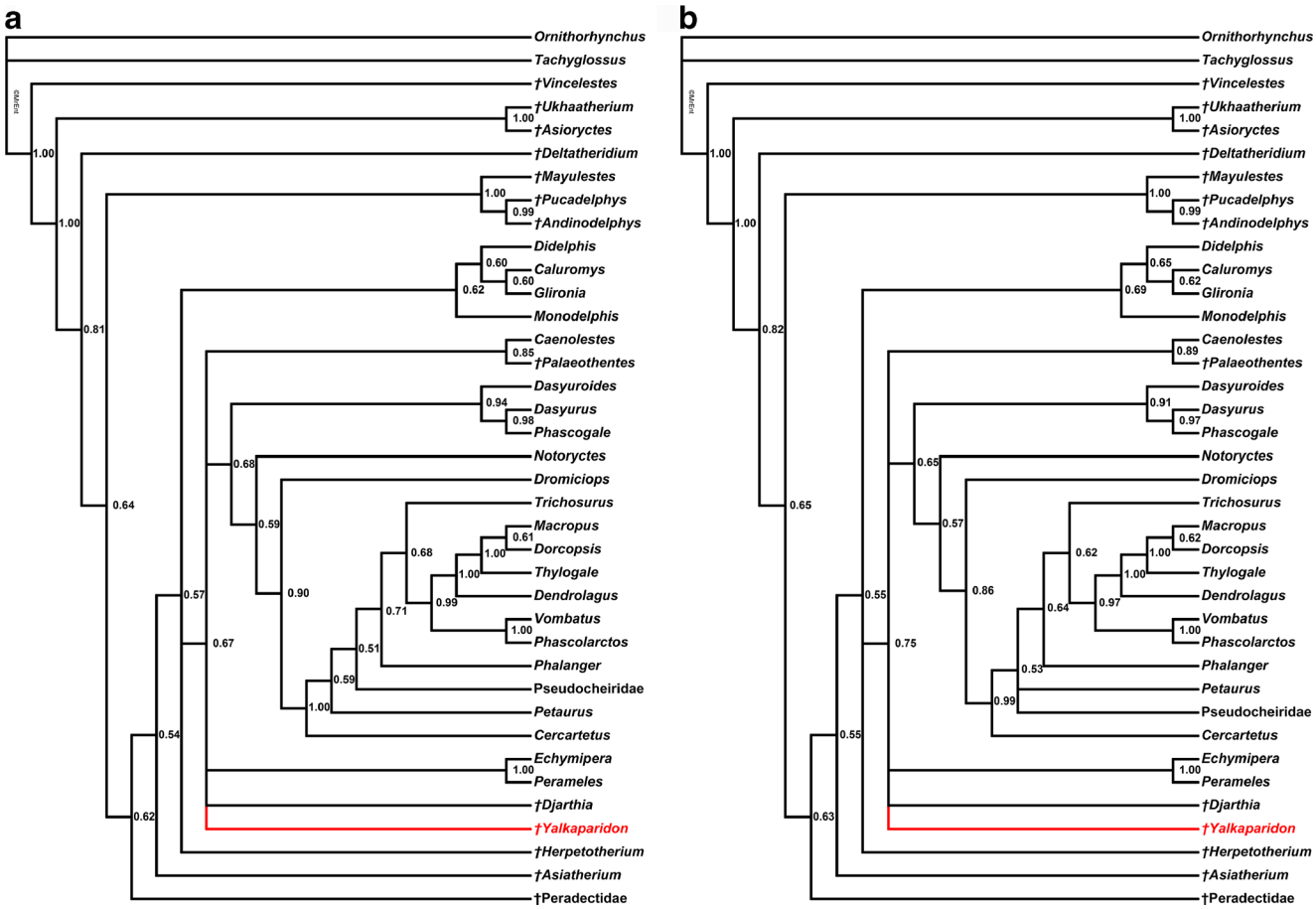

Fig. 18 Phylogenetic relationships of *Yalkaparidon* based on Bayesian analysis of the morphology-only matrix. Each analysis comprised two independent runs of 5×10^6 generations each, sampling trees every 500 generations. **a** 50 % majority rule consensus of post-burn-in trees (3.75×10^6 generations), with *Yalkaparidon* scored for craniodental characters only (harmonic mean of lnL across both runs=−3429.29). **b** 50 % majority rule consensus of post-burnin trees (3.75×10^6 generations), with *Yalkaparidon* scored for craniodental and tarsal characters (harmonic mean of lnL across both runs=−3448.63). Numbers to the right of nodes represent Bayesian posterior probabilities. Extinct taxa are identified by daggers. *Yalkaparidon* is indicated in *red* (electronic version) or *gray* (print version)

major cusp of the upper molars appears to be the metacone (i.e., the paracone has been lost); occlusal and labial surfaces of the upper molars and occlusal and lingual surfaces of the lower molars are entirely enamel-free; facial process of the maxilla with distinct rostroventral extension that overlaps the facial process of the premaxilla as far as I3; no squamosal epitympanic sinus; middle ear roofed only by alisphenoid and petrosal; alisphenoid hypotympanic sinus and small alisphenoid tympanic process present; rostral tympanic process of the petrosal crestlike and extends the entire length of the promontorium; primary foramen ovale between the alisphenoid and petrosal; transverse canal foramina posterior to the carotid foramina; entopterygoid crests very robust and extend far posteriorly; broad squamosal-alisphenoid contact; squamosal postglenoid process vestigial; ectotympanic not fused to the basicranium. If the tarsal specimens described here are correctly referred to *Yalkaparidon*, the diagnosis can be extended to encompass the following features of the tarsus: astragalus with astagalar canal; distinct ridges separating somewhat angled astragalotibial and astragalofibular facets; elongate neck; elongate sustentacular facet that extends onto the neck of the astragalus and extends the entire length of the sustentaculum of the calcaneus; proximal part of the ectal facet further proximal than the sustentacular facet; narrow connection between the ectal and sustentacular facets; calcaneus relatively elongate and slender; ectal facet of the calcaneus faces dorsomedially; no calcaneofibular facet; tripartite but weakly subdivided calcaneocuboid facet.

SPECIES *YALKAPARIDON COHENI* ARCHER ET AL., 1988

HOLOTYPE: QM F13008, a partial cranium and associated partial right mandible

PARATYPE: QM F13010, a partial right mandible.

TYPE LOCALITY: Camel Sputum Site, D-Site Plateau, Riversleigh World Heritage Area,, northwestern Queensland, Australia.

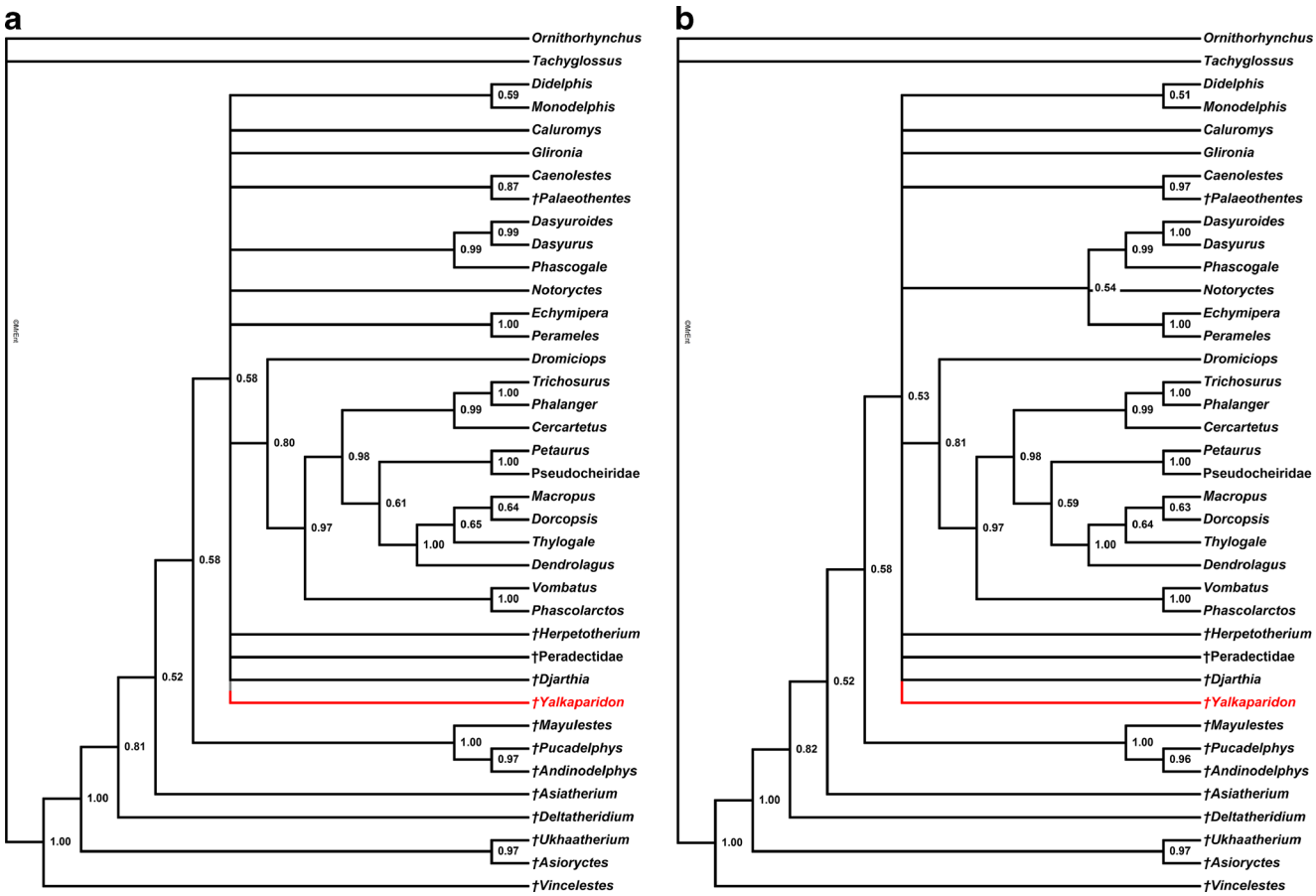

Fig. 19 Phylogenetic relationships of *Yalkaparidon* based on Bayesian analysis of the total evidence matrix. Each analysis comprised four independent runs of 10×10^6 generations each, sampling trees every 2000 generations. **a** 50 % majority rule consensus of post-burn-in trees (3.75×10^6 generations), with *Yalkaparidon* scored for craniodental characters only (harmonic mean of lnL across all four runs=−62641.72). **b** 50 % majority rule consensus of post-burnin trees (3.75×10^6 generations), with *Yalkaparidon* scored for craniodental and tarsal characters (harmonic mean of lnL across all four runs=−62655.55). Numbers to the right of nodes represent Bayesian posterior probabilities. Extinct taxa are identified by daggers. *Yalkaparidon* is indicated in *red* (electronic version) or *gray* (print version)

REFERRED SPECIMENS: see Table 1 and Electronic Supplementary Material.

DISTRIBUTION AND AGE: Riversleigh World Heritage Area, northwestern Queensland. A single *Y. coheni* specimen (QM F50794) is known from Quantum Leap Site, which may be part of Riversleigh Faunal Zone A (currently interpreted as late Oligocene in age) or may represent Faunal Zone B (P. Creaser, pers. comm., June 2008; Travouillon et al. 2013; currently interpreted as early Miocene in age). *Yalkaparidon coheni* is also known from the following Riversleigh Faunal Zone B sites: Camel Sputum Site, Creaser's Ramparts Site, Dirk's Towers Site, Inabeyance Site, Judith Horizontalis Site, Neville's Garden Site, Upper Site, and Wayne's Wok Site (see Table 1; Electronic Supplementary Material).

REVISED DIAGNOSIS: *Yalkaparidon coheni* differs from *Y. jonesi* in exhibiting at least one alveolus between i1 and m1.

NOTES: QM F13011 (a partial right maxilla) was listed as a paratype of *Y. coheni* by Archer et al. (1988) but cannot be unequivocally referred to the species under the revised diagnosis proposed here. Only *Yalkaparidon* specimens preserving the postincisive region of the mandible can be identified to species level; all other specimens (including QM F13011) should be considered as *Yalkaparidon* sp. indet.

SPECIES *YALKAPARIDON JONESI* ARCHER ET AL., 1988

HOLOTYPE: QM F13009, a partial right mandible with i1 and worn m1.

PARATYPE: none.

DISTRIBUTION AND AGE: Riversleigh World Heritage Area, northwestern Queensland. *Yalkaparidon jonesi* is represented by a single specimen (QM F13009) from Gag site, which is part of Riversleigh Faunal Zone C, and is currently interpreted as middle Miocene in age (see Table 1; Electronic Supplementary Material).

REVISED DIAGNOSIS: *Yalkaparidon jonesi* differs from *Y. coheni* in lacking any alveoli between i1 and m1.

NOTES: QM F13012 (an isolated M1) was listed as a paratype of *Y. jonesi* by Archer et al. (1988) but cannot be unequivocally referred to the species under the revised diagnosis presented here. Only *Yalkaparidon* specimens preserving the postincisive region of the mandible can be identified to species level; all other specimens (including QM F13012) should be considered as *Yalkaparidon* sp. indet.

Summary and Conclusions

The detailed description of the osteology of *Yalkaparidon* presented here corrects a number of errors (particularly regarding the dental formula) present in the original brief description by Archer et al. (1988) and provides new information on anatomical regions that are currently thought to be particularly phylogenetically informative, namely the dentition, basicranium, and tarsus. Nevertheless, we have not been able to confidently resolve the phylogenetic relationships of this taxon. Maximum parsimony analyses of morphology only suggest that *Yalkaparidon* is member of Australiadelphia (Fig. 17), but Bayesian analyses of morphology-only (Fig. 18) and of total evidence (Fig. 19) matrices are less resolved, suggesting only that *Yalkaparidon* is a probable crown-group marsupial. Nevertheless, the tarsal specimens we tentatively refer to *Yalkaparidon* exhibit characteristic australidelphian apomorphies, specifically the CLAJP and tripartite calcaneocuboid facet of the calcaneus (Szalay 1982, 1994; Beck et al. 2008b; Beck 2012); if these tarsals are correctly attributed, then *Yalkaparidon* would appear to be most likely a member of Australidelphia.

Confident resolution of the precise affinities of yalkaparidontians will probably require the discovery of plesiomorphic members of the order. It is possible that the engimatic Riversleigh taxon *Yingabalanara richardsoni* (see Archer et al. 1990) represents a plesiomorphic pre-zalambdodont yalkaparidontian, but *Yingabalanara* is currently known only from two isolated lower molars. Neither *Yalkaparidon* nor any potential close relatives have been found at any fossil site besides Riversleigh, and no fossils that might represent early yalkaparidontians have been identified from the early Eocene Tingamarra Local Fauna, which is the source of the only known Australian metatherians older than the late Oligocene (Godthelp et al. 1992, 1999; Archer et al. 1993; Beck et al. 2008b). There is also no clear evidence for yalkaparidontians in any South American fossil deposit. *Kiruwamaq chisu* (known from a single left upper molar from the ?Eocene Santa Rosa

Fig. 20 Life reconstruction of *Yalkaparidon coheni* by Filipe Martinho

fauna of Peru; Goin and Candela 2004) may represent a proto-zalambdodont metatherian that is in the process of losing the paracone; as such, it resembles the dental morphology expected in early yalkaparidontians prior to their evolution of fully zalambdodont molars. However, zalambdodonty has evolved multiple times within Theria (Asher et al. 2002; Asher and Sánchez-Villagra 2005; Seiffert et al. 2007) and the precise biogeographical links between the metatherian faunas of South America and Australia during the Cenozoic remain controversial (Woodburne and Case 1996; Goin 2003; Beck et al. 2008b; Beck 2012); thus, the relevance of *Kiruqamaq* (if any) to the origins of Yalkaparidontia cannot be confidently ascertained given current evidence. Regardless, given that the zalambdodont molars of *Yalkaparidon* are highly modified from a presumably fully tribosphenic ancestry, it may prove extremely difficult to identify more ancient, less specialized relatives of *Yalkaparidon* based on isolated dental specimens alone.

Ultimately, the origins of *Yalkaparidon* are likely to remain obscure without an enormous improvement in the quantity and quality of metatherian fossils known from Australia, Antarctica, and South America. Discovery of more of the skeleton (particularly the postcranium) of *Yalkaparidon* should also shed further light on its affinities, functional morphology, and paleobiology. Of particular interest, an associated postcranial skeleton of *Yalkaparidon* would reveal whether any of the manual digits are elongate, as would be expected if it was indeed a "mammalian woodpecker," as hypothesized by Beck (2009).

In its unusual morphology, absence of obvious close relatives, and uncertain phylogenetic relationships, *Yalkaparidon* (Fig. 20) resembles the recently described Australian fossil metatherian *Numbigilga ernielundeliusi* from the early Pliocene Bluff Downs Local Fauna (if the latter is not a highly derived peramelemorphian; Beck et al. 2008a). That two such distinctive taxa have been discovered so recently raises the prospect that equally distinctive fossil Cenozoic Australian metatherians will be found with future work. Undoubtedly, many more surprises await mammalian paleontologists working in Australia.

Acknowledgments Financial support for RMDB's research on *Yalkaparidon* has been provided by the Leverhulme Trust (via Study Abroad Studentship SAS/30110), Phil Creaser and the CREATE fund at the University of New South Wales (via a CREATE scholarship), the National Science Foundation (via grant DEB-0743039, in collaboration with Rob Voss at the American Museum of Natural History), and the Australian Research Council (via Discovery Early Career Researcher Award DE120100957). KJT is supported by the Robert Day Postdoctoral Fellowship at the University of Queensland. Additional support for research at Riversleigh has come from the Australian Research Council (DP0453262, LP0453664, LP0989969, and LP100200486 grants to MA), the XSTRATA Community Partnership Program (North Queensland), the University of New South Wales, Phil Creaser and the CREATE Fund, the Queensland National Parks and Wildlife Service, Environment Australia, the Queensland Museum, the Riversleigh Society Inc., Outback at Isa, Mount Isa City Council, and private supporters including K. and M. Pettit, E. Clark, M. Beavis, and M. Dickson. We also thank the hundreds of volunteers, staff and postgraduate students of the University of New South Wales who have assisted in field work at Riversleigh. We thank Drs Brook and Tveshor for x-raying several mandibles for us. We are grateful to the editor-in-chief John Wible and an anonymous reviewer for their thorough and constructive reviews.

References

Abello MA, Candela AM (2010) Postcranial skeleton of the Miocene marsupial *Palaeothentes* (Paucituberculata, Palaeothentidae): paleobiology and phylogeny. J Vertebr Paleontol 30:1515–1527

Amrine-Madsen H, Scally M, Westerman M, Stanhope MJ, Krajewski C, Springer MS (2003) Nuclear gene sequences provide evidence for the monophyly of australidelphian marsupials. Mol Phylogenet Evol 28:186–196

Aplin K, Archer M (1987) Recent advances in marsupial systematics with a new syncretic classification. In: Archer M (ed) Possums and Opossums: Studies in Evolution. Surrey Beatty & Sons, Sydney, pp xv–lxxii

Aplin KP (1987) Basicranial anatomy of the early Miocene diprotodontian *Wynyardia bassiana* (Marsupialia: Wynyardiidae) and its implications for wynyardiid phylogeny and classification. In: Archer M (ed) Possums and Opossums: Studies in Evolution. Surrey Beatty & Sons, Sydney, pp 369–391

Aplin KP (1990) Basicranial regions of diprotodontian marsupials: anatomy, ontogeny and phylogeny. Unpublished Ph. D. Thesis, University of New South Wales, School of Biological Sciences, 389 p

Aplin KP, Helgen KM, Lunde DP (2010) A review of *Peroryctes broadbenti*, the giant bandicoot of Papua New Guinea. Am Mus Novitates 3696:1–41

Archer M (1975) Abnormal dental development and its significance in dasyurids and other marsupials. Mem Queensland Mus 17:251–265

Archer M (1976) The basicranial region of marsupicarnivores (Marsupialia), inter-relationships of carnivorous marsupials, and affinities of the insectivorous marsupial peramelids. Zool J Linn Soc 59:217–322

Archer M (1978) The nature of the molar-premolar boundary in marsupials and a reinterpretation of the homology of marsupial cheek teeth. Mem Queensland Mus 18:157–164

Archer M (1984a) The Australian marsupial radiation. In: Archer M, Clayton G (eds) Vertebrate Zoogeography and Evolution in Australasia. Hesperian Press, Perth, pp 633–808

Archer M (1984b) Origins and early radiations of marsupials. In: Archer M, Clayton G (eds) Vertebrate Zoogeography and Evolution in Australasia. Hesperian Press, Perth, pp 585–631

Archer M, Beck R, Gott M, Hand S, Godthelp H, Black K (2011) Australia's first fossil marsupial mole (Notoryctemorphia) resolves controversies about their evolution and palaeoenvironmental origins. Proc R Soc B 278:1498–1506

Archer M, Every RG, Godthelp H, Hand S, Scally K (1990) Yingabalanaridae, a new family of enigmatic mammals from Tertiary deposits of Riversleigh, northwestern Queensland. Mem Queensland Mus 28:193–202

Archer M, Godthelp H, Hand SJ (1993) Early Eocene marsupial from Australia. Kaupia 3:193–200

Archer M, Godthelp H, Hand SJ, Megirian D (1989) Fossil mammals of Riversleigh, northwestern Queensland: preliminary overview of biostratigraphy, correlation and environmental change. Australian Zool 25:29–65

Archer M, Hand S, Godthelp H (1988) A new order of Tertiary zalambdodont marsupials. Science 239:1528–1531

Archer M, Hand SJ, Godthelp H, Creaser P (1997) Correlation of the Cainozoic sediments of the Riversleigh World Heritage fossil property, Queensland, Australia. In: Aguilar J-P, Legendre S, Michauz J

(eds) Actes du Congrès BiochroM'97. École Pratique des Hautes Études, Institut de Montpellier, Montpellier, pp 131–152
Archer M, Kirsch JAW (2006) The evolution and classification of marsupials. In: Armati PJ, Dickman CR, Hume ID (eds) Marsupials. Cambridge University Press, New York, pp 1–21
Arena DA, Archer M, Godthelp H, Hand SJ, Hocknull S (2011) Hammer-toothed 'marsupial skinks' from the Australian Cenozoic. Proc R Soc B 278:3529–3533
Argot C (2002) Functional-adaptive analysis of the hindlimb anatomy of extant marsupials and the paleobiology of the Paleocene marsupials *Mayulestes ferox* and *Pucadelphys andinus*. J Morph 253:76–108
Asher RJ (2005) Insectivoran-grade placental mammals: character evolution and fossil history. In: Rose KD, Archibald JD (eds) The Rise of Placental Mammals: Origins and Relationships of the Major Clades. Johns Hopkins University Press, Baltimore, pp 50–70
Asher RJ, Horovitz I, Martin T, Sánchez-Villagra MR (2007) Neither a rodent nor a platypus: a reexamination of *Necrolestes patagonensis* Ameghino. Am Mus Novitates 3546:1–40
Asher RJ, Horovitz I, Sánchez-Villagra MR (2004) First combined cladistic analysis of marsupial mammal interrelationships. Mol Phylogenet Evol 33:240–250
Asher RJ, McKenna MC, Emry RJ, Tabrum AR, Kron DG (2002) Morphology and relationships of *Apternodus* and other extinct, zalambdodont, placental mammals. Bull Am Mus Nat Hist 273:1–117
Asher RJ, Sánchez-Villagra MR (2005) Locking yourself out: diversity among dentally zalambdodont therian mammals. J Mammal Evol 12:265–282
Averianov AO, Martin T, Lopatin AV (2013) A new phylogeny for basal Trechnotheria and Cladotheria and affinities of South American endemic Late Cretaceous mammals. Naturwissenschaften 100:311–326
Baker ML, Wares JP, Harrison GA, Miller RD (2004) Relationships among the families and orders of marsupials and the major mammalian lineages based on recombination activating gene-1. J Mammal Evol 11:1–16
Beck RMD (2008) A dated phylogeny of marsupials using a molecular supermatrix and multiple fossil constraints. J Mammal 89:175–189
Beck RMD (2009) Was the Oligo-Miocene Australian metatherian *Yalkaparidon* a 'mammalian woodpecker'? Biol J Linn Soc 97:1–17
Beck RMD (2012) An 'ameridelphian' marsupial from the early Eocene of Australia supports a complex model of Southern Hemisphere marsupial biogeography. Naturwissenschaften 99:715–729
Beck RMD, Archer M, Godthelp H, Mackness BS, Hand SJ, Muirhead J (2008a) A bizarre new family of Marsupialia (*incertae sedis*) from the early Pliocene of northeastern Australia: implications for the phylogeny of bunodont marsupials. J Paleontol 82:749–762
Beck RMD, Godthelp H, Weisbecker V, Archer M, Hand SJ (2008b) Australia's oldest marsupial fossils and their biogeographical implications. PLoS ONE 3:e1858
Bremer K (1988) The limits of amino acid sequence data in angiosperm phylogenetic reconstruction. Evolution 42:795–803
Burk A, Westerman M, Kao DJ, Kavanagh JR, Springer MS (1999) An analysis of marsupial interordinal relationships based on 12S rRNA, tRNA valine, 16S rRNA, and cytochrome b sequences. J Mammal Evol 6:317–334
Cartmill M (1974) *Daubentonia*, *Dactylopsila*, woodpeckers, and klinorhynchy. In: Martin RD, Doyle GA, Walker AC (eds) Prosimian Biology. Gerald Duckworth and Co. Ltd., London, pp 655–670
Chimento NR, Agnolin FL, Novas FE (2012) The Patagonian fossil mammal *Necrolestes*: a Neogene survivor of Dryolestoidea. La Revista del Museo Argentino de Ciencias Naturales, new series 14:261–306
Cobbett A, Wilkinson M, Wills MA (2007) Fossils impact as hard as living taxa in parsimony analyses of morphology. Syst Biol 56:753–766
Crosby K, Norris CA (2003) Periotic morphology in the trichosurin possums *Strigocuscus celebensis* and *Wyulda squamicaudata* (Diprotodontia, Phalangeridae) and a revised diagnosis of the tribe Trichosurini. Am Mus Novitates 3414:1–14
Crosby KML (2002) Studies in the diversity and evolution of phalangeroid possums (Marsupialia; Phalangerida; Phalangeroidea). Unpublished Ph.D. Thesis, University of New South Wales
Davis BM (2007) A revision of "pediomyid" marsupials from the Late Cretaceous of North America. Acta Palaeontol Pol 52:217–256
Evans HE (1993) Miller's Anatomy of the Dog. W.B. Saunders, Philadelphia
Felsenstein J (1985) Confidence limits on phylogenies: an approach using the bootstrap. Evolution 39:783–791
Filan SL (1990) Myology of the head and neck of the bandicoot (Marsupialia : Peramelemorphia). Australian J Zool 38:617–634
Flannery TF (1994) Possums of the World: a Monograph of the Phalangeroidea. GEO Productions and the Australian Museum, Sydney
Flannery TF (1995) Mammals of New Guinea. Reed Books, Chatswood, NSW
Flynn JJ, Wyss AR (1999) New marsupials from the Eocene-Oligocene transition of the Andean Main Range, Chile. J Vertebr Paleontol 19:533–549
Flynn JJ, Wyss AR (2004) A polydolopine marsupial skull from the Cachapoal Valley, Andean Main Range, Chile. Bull Am Mus Nat Hist 285:80–92
Forasiepi AM (2009) Osteology of *Arctodictis sinclairi* (Mammalia, Metatheria, Sparassodonta) and phylogeny of Cenozoic metatherian carnivores from South America. Monografias del Museo Argentino de Ciencias Naturales 6:1–174
Fox RC, Naylor BG (2006) Stagodontid marsupials from the Late Cretaceous of Canada and their systematic and functional implications. Acta Palaeontol Pol 51:13–36
Freeman PW, Lemen CA (2008) A simple morphological predictor of bite force in rodents. J Zool 275:418–422
Gaudin TJ, Wible JR, Hopson JA, Turnbull WD (1996) Reexamination of the morphological evidence for the cohort Epitheria (Mammalia, Eutheria). J Mammal Evol 3:31–79
Gelfo JN, Lorente M (2012) The alleged astragalar remains of *Didolodus* Ameghino, 1897 (Mammalia, Panameriungulata) and a critic of isolated bone association models. Bull Geosci 87:249–259
Giannini NP, Wible JR, Simmons NB (2006) On the cranial osteology of Chiroptera. I. *Pteropus* (Megachiroptera: Pteropodidae). Bull Am Mus Nat Hist 295:1–134
Godthelp H, Archer M, Cifelli RL, Hand SJ, Gilkeson CF (1992) Earliest known Australian Tertiary mammal fauna. Nature 356:514–516
Godthelp H, Wroe S, Archer M (1999) A new marsupial from the early Eocene Tingamarra Local Fauna of Murgon, southeastern Queensland: a prototypical Australian marsupial? J Mammal Evol 6:289–313
Goin FJ (2003) Early marsupial radiations in South America. In: Jones M, Dickman C, Archer M (eds) Predators with Pouches: the Biology of Carnivorous Marsupials. CSIRO Publishing, Collingwood, pp 30–42
Goin FJ, Candela AM (2004) New Paleogene marsupials from the Amazon Basin of eastern Peru. In: Campbell Jr KE (ed) The Paleogene Mammalian Fauna of Santa Rosa, Amazonian Peru. Natural History Museum of Los Angeles County, Science Series 40, Los Angeles, pp 15–60
Gregory WK (1910) The orders of mammals. Bull Am Mus Nat Hist 27:1–524
Hammer Ø, Harper DAT, Ryan PD (2008) PAST - Palaeontological Statistics, ver. 1.81
Hershkovitz P (1982) The staggered marsupial lower third incisor (I_3). Geobios mem spec 6:191–200
Hershkovitz P (1995) The staggered marsupial third lower incisor: hallmark of cohort Didelphimorphia, and description of a new genus and species with staggered i3 from the Albian (Lower Cretaceous) of Texas. Bonner Zool Beitrage 45:153–169

Hooker JJ (2001) Tarsals of the extinct insectivoran family Nyctitheriidae (Mammalia): evidence for archontan relationships. Zool J Linn Soc 132:501–529

Horovitz I (1999) A phylogenetic study of living and fossil platyrrhines. Am Mus Novitates 1–40

Horovitz I, Ladevèze S, Argot C, Macrini TE, Martin T, Hooker JJ, Kurz C, de Muizon C, Sánchez-Villagra MR (2008) The anatomy of *Herpetotherium* cf. *fugax* Cope, 1873, a metatherian from the Oligocene of North America. Palaeontographica Abt A 284:109–141

Horovitz I, Martin T, Bloch J, Ladevèze S, Kurz C, Sánchez-Villagra MR (2009) Cranial anatomy of the earliest marsupials and the origin of opossums. PLoS ONE 4:e8278

Horovitz I, Sánchez-Villagra MR (2003) A morphological analysis of marsupial mammal higher-level phylogenetic relationships. Cladistics 19:181–212

Kear BP, Archer M, Flannery TF (2001a) Bulungamayine (Marsupialia: Macropodoidea) postcranial remains from the late Miocene of Riversleigh, northwestern Queensland. Mem Assoc Australasian Palaeontol 25:103–122

Kear BP, Archer M, Flannery TF (2001b) Postcranial morphology of *Ganguroo bilamina* Cooke, 1997 (Marsupialia: Macropodidae) from the middle Miocene of Riversleigh, northwestern Queensland. Mem Assoc Australasian Palaeontol 25:123–138

Kear BP, Cooke BN, Archer M, Flannery TF (2007) Implications of a new species of the Oligo-Miocene kangaroo (Marsupialia: Macropodoidea) *Nambaroo*, from the Riversleigh World Heritage Area, Queensland, Australia. J Paleontol 81:1147–1167

Kemp TS (2005) The Origin and Evolution of Mammals. Oxford University Press, Oxford

Kielan-Jaworowska Z, Cifelli RL, Luo Z-X (2004) Mammals from the Age of Dinosaurs: Origins, Evolution, and Structure. Columbia University Press, New York

Kirsch JAW, Lapointe FJ, Springer MS (1997) DNA-hybridization studies of marsupials and their implications for metatherian classification. Australian J Zool 45:211–280

Koenigswald W von (1990) Die Paläobiologie der Apatemyiden (Insectivora s.l.) und die Ausdeutung der Skelettfunde von *Heterohyus nanus* aus dem Mitteleozän von Messel bei Darmstadt. Palaeontographica Abt A 210:41–77

Kupczik K, Spoor F, Pommert A, Dean MC (2005) Premolar root number variation in hominoids: genetic polymorphism vs. functional significance In: Zadzinska E (ed) Current Trends in Dental Morphology Research. University of Lodz Press, Lodz, pp 257–268

Ladevèze S (2004) Metatherian petrosals from the late Paleocene of Itaboraí (Brazil), and their phylogenetic implications. J Vertebr Paleontol 24:202–213

Ladevèze S (2007) Petrosal bones of metatherian mammals from the late Palaeocene of Itaboraí (Brazil), and a cladistic analysis of petrosal features in metatherians. Zool J Linn Soc 150:85–115

Ladevèze S, Asher RJ, Sánchez-Villagra MR (2008) Petrosal anatomy in the fossil mammal *Necrolestes*: evidence for metatherian affinities and comparisons with the extant marsupial mole. J Anat 213:686–697

Ladevèze S, Muizon C de (2007) The auditory region of early Paleocene Pucadelphydae (Mammalia, Metatheria) from Tiupampa, Bolivia, with phylogenetic implications. Palaeontol 50:1123–1154

Ladevèze S, Muizon C de (2010) Evidence of early evolution of Australidelphia (Metatheria, Mammalia) in South America: phylogenetic relationships of the metatherians from the late Palaeocene of Itaboraí (Brazil) based on teeth and petrosal bones. Zool J Linn Soc 159:746–784

Lanfear R, Calcott B, Ho SY, Guindon S (2012) Partitionfinder: combined selection of partitioning schemes and substitution models for phylogenetic analyses. Mol Biol Evol 29:1695–1701

Lester KS, Archer M, Gilkeson CF, Rich T (1988) Enamel of *Yalkaparidon coheni*: representative of a distinctive order of Tertiary zalambdodont marsupials. Scanning Microscopy 2:1491–1501

Lewis PO (2001) A likelihood approach to estimating phylogeny from discrete morphological character data. Syst Biol 50:913–925

Long JA, Archer M, Flannery TF, Hand SJ (2002) Prehistoric Mammals of Australia and New Guinea: One Hundred Million Years of Evolution. UNSW Press, Sydney

Luckett WP (1993) An ontogenetic assessment of dental homologies in therian mammals. In: Szalay FS, Novacek MJ, McKenna MC (eds) Mammal Phylogeny, Volume 1: Mesozoic Differentiation, Multituberculates, Monotremes, Early Therians, and Marsupials. Springer Verlag, New York, pp 182–204

Luo Z-X, Ji Q, Wible JR, Yuan C-X (2003) An Early Cretaceous tribosphenic mammal and metatherian evolution. Science 302:1934–1940

Maga AM (2008) Systematic paleontological investigation of the metatherian fauna from the Paleogene Uzunçarşıdere Formation, Central Turkey, Unpublished Ph. D. Thesis, The University of Texas at Austin

Marshall LG (1982) Systematics of the extinct South American marsupial family Polydolopidae. Fieldiana Geol 12:1–109

Marshall LG, Case JA, Woodburne MO (1990) Phylogenetic relationships of the families of marsupials. Current Mammal 2:433–505

Marshall LG, Muizon C de (1995) *Pucadelphys andinus* (Marsupialia, Mammalia) from the early Paleocene of Bolivia. Mem Mus Natl d'Hist Nat 165:1–164

Marshall LG, Sigogneau-Russell D (1995) Postcranial skeleton. In: Muizon C de (ed) *Pucadelphys andinus* (Marsupialia, Mammalia) from the early Palaeocene of Bolivia. Mem Mus Natl d'Hist Nat 165:91–164

Martin GM (2007) Dental anomalies in *Dromiciops gliroides* (Microbiotheria, Microbiotheriidae), *Caenolestes fuliginosus* and *Rhyncholestes raphanurus* (Paucituberculata, Caenolestidae). Revista Chilena de Historia Natural 80:393–406

McCoy DE, Norris CA (2012) The cranial anatomy of the Miocene notoungulate *Hegetotherium mirabile* (Notoungulata, Hegetotheriidae) with preliminary observations on diet and method of feeding. Bull Peabody Mus Nat Hist 53:355–374

McKenna MC, Bell SK (1997) Classification of Mammals Above the Species Level. Columbia University Press, New York

Meredith RW, Janecka JE, Gatesy J, Ryder OA, Fisher CA, Teeling EC, Goodbla A, Eizirik E, Simao TL, Stadler T, Rabosky DL, Honeycutt RL, Flynn JJ, Ingram CM, Steiner C, Williams TL, Robinson TJ, Burk-Herrick A, Westerman M, Ayoub NA, Springer MS, Murphy WJ (2011) Impacts of the Cretaceous Terrestrial Revolution and KPg extinction on mammal diversification. Science 334:521–524

Meredith RW, Krajewski C, Westerman M, Springer MS (2009a) Relationships and divergence times among the orders and families of Marsupialia. Mus North Ariz Bull 65:383–406

Meredith RW, Westerman M, Case JA, Springer MS (2008) A phylogeny and timescale for marsupial evolution based on sequences for five nuclear genes. J Mammal Evol 15:1–36

Meredith RW, Westerman M, Springer MS (2009b) A phylogeny of Diprotodontia (Marsupialia) based on sequences for five nuclear genes. Mol Phylogenet Evol 51:554–571

Muirhead J (1994) Systematics, evolution and palaeobiology of recent and fossil bandicoots (Marsupialia: Peramelemorphia). Unpublished Ph.D. Thesis, University of New South Wales

Muirhead J (2000) Yaraloidea (Marsupialia, Peramelemorphia), a new superfamily of marsupial and a description and analysis of the cranium of the Miocene of *Yarala burchfieldi*. J Paleontol 74:512–523

Muirhead J, Wroe S (1998) A new genus and species, *Badjcinus turnbulli* (Thylacinidae: Marsupialia), from the late Oligocene of Riversleigh, northern Australia, and an investigation of thylacinid phylogeny. J Vertebr Paleontol 18:612–626

Muizon C de (1998) *Mayulestes ferox*, a borhyaenoid (Metatheria, Mammalia) from the early Palaeocene of Bolivia: phylogenetic and palaeobiologic implications. Geodiversitas 20:19–142

Muizon C de (1999) Marsupial skulls from the Deseadan (late Oligocene) of Bolivia and phylogenetic analysis of the Borhyaenoidea (Marsupialia, Mammalia). Geobios 32:483–509

Muizon C de, Argot C (2003) Comparative anatomy of the Tiupampa didelphimorphs: an approach to locomotory habits of early marsupials. In: Jones M, Dickman C, Archer M (eds) Predators with Pouches: the Biology of Carnivorous Marsupials. CSIRO Publishing, Collingwood, pp 43–62

Müller K (2005) SeqState—primer design and sequence statistics for phylogenetic DNA data sets. Applied Bioinformatics 4:65–69

Murray P, Wells R, Plane M (1987) The cranium of the Miocene thylacoleonid, *Wakaleo vanderleuri*: click go the shears—a fresh bite at thylacoleonid systematics. In: Archer M (ed) Possums and Opossums: Studies in Evolution. Surrey Beatty & Sons, pp 433–466

Murray PF, Megirian D (2006) The Pwerte Marnte Marnte Local Fauna: a new vertebrate assemblage of presumed Oligocene age from the Northern Territory of Australia. Alcheringa Spec Iss 1:211–228

Myers TJ (2001) Marsupial body mass prediction. Australian J Zool 49:99–118

Nilsson MA, Arnason U, Spencer PBS, Janke A (2004) Marsupial relationships and a timeline for marsupial radiation in South Gondwana. Gene 340:189–196

Nilsson MA, Churakov G, Sommer M, Tran NV, Zemann A, Brosius J, Schmitz J (2010) Tracking marsupial evolution using archaic genomic retroposon insertions. PLoS Biology 8:e1000436

Osgood WH (1921) A monographic study of the American marsupial *Caenolestes*. Field Mus Nat Hist Zool Ser 14:1–162

Phillips MJ, McLenachan PA, Down C, Gibb GC, Penny D (2006) Combined mitochondrial and nuclear DNA sequences resolve the interrelations of the major Australasian marsupial radiations. Syst Biol 55:122–137

Pledge NS (2005) The Riversleigh wynyardiids. Mem Queensland Mus 51:135–169

Ride WDL (1962) On the evolution of Australian marsupials. In: Leeper GW (ed) The Evolution of Living Organisms. Melbourne University Press, Melbourne, pp 281–306

Ronquist F, Huelsenbeck JP, van der Mark P (2005) MrBayes 3.1 manual

Ronquist F, Teslenko M, van der Mark P, Ayres DL, Darling A, Hohna S, Larget B, Liu L, Suchard MA, Huelsenbeck JP (2012) MrBayes 3.2: efficient Bayesian phylogenetic inference and model choice across a large model space. Syst Biol 61:539–542

Rougier GW, Wible JR (2006) Major changes in the ear region and basicranium of early mammals. In: Carrano MT, Gaudin TJ, Blob RW, Wible JR (eds) Amniote Paleobiology: Perspectives on the Evolution of Mammals, Birds, and Reptiles. The University of Chicago Press, Chicago, pp 269–311

Rougier GW, Wible JR, Beck RM, Apesteguia S (2012) The Miocene mammal *Necrolestes* demonstrates the survival of a Mesozoic nontherian lineage into the late Cenozoic of South America. Proc Natl Acad Sci USA 109:20053–20058

Rougier GW, Wible JR, Novacek MJ (1998) Implications of *Deltatheridium* specimens for early marsupial history. Nature 396:459–463

Rowe TB, Eiting TP, Macrini TE, Ketcham RA (2005) Organization of the olfactory and respiratory skeleton in the nose of the gray short-tailed opossum *Monodelphis domestica*. J Mammal Evol 12:303–336

Salton JA (2005) Evolutionary morphology of the postcranial skeleton in Afro-Malagasy Tenrecoidea (Mammalia). Unpublished Ph. D. Thesis, City University of New York, Graduate Faculty in Biology, 234 p

Sánchez-Villagra MR (2001) Ontogenetic and phylogenetic transformations of the vomeronasal complex and nasal floor elements in marsupial mammals. Zool J Linn Soc 131:459–479

Sánchez-Villagra MR, Ladevèze S, Horovitz I, Argot C, Hooker JJ, Macrini TE, Martin T, Moore-Fay S, Muizon C de, Schmelzle T, Asher RJ (2007) Exceptionally preserved North American Paleogene metatherians: adaptations and discovery of a major gap in the opossum fossil record. Biol Letters 3:318–322

Sánchez-Villagra MR, Smith KK (1997) Diversity and evolution of the marsupial mandibular angular process. J Mammal Evol 4:119–144

Sánchez-Villagra MR, Wible JR (2002) Patterns of evolutionary transformation in the petrosal bone and some basicranial features in marsupial mammals, with special reference to didelphids. J Zool Syst Evol Res 40:26–45

Segall W (1969) The middle ear region of *Dromiciops*. Acta Anat 73:489–501

Seiffert ER, Simons EL, Ryan TM, Bown TM, Attia Y (2007) New remains of Eocene and Oligocene Afrosoricida (Afrotheria) from Egypt, with implications for the origin(s) of afrosoricid zalambdodonty. J Vertebr Paleontol 27:963–972

Sereno PC (2006) Shoulder girdle and forelimb in multituberculates: evolution of parasagittal forelimb posture in mammals. In: Carrano MT, Gaudin TJ, Blob RW, Wible JR, (eds) Amniote Paleobiology: Perspectives on the Evolution of Mammals, Birds, and Reptiles. University of Chicago Press, Chicago, pp 315–366

Simmons MP, Ochoterena H (2000) Gaps as characters in sequence-based phylogenetic analyses. Syst Biol 49:369–381

Simpson GG (1970) The Argyrolagidae, extinct South American marsupials. Bull Mus Comp Zool 139:1–86

Springer MS, Kirsch JAW, Case JA (1997) The chronicle of marsupial evolution. In: Givnish T, Sytsma K (eds) Molecular Evolution and Adaptive Radiation. Cambridge University Press, New York, pp 129–161

Springer MS, Westerman M, Kavanagh JR, Burk A, Woodburne MO, Kao DJ, Krajewski C (1998) The origin of the Australasian marsupial fauna and the phylogenetic affinities of the enigmatic monito del monte and marsupial mole. Proc R Soc B 265:2381–2386

Swofford DL (2002) PAUP*: phylogenetic analysis using parsimony (*and other methods). Sinauer Associates, Inc., Sunderland, Massachusetts

Szalay FS (1982) A new appraisal of marsupial phylogeny and classification. In: Archer M (ed) Carnivorous Marsupials. Royal Zoological Society of New South Wales, Mosman, New South Wales, pp 621–640

Szalay FS (1994) Evolutionary History of the Marsupials and an Analysis of Osteological Characters. Cambridge University Press, Cambridge

Szalay FS, Sargis EJ (2001) Model-based analysis of postcranial osteology of marsupials from the Palaeocene of Itaboraí (Brazil) and the phylogenetics and biogeography of Metatheria. Geodiversitas 23:139–302

Szalay FS, Sargis EJ (2006) Cretaceous therian tarsals and the metatherian-eutherian dichotomy. J Mammal Evol 13:171–210

Travouillon KJ, Archer M, Hand SJ, Godthelp H (2006) Multivariate analyses of Cenozoic mammalian faunas from Riversleigh, northwestern Queensland. Alcheringa Spec Iss 1:323–349.

Travouillon KJ, Gurovich Y, Archer M, Hand SJ, Muirhead J (2013) The genus *Galadi*: three new bandicoots (Marsupialia, Peramelemorphia) from Riversleigh's Miocene deposits, Northwestern Queensland, Australia. J Vertebr Paleontol 33:153–168

Turnbull WD (1970) Mammalian masticatory apparatus. Fieldiana: Geol 18:149–356

Voss RS, Jansa SA (2003) Phylogenetic studies on didelphid marsupials II. Nonmolecular data and new IRBP sequences: separate and combined analyses of didelphine relationships with denser taxon sampling. Bull Am Mus Nat Hist 276:1–82

Voss RS, Jansa SA (2009) Phylogenetic relationships and classification of didelphid marsupials, an extant radiation of New World metatherian mammals. Bull Am Mus Nat Hist 322:1–177

Vullo R, Gheerbrant E, Muizon C de, Neraudeau D (2009) The oldest modern therian mammal from Europe and its bearing on stem marsupial paleobiogeography. Proc Natl Acad Sci USA 106:19910–19915

Waddell PJ, Kishino H, Ota R (2001) A phylogenetic foundation for comparative mammalian genomics. Genome Informatics 12:141–151

Warburton NM (2003) Functional morphology and evolution of marsupial moles (Marsupialia; Notoryctemorphia). Unpublished Ph.D. Thesis, University of Western Australia

West RM (1973) Review of the North American Eocene and Oligocene Apatemyidae (Mammalia: Insectivora). Spec Publ Mus Texas Tech Univ 3:1–42

Wible JR (1990) Late Cretaceous marsupial petrosal bones from North America and a cladistic analysis of the petrosal in therian mammals. J Vertebr Paleontol 10:183–205

Wible JR (2003) On the cranial osteology of the short-tailed opossum *Monodelphis brevicaudata* (Marsupialia, Didelphidae). Ann Carnegie Mus 72:137–202

Wible JR, Novacek MJ, Rougier GW (2004) New data on the skull and dentition in the Mongolian Late Cretaceous eutherian mammal *Zalambdalestes*. Bull Am Mus Nat Hist 281:1–144

Wible JR, Rougier GW, Novacek MJ (2005) Anatomical evidence for superordinal/ordinal eutherian taxa in the Cretaceous. In: Rose KD, Archibald JD (eds) The Rise of Placental Mammals: Origins and Relationships of the Major Extant Clades. Johns Hopkins University Press, Baltimore, pp 15–36

Wible JR, Rougier GW, Novacek MJ, McKenna MC (2001) Earliest eutherian ear region: a petrosal referred to *Prokennalestes* from the Early Cretaceous of Mongolia. Am Mus Novitates 3322:1–44

Williamson TE, Brusatte SL, Carr TD, Weil A, Standhardt BR (2012) The phylogeny and evolution of Cretaceous-Palaeogene metatherians: cladistic analysis and description of new early Palaeocene specimens from the Nacimiento Formation, New Mexico. J Syst Palaeontol 10:625–651

Woolley PA (2011) *Pseudantechinus mimulus*: a little known dasyurid marsupial. Australian Mammal 33 :57–67

Woodburne MO, Case JA (1996) Dispersal, vicariance, and the Late Cretaceous to early Tertiary land mammal biogeography from South America to Australia. J Mammal Evol 3:121–161

Worthy TH, Tennyson AJD, Archer M, Musser AM, Hand SJ, Jones C, Douglas BJ, McNamara JA, Beck RMD (2006) Miocene mammal reveals a Mesozoic ghost lineage on insular New Zealand, southwest Pacific. Proc Natl Acad Sci USA 103:19419–19423

Wroe S (1997) A reexamination of proposed morphology-based synapomorphies for the families of Dasyuromorphia (Marsupialia). 1. Dasyuridae. J Mammal Evol 4:19–52

Wroe S (1999) The geologically oldest dasyurid (Marsupialia), from the Miocene Riversleigh, northwestern Queensland. Palaeontology 42:1–27

Wroe S, Brammall J, Cooke BN (1998) The skull of *Ekaltadeta ima* (Marsupialia, Hypsiprymnodontidae?): an analysis of some cranial features within Marsupialia and a re-investigation of propleopine phylogeny; with notes on the inference of carnivory among mammals. J Paleontol 72:738–751